High porosity carbon cathodes for seawater batteries

João Ferreira
MSc. Engineering Physics
Departamento de Física e Astronomia
2022

Supervisor
Prof. Dra. Joana Oliveira, Faculdade de Engenharia

Co-supervisor
Prof. Dr. João Ventura, Faculdade de Ciências

All corrections determined by the jury, and only those, were made.

The President of the Jury,

Porto,_____/_____/_____

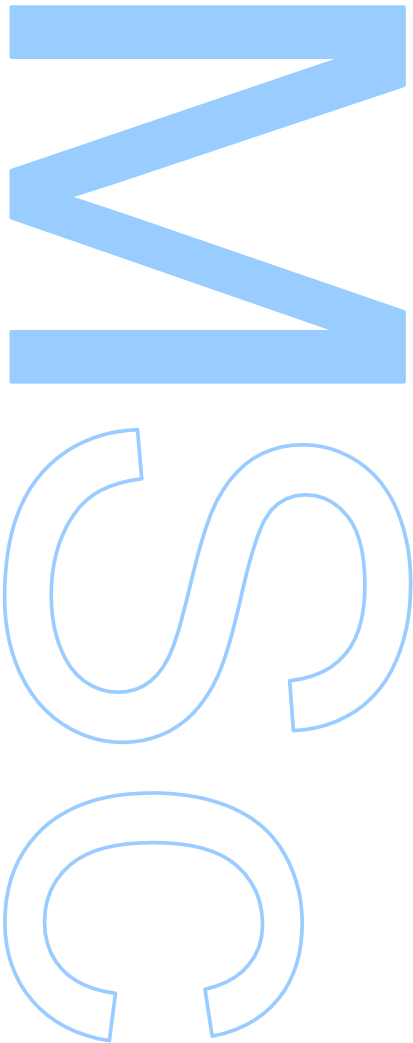

UNIVERSIDADE DO PORTO

MASTERS THESIS

High porosity carbon cathodes for seawater batteries

Author:
João FERREIRA

Supervisor:
Prof. Dra. Joana Oliveira

Co-supervisor:
Prof. Dr. João Ventura

A thesis submitted in fulfilment of the requirements
for the degree of MSc. Engineering Physics

at the

Faculdade de Ciências da Universidade do Porto
Departamento de Física e Astronomia

December 21, 2022

" Never doubt that a small group of thoughtful, committed citizens can change the world; indeed, it is the only thing that ever has. "

Margaret Mead

Sworn Statement

I, João Pedro André Ferreira, enrolled in the Master Degree Engineering Physics at the Faculty of Sciences of the University of Porto hereby declare, in accordance with the provisions of paragraph a) of Article 14 of the Code of Ethical Conduct of the University of Porto, that the content of this dissertation reflects perspectives, research work and my own interpretations at the time of its submission.

By submitting this dissertation, I also declare that it contains the results of my own research work and contributions that have not been previously submitted to this or any other institution.

I further declare that all references to other authors fully comply with the rules of attribution and are referenced in the text by citation and identified in the bibliographic references section. This dissertation does not include any content whose reproduction is protected by copyright laws.

I am aware that the practice of plagiarism and self-plagiarism constitute a form of academic offense.

João Pedro André Ferreira 20 de dezembro de 2022

Acknowledgements

First and foremost, I would like to extend my gratitude to my supervisors, Prof. Joana Espain de Oliveira and Prof. João Ventura, who provided encouragement and guidance throughout the entire process and inspired me to pursue a doctoral degree as the next chapter. Without their knowledge and the open communication environment that they created, this dissertation would not be possible. They allowed me to learn and to explore the themes that I am passionate about, always being there to ensure that a good and sustainable scientific contribution was the outcome of the research work.

A special thanks to Rita Veloso, who was always available to help and teach me the proper way to use the laboratory equipment that I needed, while also supporting me and providing encouragement. Being from a different scientific field, she taught me a lot and was always checking up on me to see if there was anything that I need, and for this I am thankful.

I would also like to thank Tiago Salgueiro that helped me in some parts of this dissertation, greatly contributing the outcome of this research work, and the IFIMUP team, whose members were always ready to help, whether themselves or indicating others, creating an environment full of scientific exchanges that is very important for the evolution of science in general.

This dissertation concludes my 5 year integrated master's degree, so I would like to thank to all of my colleagues and friends that helped me reach this final stage. From all, I would like to mention Inês Ornelas, Beatriz Lopes and Filipa Ribeiro, who have grown to be very important throughout these 5 years, always helping me academically and personally to be the best that I can. Without their friendship and support this journey would have been much harder, as almost nothing can be done alone.

Lastly but most importantly, I would like to thank my parents and my sister. They have supported me from the very beginning, allowing me to chose the best path for my life having only the condition that I was happy with my choices. Without the patient and familiar environment that they created, I would not be able to come as far as I did. They gave something to aspire to, which drove me to always be and give the best that I can.

UNIVERSIDADE DO PORTO

Abstract

Faculdade de Ciências da Universidade do Porto
Departamento de Física e Astronomia

MSc. Engineering Physics

High porosity carbon cathodes for seawater batteries

by João FERREIRA

Humanity is reaching a tipping point where new sustainable energy solutions are needed. Oceans, covering more than 70% of Earth surface, can become the key asset in this fight. Many technologies have taken advantage of this resource, such as seawater desalination, offshore power storage and sea vessels electrification. Rechargeable sodium seawater batteries (SWB) are assuming the world leadership of high voltage batteries in marine environment and can be a great addition to the previously mention technologies. SWB have several applications as main or auxiliary power sources for a wide range of maritime sectors, such as life jackets integrated with GPS, light buoys, where SWB would store energy generated by solar power, and many others. On the other hand, any energy storage application needs to be sustainably scalable. In this way, the use of carbon waste is a basic rule in the technologies to be developed from now on. A good bio-waste precursor are peanut shells whose global annual volume is around 7.44 million tons and their use for animal feed or fuel is very limited. With natural seawater as the active material, the SWB can be supplied infinitely with Na cations. Because of their open structure cathode, the performance of the battery is dependent on the characteristics of the cathode material, such as its specific surface area, porosity, functionalisation and wettability. The redox reactions involved in SWBs are slow electrochemical processes. With increased surface area, a much faster capacitive mechanism arises with an important contribution of the electric double layer (EDL) formed at the cathode interface.

Therefore, in this work, we studied how the performance of a seawater cell depends on four different cathodes, commercial, heated and activated carbon felts and a peanut shell bio-waste activated carbon electrode. Their performance was evaluated through galvanostic charge and discharge cycles and cyclic voltammetries. Their morphologies were

analysed by scanning electron microscopy (SEM), energy dispersive X-ray spectroscopy (EDS) and their wettability was measured. The performed electrochemical characterisation allowed to observe a gradual improvement of the cathode performance with the increase of the specific surface due to an enhancement of the capacitive behaviour contribution. The peanut shell bio-waste cathode revealed a voltage gap similar to that of the activated carbon, being even smaller for the highest current. The cyclic voltammetry showed a great capacitive effect and the calculated gravimetric capacitance of the full seawater cell was close to that of the activated carbon. The obtained performance demonstrates that the bio-waste electrode shows good performance due to the combination of a strong EDL formation contribution and the improvement of the OER/ORR activity efficiency. This is caused by the highly porous structure of the electrocatalyst with macroporous cores that act as secondary ion-buffering reservoirs, mesoporous walls that provide pathways with low resistance, and micropores that can afford the electric double layer capacitance. Adding to these, a highly functionalised surface where oxygen functional groups result in excellent active sites for OER/ORR activity. This work opens a new path for the integration of bio-waste in seawater batteries towards a more sustainable future.

Keywords: Seawater Battery · Peanut Shells · Bio-waste · Activated Carbon · Electrocatalyst · Electrical Double Layer · Sustainability

UNIVERSIDADE DO PORTO

Resumo

Faculdade de Ciências da Universidade do Porto
Departamento de Física e Astronomia

Mestrado Integrado em Engenharia Física

Cátodos de carbono altamente porosos para baterias de água do mar

por João FERREIRA

A humanidade está a atingir um ponto de viragem em que são necessárias novas soluções energéticas sustentáveis. Os oceanos, cobrindo mais de 70% da superfície terrestre, podem tornar-se numa mais-valia nesta luta. Muitas tecnologias aproveitam este recurso, tais como a dessalinização da água do mar, o armazenamento de energia no mar e a eletrificação de embarcações marítimas. As baterias recarregáveis de água do mar de sódio (SWB) estão a assumir a liderança mundial de baterias de alta voltagem em ambiente marinho e podem ser uma boa adição às tecnologias anteriormente mencionadas. As SWB têm várias aplicações como fontes de energia principal ou auxiliar para uma vasta gama de sectores marítimos, tais como coletes salva-vidas integrados com GPS, boias de luz, onde as SWB armazenariam a energia gerada por energia solar, e muitas outras. Por outro lado, qualquer aplicação de armazenamento de energia precisa de ser escalável de forma sustentável. Desta forma, a utilização de resíduos de carbono é uma regra básica nas tecnologias a serem desenvolvidas a partir de agora. Um bom precursor de bio resíduos são as cascas de amendoim cujo volume anual global é de cerca de 7,44 milhões de toneladas e a sua utilização para alimentação animal ou combustível é muito limitada. Com água do mar natural como material ativo, a SWB pode ser fornecida infinitamente com iões de sódio. Devido à sua estrutura catódica aberta, o desempenho da bateria depende das características do material catódico, tais como a sua área de superfície específica, porosidade, funcionalização e hidrofilicidade. As reações redox envolvidas nas SWBs são processos eletroquímicos lentos. Com o aumento da área de superfície, surge um mecanismo capacitivo mais rápido com uma importante contribuição da dupla camada elétrica (EDL) formada na interface entre o cátodo e a água de mar.

Assim, neste trabalho, estudámos como o desempenho de uma célula de água do mar depende de quatro cátodos diferentes: feltros de carbono comercial, aquecido e ativado e um elétrodo de carbono ativado de bio resíduos de casca de amendoim. O seu desempenho foi avaliado através de ciclos de carga e descarga galvanósticos e voltametrias cíclicas. As suas morfologias foram analisadas por microscopia eletrónica de varrimento (SEM), espectroscopia de raios X dispersiva de energia (EDS) e a sua hidrofilicidade foi medida. A caracterização eletroquímica realizada permitiu observar uma melhoria gradual do desempenho catódico com o aumento da superfície específica devido a uma melhoria da contribuição do comportamento capacitivo. O cátodo de bio resíduos de cascas de amendoim revelou uma diferença de potencial final semelhante à do carbono ativado, sendo ainda menor para a corrente mais elevada. A voltametria cíclica mostrou um grande efeito capacitivo e a capacitância gravimétrica calculada para a célula de água do mar completa era próxima da do carbono ativado. O desempenho obtido demonstra que o elétrodo de bio resíduos apresenta um bom desempenho devido à combinação de uma forte contribuição da formação EDL e de uma melhoria da eficiência da atividade OER/ORR. Isto é causado pela estrutura altamente porosa do electrocatalisador, com núcleos macro porosos que atuam como reservatórios secundários de amortecimento iónico, paredes meso porosas que proporcionam vias de baixa resistência, e microporos que podem permitir a capacitância elétrica de dupla camada. Acrescentando a estes, uma superfície altamente funcional onde grupos funcionais de oxigénio resultam em excelentes locais ativos para a atividade OER/ORR. Este trabalho abre um novo caminho para a integração de bio resíduos em baterias de água do mar rumo a um futuro mais sustentável.

Palavras-chave: Bateria de Água do Mar · Casca de Amendoim · Bio-resíduo · Carbono Ativado · Eletrocatalisador · Dupla Camada Elétrica · Sustentabilidade

Contents

List of Figures

List of Tables

Glossary

ACF	Activated carbon felt
ACPS	Activated and carbonised peanut shells
AEM	Anion Exchange Membrane
AgCl	Silver(I) chloride
BO_3^{2-}	Borate ion
Br^-	Bromide ion
C	Carbon
Ca	Calcium
Ca^{2+}	Calcium ion
CCC	Cathode current collector
CCF	Commercial carbon felt
CDI	Capacitive deionisation
CE	Coulomb efficiency
CF	Carbon felt
Cl^-	Chloride ion
CO	Carbon monoxide
CO_2	Carbon dioxide
CO_3^{2-}	Carbonate
CPS	Carbonised peanut shells
CV	Cyclic voltammetry
DMF	Dimethylformamide

DO	Dissolved oxygen
ED	Electrodialysis
EDL	Electric double-layer
EDLC	Electric double-layer capacitor
EDS	Energy dispersive X-ray spectroscopy
EES	Electrical energy storage
EIS	Electrochemical impedance spectroscopy
ESR	Equivalent series resistance
F^-	Fluoride ion
FEG	Field emission gun
H^+	Hydrogen ion
H_2	Hydrogen
H_2CO_3	Carbonic acid
H_2SO_4	Sulphuric acid
H_3O^+	Hydronium
HCCF	Heated commercial carbon felt
HCL	Hydrogen chloride
HCO_3^-	Bicarbonate ion
HER	Hydrogen-evolution reaction
HES	Hybrid energy storage
K	Potassium
K^+	Potassium ion
K_2CO_3	Potassium carbonate
K_2O	Potassium oxide
KOH	Potassium hydroxide
Li	Lithium
LIB	Lithium-ion battery

MDC	Membrane distillation crystallisation
Mg	Magnesium
Mg^{2+}	Magnesium ion
MnO_2	Manganese dioxide
N_2	Nitrogen
Na	Sodium
Na^+	Sodium ion
Na_2CO_3	Sodium carbonate
NaCl	Sodium chloride
NaOH	Sodium hydroxide
NASICON	NA Super Ion CONductor
NH_4^+	Ammonium
NO_2^-	Nitrite
NO_3^-	Nitrate
O_2	Oxygen
OER	Oxygen-evolution reaction
ORR	Oxygen-reduction reaction
PAN	Polyacrylonitrile
pH	Potential of hydrogen
PS	Peanut shells
PSCF	Peanut shell coated heated commercial carbon felt
Redox	Oxidation-reduction
RO	Reverse osmosis
SEI	Solid electrolyte interphase
SEM	Scanning electron microscopy
SHE	Standard hydrogen electrode
Si	Silicon

SIB	Sodium ion battery
SO_4^{2-}	Sulfate ion
Sr^{2+}	Strontium ion
SWB	Seawater battery
TEGDME	Tetraethylene glycol dimethyl ether
UPS	Uninterruptible power supply
Zn	Zinc
$ZnCl_2$	Zinc chloride

Chapter 1

Introduction

The technological advances in the last decades that have greatly improved our everyday lives has also propelled the need for the development of new technologies and the improvement of the ones already in existence. Concerns regarding energy and environmental challenges, such as the reliance on fossil fuels for energy, pollution, global warming, and climate change, are on the rise [1]. Fossil fuels are one of the major causes for global warming due to carbon dioxide emissions and they are being quickly depleted [2]. These concerns have propelled the interest in renewable energies, such as solar, wind, wave and geothermal. They are seen by many as an important part of the solution and a path to an efficient energy use that allows for a sustainable development of society. Accompanying these growing concerns is the gradual increase in energetic demand by the population. Renewable energies are abundant but have an intermittent nature with irregularities and power variations [3], because of their dependence in natural and uncontrollable elements. Electrical storage devices are a great solution for matching fluctuating electricity supply with demand [4], transforming renewable energy into a usable form.

Electricity is the foundation of modern civilisation [5], being a very important scientific field, regarding its production and storage. Electrical energy storage (EES) devices, such as rechargeable batteries, flow batteries and capacitors, exist all around us in our everyday lives. They can offer low maintenance, high round-trip efficiency, long cycle life, and flexible power and energy features [4]. Important factors to consider while choosing an energy storage device are specific energy, specific power, lifetime, dependability, and protection, keeping in mind the sustainability of the materials used to build said EES [3]. Rechargeable batteries are expected to have a major role in a low-carbon footprint and sustainable future. Li-ion batteries (LIBs) are one of the most widely used EES device

nowadays in various fields because of their high energy and power densities, ease of installation and lifetime [2]. However, this industry currently requires almost 50% of the available resources of lithium and cobalt (the main components of LIBs) to meet the high energetic demand, which can cause many economic and supply problems in a long term point of view [1]. Besides, the extraction of raw lithium containing materials has severe environmental issues.

A good way to make a technology more sustainable and a better long-term solution is by using abundant materials with an environmentally friendly extraction process. Rechargeable seawater batteries (SWBs) use the abundant seawater as the active material. SWBs utilise the sodium ions present in natural seawater without needing any additional extraction process. They store electrochemical energy through chemical bonds of sodium, with the oxidation of seawater in the cathode and the reduction of sodium ions in the anode. The stored electrochemical energy is transformed in electricity during discharge through the release of sodium ions back to seawater. SWBs have an open-structure cathode configuration that enables the continuous and almost infinite supply of sodium ions, while the reaction products and reactants are continuously replaced for new ones. The use of seawater as the catholyte can mean a reduction in material and manufacturing costs. The main prospect applications of SWBs are offshore and stationary applications where they can be coupled with renewable energy sources that drawn from the surrounding elements, such as solar and wave motion energy. With this in mind, SWB are a cheaper and more environmentally friendly alternative to LIBs in large-scale applications, but compared to LIBs, SWBs research is still in an embryonic stage for commercialisation [1, 4].

The cathode is the positive electrode of a seawater battery and on its surface is where the main reactions that allow for the operation of the battery take place, being a very important part of a SWB. Its study and alterations can improve the performance of a seawater battery. Carbon felts are widely used as cathodes and play an important role in the development of clean energy storage and conversion technologies, as they are resistant to ecological environmental deterioration and have good characteristics, such as strength, stability, conductivity and cost-effectiveness [6]. SWBs with carbon felts as cathodes can show low voltage efficiency and large voltage gaps between the charge and discharge profiles because of the sluggish kinetics of the redox reactions taking place. This can be improved by the addition of an electrocatalyst such as noble metal based (Ir, Ru, and Pt) catalysts, being these the ones that are most used in the battery industry. However, they

are not a scalable solution as they are derived from expensive and scarce materials, and offer poor stability which impede their widespread use in large-scale stationary systems [7]. Furthermore, carbon-based materials mostly come from non-renewable sources like coal, petrochemicals and natural gas. These resources are limited and are being increasingly depleted, becoming imperative to seek alternatives that are derived from sustainable and abundant carbon resources for the production of carbon-based materials [6].

Bio-waste derived carbon materials are great candidates for the production of activated carbon with large specific surface area, porous nature, chemical stability, a high degree of surface activity, and adequate electrical conductivity [8, 9]. They are promising alternatives since bio-waste is an affordable, widely accessible, naturally renewable, and environmentally friendly precursor that can be used in a scalable production for large-scale applications at a low cost [7]. A possible bio-waste source are agricultural waste materials that have received a lot of attention recently. In particular, peanut shells are a clean, extensive, inexpensive and renewable industrial waste product with a global annual volume of about 7.44 million tons [6] that can be used as a biomass precursor for activated carbon production. Their utilisation in EES devices can alleviate some of the environmental burden. The ability to tune the chemical composition, material morphology, surface functionalities and carbon properties of peanut shells makes them a good precursor to produce activated carbon [8]. The utilisation of peanut shell derived materials has been reported in the preparation of absorbents to remove heavy metal ions and organic dyes from wastewater and as electrode materials in energy storage devices such as supercapacitors, LIBs and metal-air batteries [6].

1.1 Thesis Structure

The research work presented in this thesis is focused on the development of optimised SWBs cathode current collectors and the study of their influence on the SWB performance in a laboratory environment.

The first part of the research work aimed to better understand the working mechanism of a seawater cell using known cathode current collectors such as commercial carbon felts, pristine and annealed, and an activated carbon felt with an unconventional manufacturing process. These three cathode currents collectors had already been studied in the literature to some extent, allowing for a good understanding of the working mechanism of a seawater full cell.

The second part of the research work focused on the synthesis of an electrocatalyst to be applied on the heated commercial carbon felt to improve the SWB performance. Being sustainability a very important parameter to have in consideration, we decided to chose peanut shells as the raw material for the electrocatalyst, as they are a waste product and possess interesting properties that make it a promising material. The electrocatalyst manufacturing process consisted mainly of a carbonisation followed by an activation with potassium hydroxide (KOH), whose process was optimised. This peanut shell coated electrode increased the sustainability of the seawater battery with a simple and cheap manufacturing process, making sure that, once optimised, it could still be employed in large-scale applications with a low carbon footprint and low cost.

Chapter 2

Seawater Batteries

2.1 Batteries

2.1.1 The brief evolution of batteries

Modern civilisation is built on electricity. For many years after the discovery of electricity, electrochemical cells were the only way to store electrical power, having still a crucial role in modern electrical technology [5].

A battery is a device that exchanges electrical with electrochemical energy in a dynamic process, working as a limited source of electricity. The term battery was first used by Benjamin Franklin in 1740s, but evidence was found that indicate that the notion of a battery to store energy could be as old as 2000 years. In 1800, Alessandro Volta developed the first actual electrochemical battery, which was made up of two zinc and copper discs spaced by a piece of cloth dipped in an aqueous solution with a high concentration of salt. The growth of batteries continued to evolve leading to the development of the first primary lithium anode batteries in 1970, which was the beginning of the creation that led to the batteries most used today, in our phones, cars, tablets, laptops and so many other everyday life devices [5].

From all battery types, lithium-ion batteries have received the most attention and research. John B. Goodenough, M. Stanley Whittingham and Akira Yoshino were awarded with the Nobel Prize in Chemistry by the Royal Swedish Academy of Sciences in 2019 for their vital contributions to the development of lithium-ion batteries that laid the foundation for wireless electronics, shaping the world we live in today.

However, with the increasing concerns regarding lithium batteries (which will be further explored in section 2.1.4.1), alternatives have been developed over the years, replacing lithium with other active materials such as Sodium (Na), Zinc (Zn), Magnesium (Mg), among many others.

2.1.2 Battery general working principle

Batteries are a type of electrical energy storage devices (EES), that store electrochemical energy and later convert it to electricity. Ideally, a battery storage system has low resistance, simplicity and ease of construction, durability, and low cost [10]. Their main working mechanism is the oxidation-reduction reaction (also known as a redox reaction) at the anode and the cathode. These reactions produce ions and electrons that will travel through the electrolyte and an external electrical circuit, respectively, to ensure charge neutrality. The pathways of the charge particles can be observed in Figure 2.1, where a typical battery is illustrated. The transfer of electrons between electrodes results in an electrical current, from which energy can be extracted.

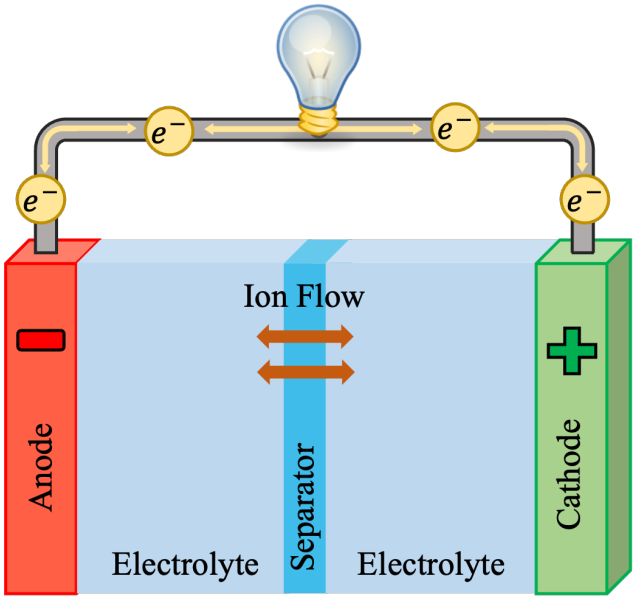

FIGURE 2.1: Illustration of a typical battery.

Usually, a battery is a set of galvanic cells working together, where electrons and ions move spontaneously converting electrochemical energy into electricity. The cell's voltage and capacity are two parameters that quantify the energy delivered by it. The cell's voltage is the difference of potential between the two electrodes and can be defined as the

work done to move a unit charge from one electrode to the other. The cell voltage can be described by:

$$E^o_{Cell} = E^o_{Cathode} - E^o_{Anode}, \tag{2.1}$$

where the electrochemical potential is an element characteristic and it is a measure of the difference between the average energy of an element's or molecule's outermost electrons in its two valence states. The differences in electrochemical potentials between various phases, where species will attempt to migrate from a phase with greater electrochemical potential to a phase with lower electrochemical potential, are what drive redox reactions in a cell [11]. The cell potential depends on the materials chosen to build the battery, having many possible combinations to achieve a desired voltage. The theoretical cell potential can be obtained with the redox potentials of the chosen materials. The potential of the actual developed battery can differ from the theoretical value because of the presence of resistive elements, being also influenced by temperature and humidity [5].

Another critical parameter is the amount of charge, in Coulomb (C), stored in the cell. The motion of the charged particles creates a current (I) that is the amount of charge flowing per unit of time, with ampere (A) as the unit. Usually, when addressing batteries, the amount of charge is normally expressed in ampere-hours (Ah), referring to the capacity of the battery. It is the total charge (measured in Ah) that exists in the battery under a certain set of conditions. Theoretically, the cathode and anode materials will influence the capacity (Q) that can be calculated with [5]:

$$Q = I. \cdot t \quad [Ah] \tag{2.2}$$

With these two parameters we can measure the energy (E) stored in a cell:

$$E = Q \cdot V, \quad [J \ \ or \ \ Wh] \tag{2.3}$$

and its power (P):

$$P = \frac{E}{t} = \frac{Q \cdot V}{t}. \quad [W] \tag{2.4}$$

The batteries' energy and power are strongly influenced by the chosen materials, so research on energy storage devices has focused, since the beginning, on the development of new materials that can supply greater amounts of energy and higher power outputs.

The way to classify a battery has changed over the years. In the beginning, batteries were named after the scientist who created them or their main characteristics. Currently, batteries are categorised according to their main active material or metal electrode (e.g. sodium or lithium batteries), their mechanism of reaction in the electrodes, or their intended use, shape or size. Nonetheless, batteries are primarily classified according to their ability to be or not recharged, being called a secondary or primary battery, respectively [5].

2.1.3 Primary batteries

Primary batteries are discarded after one use since they cannot be successfully recharged, generally because the involved electrochemical reaction is irreversible. Even though their inability to be reused, primary batteries make up about 90% of the battery market, because they are generally cheaper, simpler and more compact than rechargeable batteries. They generally also have higher capacities, initial voltage and energy density when compared to secondary batteries according to the ratio weight/volume criteria [12]. In this work we will be working with rechargeable seawater batteries, so a brief introduction to primary SWBs will be done in this context.

The first and most frequently used seawater battery is the disposable, non-rechargeable "seawater-activated battery", that was created in the 1940s. Over time, many primary seawater batteries were developed by changing their materials, but always maintaining metal as the anode material that throughout the cell's life will continuously dissolve in seawater. In the late 1980s, seawater batteries were developed for deep-sea applications and long-term operation, by using the seawater as the electrolyte and also as the source of active material. This development decreased the weight and volume of the cathode material, allowing higher energy densities. They use the dissolved oxygen or the water decomposition reactions that occur naturally in seawater as the working mechanisms. Many other types of material combinations exist that give variety to the amount of primary seawater batteries developed, but even though they have a long history they were always developed to meet a specific goal, so the range of applications for primary seawater batteries is still narrow [5].

The general composition of a primary seawater battery is comprised of a positive and negative electrode, a separator, an electrolyte (seawater), a termination and a casting, which can be seen in the illustration in Figure 2.2. They are usually multiple cells

connected in series or parallel to maximise the output.

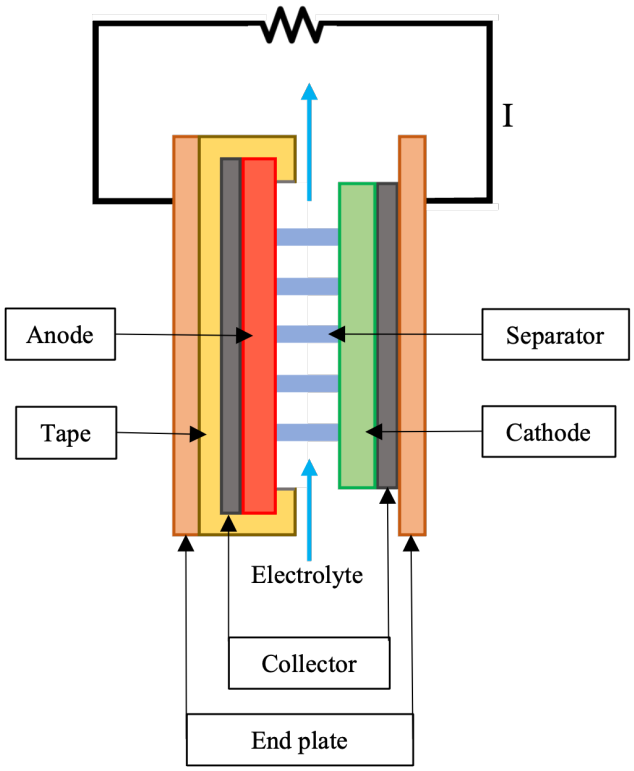

FIGURE 2.2: Illustration of a typical primary seawater battery.

As said before, several metals have been used as the anode in primary seawater batteries, such as zinc, aluminium, lead, lithium, sodium, potassium and magnesium, the latter being the most common anode material because it generates a fairly stable output. For the cathode, materials such as silver(I) chloride (AgCl) with a salt solution electrolyte and manganese dioxide (MnO_2) and an alkaline electrolyte are just an example of the many materials that have been used. These kinds of batteries are meant for irregular use, having a high output for a short period of time and a long inactive life span, where the electrolyte (i.e. seawater) is only supplied when the battery is ready to be used. The major applications for primary seawater batteries are military and communications devices [5].

In general, most batteries that use metal as the anode are primary batteries even though a metallic anode is considered to be a good negative electrode. A metallic anode in a rechargeable battery means a higher theoretical capacity, lower electrochemical potential, faster charging times and higher energy density. The high energy density of metals is because their atoms are packed closely together in a small space due to metallic bonding, which is a strong electrostatic attraction between metal cations and dispersed electrons. The higher the energy density of a system or material, the greater the amount

of energy it has stored. In the beginning of the development of rechargeable batteries, metallic anodes were studied but was soon realised that the advantages that they bring were countered by their pressing disadvantages such as dendrite formation and unstable interfaces. These problems caused safety issues, irreversible capacity loss, low coulombic efficiency, and ultimately shorter cycling life in rechargeable metal batteries [13]. Due to these issues, the metallic anodes were mostly used for the primary batteries, putting the development of secondary batteries with metal as the negative electrode in the back seat as a priority. Nowadays, with the increasing energetic demand, new research is being made in order to further study ways to mitigate the problems of a rechargeable battery with metal as the anode, such as solid state electrolytes and polymeric electrolytes that offer better safety regarding dendrite formation. Many improvements have been made that allow the use of these kind of batteries, in particular the rechargeable sodium seawater battery that is the main focus of this study and has metallic sodium as the anode. Its composition and structure will be better described further ahead, in section 2.2.

2.1.4 Secondary batteries

Secondaries batteries mainly differ from primary batteries because of their ability to be recharged, or regain cell potential, making them reusable. They can be recharged numerous times because the cell reactions responsible for the working of the battery are reversible. This means that, by allowing current to flow into the cell, its original chemical conditions can be restored [10]. There are many types of secondary batteries, as their classification is based on whether they are sealed or vented, the kind of electrolyte or active material used, or their application and end use. They can be used in long-term applications, with long storage time when inactive, remote activation, and can operate under harsh weather conditions. To this day, no secondary battery can respond to all these ends. Examples of these batteries applications are automotive and aircraft systems, uninterruptible power supply (UPS), hybrid vehicles, portable consumer electronics, power tools, and so on, having a much wider range of applications than the previous mentioned primary batteries [12], being mainly divided in mobile and stationary applications.

Figure 2.3 illustrates a comparison between some of the existing secondary batteries. The most common secondary batteries are lead-acid batteries, nickel-cadmium batteries, silver-zinc batteries, lithium-ion batteries and sodium-ion batteries.

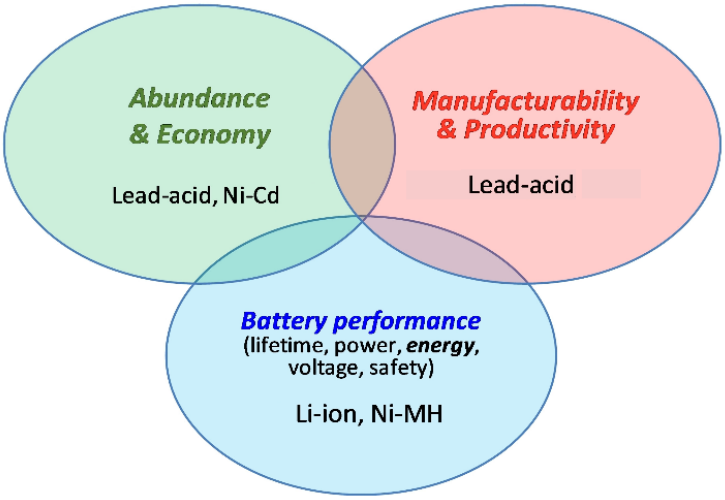

FIGURE 2.3: Schematised comparison of some of the existing secondary batteries. Figure from reference [14].

2.1.4.1 Lithium-ion vs Sodium-ion batteries

Lithium-ion batteries (LIBs) are rechargeable and have become the most known type of EES device in the last two decades because they are present in a large number of devices that we use on our everyday lives. Their development resulted in a rapid evolution of wireless and portable instruments and electric vehicles, being one of the options for the main energy storage for electric and hybrid cars in the near future. They are a wonderful and efficient technology, but they still have some drawbacks that propel the need to have alternatives that mitigate those disadvantages and still meet the needs that they are set to fulfil. Another type of battery that is gaining more and more attention these days is the sodium ion battery (SIB). These batteries can mitigate some of the disadvantages of LIBs, but their stage of development is not advanced enough to replace LIBs all together. In this section we are going to compare these two EES devices and show some advantages and disadvantages of each.

Lithium is the 27th most abundant metal on Earth, being the lightest alkali, highly reactive and flammable, with a low atomic mass and a small radius. Lithium metal possesses a high specific capacity (3.86 Ah g^{-1}) and an extremely low electrode potential (-3.04 V vs. standard hydrogen electrode). One of the biggest disadvantages of LIBs technology is the extraction of raw materials containing lithium, since pure lithium is never found in nature due to its high reactivity. It is generally found as a ion dissolved in water, so its extraction sites are normally brines and clays, being obtained from a mixture of lithium and potassium chloride [15]. To make matters worse, lithium resources

are unevenly distributed throughout the globe, only existing in North and South America, China, Australia, Portugal and Zimbabwe. The increasing demand for lithium as the active material is causing concerns regarding the feasibility and sustainability of the ratio demand vs supply. The ratio will only increase significantly from now on, since the battery industry requires almost 50% of the resources available of lithium and cobalt already [1, 16]. If the need for lithium continuous to increase, there is the risk of lithium resources scarcity, which will result in very high lithium market prices. Most reports state that the cost of LIBs is highly dependent on the material cost, such as lithium and cobalt, which accounts for more than 70% of the total manufacturing cost [1]. The extraction of lithium resources has another major problem in terms of environmental sustainability. Lithium mining has severe environmental side effects such as water loss, ground destabilisation, biodiversity loss, increased rivers' salinity, soil contamination and toxic waste. The climate crisis we already live in is only going to get worse, so being energetically dependent on a technology that causes so much environmental damage in order to work should not be one of the main options. All these factors regarding the cost, availability and sustainability of lithium as the active material for EES devices indicate that LIBs could become a nonviable long-term solution, economically and environmentally wise.

Such problems are drastically mitigated when addressing SIBs. Their active material is sodium which is similar to lithium in being an alkali and highly reactive metal, but their most significant difference is that sodium is the 6th most abundant element on Earth's crust, being usually found in the form of sodium chloride in the oceans [17]. The abundance of sodium is its greatest advantage because it significantly reduces the cost of active material extraction and also mitigates the concerns regarding the increase of the ratio demand vs supply. Sodium is so abundant that the risk of under supply is not really considered to be a problem in the future. The costliest component of a LIB is the cathode, comprising about 25% of the total cost. When comparing the cathodes of a LIB and a SIB, the material of the cathode is the main difference. Since the cost of preparing the cathode from raw materials is essentially the same for LIBs and SIBs, the main distinction is the active material, which will result in a production cost reduction of SIBs. It is predicted that SIBs will cost roughly 10–20% less than LIBs based on the information currently available [18] .

Another advantage in favour of SIBs is the fact that the initial investment needed to produce SIBs instead of LIBs would be low and the learning curve would be shortened

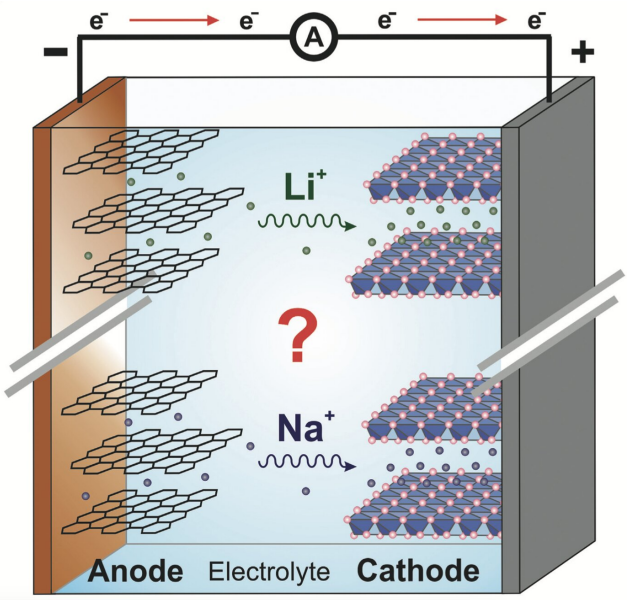

FIGURE 2.4: Illustration of the similar working principle of a LIB and a SIB, being the main difference the ion. Figure from reference [19]

because the manufacturing of SIBs consists in similar materials and production lines that already exist for LIBs [14], as it is illustrated in Figure 2.4. This increases the sustainability of SIBs because we can use factories that already exist, having no need to create new ones. So far, we can already see that, when the under supply of lithium resources becomes a serious problem, the replacement of LIBs with SIBs, as a sustainable and low cost alternative, is a great solution to consider [14].

Up to this point, we have only compared the cost and the environmental impact of the two EES devices, but by comparing their performances, we understand why LIBs have received much more attention and investment than SIBs, in a time where the risk of lithium resource under supply is still a future issue. The energy density of modern LIBs, which ranges from 150 to 190 Wh kg^{-1}, is significantly higher than that of the remaining battery types, including silver-zinc batteries [20]. The energy associated with each lithium ion is high and they can exist in higher quantities in the same volume due to their small radius. They also have very high efficiency, low weight and one of the highest upper limits of the cut off potential, being around 4.3 V vs Li^+/Li in conventional LIBs [14]. It is in the performance and range of possible applications that LIBs clearly have the advantage over SIBs. Lithium-ion batteries have a very wide range of applications that includes wireless and portable consumer devices (e.g. mobile phones, laptops), power tools, electric mobility (e.g. electric bicycles and scooters), automotive industry (e.g. hybrid and electric

cars, buses and trucks), and also stationary applications, such as smaller storage devices in larger plants [21].

On the other hand, the sodium in SIBs has lower ionisation potential when compared to lithium, leading to a theoretical upper limit cut off potential of $\sim$ 4.0 V vs Na^+/Na and a lower energy density. Another setback of SIBs is the fact that Na^+ ions are larger and heavier than Li^+ ions, leading to slower diffusion within a solid electrolyte and often larger volume expansion of the electrode when compared to LIBs. To compensate this, SIBs have to employ high-capacity positive electrodes [14, 16]. Nonetheless, recent studies have reported [18] that SIBs are rapidly reaching a satisfactory level to be commercialised considering their energy density and life cycle, since, currently, the main applications for SIBs are stationary large-scale electrical storage.

Parameters	LIBs	SIBs
Active Material	Scarce and unevenly distributed	Abundant
Production Cost	High	Lower
Extraction	Difficult	Easier
Energy Density and Cycle Life	High	Lower
Environmental Impact	Very high	Minimal
Applications	Wide range, from mobile to stationary	Mainly stationary

TABLE 2.1: Comparison between LIBs and SIBs.

The main comparison points between these two technologies are summarised in Table 2.1. We can have one major advantage and disadvantage in each, whereas for LIBs we have the advantage of better performance overall, which is very important in order to meet the increasing energetic demand of the population, but they also bring serious environmental issues and the fact that LIBs probably are not a feasible long-term solution. On the other hand, SIBs offer sustainability, which is very important when striving for a carbon emission free world, lower cost and environmental impact, and a very abundant active material, while having a lower performance and a narrower range of applications.

The interest in SIBs have increased a lot over the years so it is foreseeable that, in the future, SIBs are going to become an even better alternative to Lithium ion batteries for uses like short-range electric vehicles and large-scale energy storage in a world where wind, solar, and hydroelectric power are becoming more and more prevalent. These applications require battery energy storage for continuous, round-the-clock performance [18].

2.1.5 Bio-waste carbon cathode

There are many ways to improve the performance of a battery, being the addition of an electrocatalyst one of them. They alter the characteristics of the cathode and can be deposited on its surface. Electrocatalysts are substances that accelerate electrochemical reactions without being consumed in the process [17]. The electrocatalysts applied to the cathode of a battery, in particular a seawater battery, more commonly used, are Pt/C, a standard industry ORR catalyst, and RuO_2 and IrO_2, standard industry OER catalysts. They improve the battery's performance by increasing the efficiency of the redox reactions. Nonetheless, these electrocatalysts have low cost-efficiency as they are derived from expensive and scarce materials, and offer poor stability which prevents their widespread use in large-scale stationary systems [7].

2.1.5.1 Biomass derived activated carbon

An alternative to this electrocatalysts are carbon-based materials like activated carbon, which has been been widely used in important technologies like energy storage (supercapacitors and batteries), energy conversion (fuel and solar cells), sensors, environmental protection and catalysts, because of their electrical conductivity and structural diversity. They are characterised by high specific surface area and high porosity and consist of hydrophobic graphene layers and hydrophilic surface functional groups. In addition, they have been reported to be highly resistant to corrosive (acidic and basic) and toxic environments. Nonetheless, the majority of activated carbons available commercially originate from non-renewable resources such as coal and petroleum pitch [6]. These resources are limited, have a non-uniform global distribution and are being increasingly depleted. Because there are so many uses for activated carbon, the supply and demand gap is widening which can cause scarcity of the raw materials in a long-term perspective. So, it is becoming imperative to seek alternatives for the activated carbon precursors that are derived from sustainable and abundant carbon resources while maintaining its properties,

such as high specific surface area, micro- or mesoporosity, surface functionality, thermal stability, carbon purity and chemical composition [22].

Biomass carbons are great candidates as precursors to produce activated carbon. The entire biological material derived from plants, animals, and the products of their natural or induced transformation is referred to as biomass. Biological waste from agricultural, industrial, and municipal operations is also covered by this concept [23]. Activated carbons can be manufactured in two ways, through physical or chemical processes, after being properly washed and dried [24].

Many agricultural and industrial waste products have been reported to be good candidates as precursors to produce activated carbon, such as almonds shells, hazelnut shells, coconut shells, olive seeds, apricots, peach seeds, corn husks, oak, rice straw and husks, pecan shells, oil palm wastes, peanut shells and many others (Figure 2.5) [24].

Biomass derived activated carbons have been already applied to a wide variety of applications, such as water and gas purification technologies (where the used activated carbon can be recycled), air pollution control, CO_2 capture technologies, wastewater treatment, photocatalytic applications and many others [25–29].

FIGURE 2.5: Schematic of possible bio-waste precursors to produce activated carbon. Figure adapted from reference [30].

2.1.5.2 Peanut shell activated carbon

In this thesis, the chosen biomass precursor for the production of an activated carbon electrocatalyst were peanut shells. The peanut industry is one of the major sources of agro-industrial waste (shells) and exploring this wasted biomass' high energy content is worthwhile. The peanut shell represents around 25% and 30% of the total mass of the legume, being discarded as residues in the final stage, whether for oil productions or direct consumption, when it can be used as a biofuel to reduce CO_2 emissions [23]. However, even though it has a global annual volume around 7.44 million tons, their use for animal feed or fuel is very limited. The application of peanut shells in electrical energy storage systems can help to alleviate that burden and give another purpose to this waste material.

Peanut shells are a clean, extensive, cheap and renewable biomass resource, with a high carbon content, and level of porosity [6, 9]. Their different chemical composition, material morphology, surface functionalities and carbon properties make peanut shells a good candidate as a precursor to produce an activated carbon electrode that is capable of storing charge. To enhance the natural characteristics of peanut shells, different activating agents have been used such as zinc chloride ($ZnCl_2$), potassium hydroxide (KOH), potassium carbonate (K_2CO_3), sulphuric acid (H_2SO_4), sodium carbonate (Na_2CO_3), sodium hydroxide (NaOH), and many others [8]. The chosen activating agent was KOH because it is the one that showed more promising results in terms of specific surface area of the peanut shell activated carbon, ranging from 1430 to 2500 $m^2\ g^{-1}$, and its activation process is known to achieve highly disordered and uniform micro porous activated carbon [31, 32].

The natural multiple channel and porous structure of the peanut shells is maintained throughout the carbonisation and activation process. IUPAC categorises pores into three groups: micropores (diameter < 2 nm), mesopores (diameter between 2 nm and 50 nm), and macropores (diameter > 50 nm) [33]. According to [33], most of the porous carbon materials possess micro-, meso- and macropores due to the burn-off of non-carbon elements, such as oxygen, nitrogen and hydrogen, and carbon containing compounds during the process of carbonisation. All of these different sized pores are connected to each other through channels, creating an intricate network that allows the motion of charges and contributes to the electric double-layer (EDL) formation. Each pore type has a different function. Micropores act as sites for ion storage and charge transfer reactions during

charge/discharge processes, with high ion accessible surface area. On the other hand, mesopores provide fast mass transport pathways and macropores can act as ion-buffer reservoirs that minimise the diffusion paths. Because of these properties, it is believed that the peanut shell electrocatalyst will have macroporous cores that act as secondary ion-buffering reservoirs, mesoporous walls that provide pathways with low resistance, and micropores that can afford the electric double layer capacitance [33], all which could lead to an improvement in the performance of a seawater battery.

Another property ascribed to peanut shell derived activated carbon is a highly functionalised surface. During the carbonisation in an inert atmosphere, the majority of oxygen and hydrogen is removed in the form of different gases. The defective carbon atoms are produced on aromatic (graphene-like) sheets while the remaining carbon atoms self-organise into a group and form aromatic sheets. Because some of these defective carbon atoms have unpaired electrons or unsaturated valences, they can interact with other heteroatoms (such as oxygen and hydrogen) to form different types of surface functional groups [7, 34]. It has been reported that an abundant amount of surface functional groups can improve the wettability and hydrophilicity of the materials [9]. These defects also result in a charge population and density enhancement, where defective carbon atoms can act as active sites for the electrochemical activity of the seawater battery. Oxygen functional groups, such as $C = O$ and $C - O$, result in excellent active sites for OER/ORR activity efficiency, providing a synergetic contribution [7].

All of these factors indicate that the application of peanut shell derived electrocatalyst coated electrodes in a seawater cell could lead to an improvement of its performance.

2.1.5.3 Application of peanut shell derived activated carbon in EES devices

To the best of our knowledge, the use of peanut shell derived electrodes in rechargeable seawater batteries is novel. Nonetheless, they have been used in other electrical energy storage systems such as supercapacitors, sodium ion batteries, lithium-ion batteries, zinc-air batteries, and others.

Peanut shell derived hard carbons were used as anodes for sodium ion batteries, achieving a Coulomb efficiency of 29% to 34%, a discharge capacity of 174 to 431 mAh g^{-1} and a current density of 100 mA g^{-1} [31]. Y. Qiao et al. [6] reported the used of peanut shell derived electrodes in zinc-air batteries, where a peak power density of 141

mW cm^{-2} and a specific capacity of 767 mAh g^{-1} was achieved and these results are better than the ones obtained when using the commercial electrocatalyst mentioned before, Pt/C. C. Zhao et al. [35] reported the use of a high performance lithium ion cathode derived from peanut shells with an initial discharge capacity of 590.6 mAh g^{-1} and Coulomb efficiency of 71.6%. M. Balasubramanian et al. [32] reported the use of a peanut shell carbon–derived electrode material for a supercapacitor with a high surface area that showed a specific capacitance of 239.88 F g^{-1}.

These are just some examples of the good capacities of peanut shell derived activated carbons applied in electrical energy storage devices, so it is expected that the use of peanut shell derived electrocatalyst coated electrodes in seawater batteries will result in good performance. Adding to this, the seawater battery's sustainability increase is also relevant and could be a first step in the research leading to the application of these cost-effective biomass activated carbon electrodes in large-scale applications.

2.2 Rechargeable sodium seawater battery

As was previously stated, sodium batteries have recently drawn large interest. The rechargeable sodium saltwater battery is one of the batteries that came out of that development effort.

The SWB uses the abundant seawater as the direct source of active material, without needing any treatment. Seawater is a natural liquid electrolyte with high ionic conductivity and salinity of 35 g L^{-1}, filled with Na^+ and Cl^- ions. A SWB is a secondary battery (i.e. can be recharged) and stores energy through the bonds of sodium (Na) via the oxidation of seawater in the cathode and the reduction of sodium ions in the anode. During discharge, the battery generates electricity from the transfer of electrons through an external circuit that connects the two electrodes, much like a regular battery, as it is illustrated in Figure 2.6.

A SWB consists of an open structured cathode with Na metal [with a potential of -2.73 V vs standard hydrogen electrode (SHE)] or Na-inserting materials as the anode creating a high-voltage electrochemical cell. Separating these two components is a sodium ion conducting membrane that only allows the passage of Na^+ to and from the anode, acting as a solid separator that prevents humidity and other ions from reaching the anode. The anode part is sealed, having only the separator exposed to seawater because the Na metal is highly reactive and being exposed to humidity would pose a great danger. Inside of

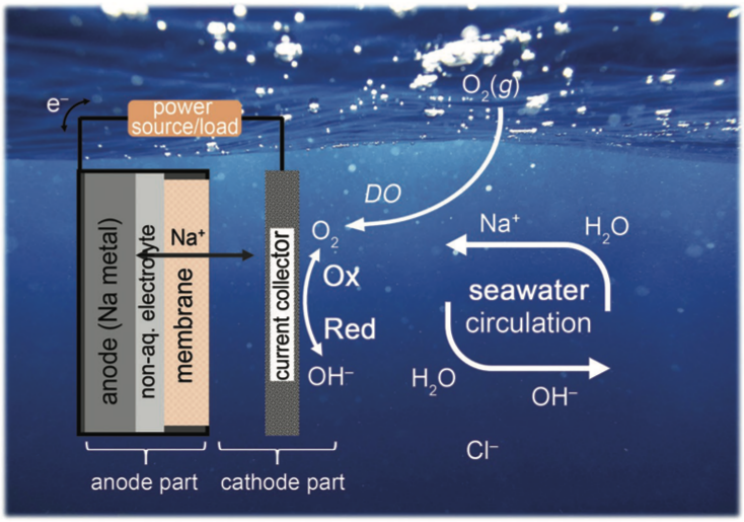

FIGURE 2.6: Scheme if a SWB cell structure and operating mechanism upon charging and discharging. Figure from reference [1]

the anode, the Na metal is attached to a current collector and immersed in a non-aqueous liquid electrolyte, used as a buffer layer between the Na metal and the solid separator to ease Na^+ transfer [1].

One of the characteristics that separates SWBs from more common batteries is their open-structured cathode configuration, which allows for a continuous supply of fresh seawater, that is the catholyte (being simultaneously the cathode and the electrolyte), during cell operation. The access to an unlimited source of working ions, with no need to store them in the electrodes, offers other perks such as cost reduction, thermal management and long cycle span. The fact that the SWB will be immersed in circulating seawater facilitates effective heat transfer from the cells, which excludes the need for internal active cooling systems. This eases the burden of thermal management and improves safety. Another benefit associated with the absence of thermal management is that the battery's size and weight are not required to be reduced to assure its safe operation. SWBs offer a significant reduction of the material and manufacturing costs, because it uses the very abundant seawater as the cathode material, needing no further materials or treatments in this side of the battery, as occurs in regular batteries [1]. Lastly, the open-structure cathode has another perk in terms of volume of the cathode current collector. Most batteries are compact, being the cathode current collector limited by the available space. In SWBs there is more than enough space to have the best cathode current collector, regardless of size.

Most renewable energies harvested from natural sources have the difficulty of supplying electrical energy directly to the consumer because this energy has an intermittent

nature and is still costly. Thus the development of large-scale and efficient EES systems is highly desirable to reduce our energetic dependence on fossil fuels [36]. In this regard, seawater batteries would be less expensive and less harmful to the environment than the existing batteries, including LIBs, making them a desirable option for low-cost, large-scale EES applications. They can be coupled with renewable energy sources, such as wind, solar or ocean energy, transforming renewable energy into usable electricity on demand, by creating an almost independent low-cost and environmentally friendly energy system. In particular, the majority of the produced marine renewable energy that is converted to electricity is either transmitted onshore through a submerged cable or immediately used on the production platform if located far offshore [37]. Rechargeable SWBs can be a good way to store energy in offshore platforms for marine renewable energy production. In the following, we will introduce the main components of a SWB.

2.2.1 Anode

The anode compartment is very important because it determines the energy density of the battery, being the place where the sodium ions will be stored during charge. Due to the open-structure cathode configuration, the cell has an almost infinite supply of Na^+, which means that the capacity of the SWB will greatly depend on the storage capability of the anode itself. The anode has two major components, the active material and the liquid non-aqueous electrolyte (Figure 2.7).

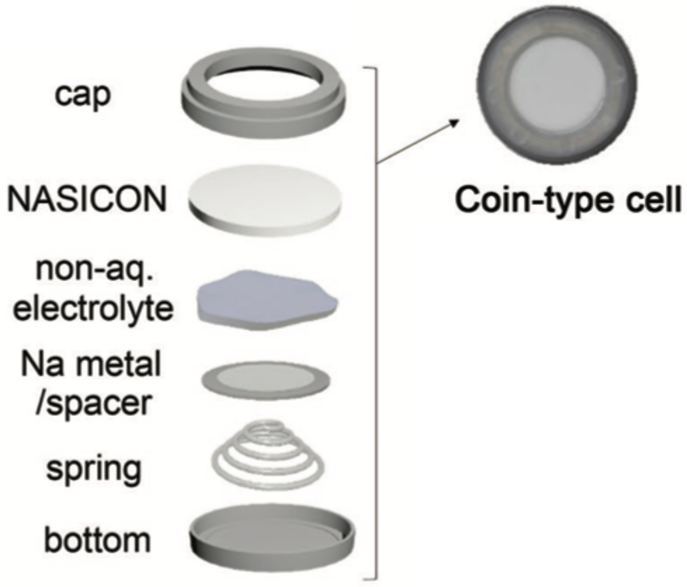

FIGURE 2.7: Parts of a seawater coin-cell. Figure from reference [1]

A SWB anode's material must have a redox potential near $E_{Na^+/Na}$, high reversible capacity, stable structural/electrochemical characteristics, and high electrical conductivity [17]. There are different anode configurations, such as sodium metal or the anode-free configuration, where a material such as hard carbon is used as the anode without any trace of active material in the beginning. In the first charge of the battery operation, active material will be deposited in the hard carbon creating a layer of sodium metal removing the need of having metallic sodium in the cell manufacturing.

As stated before, using a metal as the anode material is, theoretically, the perfect choice due to its high capacity, low electrochemical potential and fast charging times, although in reality, this configuration brings some challenges. This obviously applies to the use of sodium metal as the anode, which nevertheless was the chosen material throughout this thesis. Metallic sodium is highly reactive, being rare in its pure form in nature. It has the advantages of having very high theoretical capacity (1165 mAh $g^{-}1$) and a low electrochemical potential (- 2.73 V vs SHE), which leads to very high theoretical energy densities. The Na metal anode half-cell reaction in a convectional liquid electrolyte is given by [17]:

$$Na^+ + e^- \leftrightarrow Na, \qquad E = -2.73 \quad (vs \ \ SHE). \tag{2.5}$$

One of the disadvantages associated with the use of sodium metal is the possibility of dendrites formation and short circuits. Dendrite formation occurs during the charge process, where the deposition of Na metal takes place. This deposition is influence by an uneven distribution of current and irregular anode surface morphology. Their growth is also affected by the formation of a solid electrolyte interphase (SEI) between the liquid electrolyte and the Na metal anode. All of these factors combined can lead to a non-uniform Na^+ ion flux with preferential deposition sites where a dendrite will grow. This growth can reach such levels that the separator is pierced and cause shorts circuits. In a seawater battery, the danger of piercing the separator still exists, but, because of the open cathode structure, the cathode current collector is further away than in normal cells, minimising the risk of short circuits. Other disadvantages include low Coulomb efficiency (CE) and poor cycling performance, due to the decomposition of the liquid electrolyte during SEI layer formation, where the consumption of electrolyte and electrons leads to irreversible capacity and low CE [17].

Due to its highly reactivity, to ensure a safe operation, the reversible deposition/stripping performance of Na metal is very important. For this to happen, a stable SEI layer is needed on the surface, as well as a reversible behaviour, which can be obtained via anode components such as a non-aqueous electrolyte and the anode current collector.

During cell operation, the non-aqueous liquid electrolyte functions as ionic transport channels between the solid electrolyte and the anode and ensures the stability of the anode's electrochemical performance. They should have minimal electrical conductivity to avoid short circuits, high ionic conductivity, electrochemical stability at low voltage ranges, thermal stability, low cost and low toxicity. High ionic conductivity is very important since a rapid ion mobility results in a cell with higher power. Another important characteristic of the non-aqueous electrolyte is that it should not damage the structure of the anode material nor react with it [4].

There are many types of liquid electrolytes and all that are sodium-based can be used in SWBs. The three major categories are organic liquid electrolytes, ionic liquids, and anolytes. The liquid non-aqueous electrolyte used in this work was 1 M $NaCF_3SO_3$ in TEGDME (tetraethylene glycol dimethylether), being an organic liquid electrolyte. After being studied and compared to others, TEGDME showed an improvement of the battery life cycle and a small cell resistance which led to high charge delivery and discharge capabilities [17]. This is because 1 M $NaCF_3SO_3$ in TEGDME as the electrolyte supports the formation of a thin, efficient and stable SEI layer [4] and has a good binder stability, offering high cycle performance to the SWB.

2.2.2 NASICON solid electrolyte (separator)

The main purpose of the solid ceramic electrolyte is to protect the anode from direct contact with seawater. It only allows the passage of sodium ions and nothing else, from the cathode to the anode and vice-versa during cell operation. It is also called separator because it literally separates the two electrodes.

The separator should have properties such as high ionic conductivity for Na^+ under low temperature conditions, low electrical conductivity (i.e. insulator), high chemical stability in the presence of seawater and non-aqueous electrolytes, electrochemical stability in a wide electrochemical range, and high mechanical/physical strength [17].

According to literature, there are many solid electrolytes that have high Na^+ conductivity, but NASICON, an oxide solid electrolyte, is typically regarded as the best [4, 17].

NASICON stands for NA Super Ion CONductor and has a complex composition represented by $Na_{1+x}Zr_2P_{3-x}Si_xO_{12}$, with $0 \leq x \leq 3$. The material is formed from a solid solution of $NaZr_2P_3O_{12}$, where P is partially replaced by Si. NASICON generally forms in two phases, the rhombohedral and the monoclinic. The different phase formation depends on the composition and synthesis temperature, but both phases have 3D linked ZrO_6 octahedra sharing corners with SiO_4 and PO_4 tetrahedra and offer a three-dimensional pathway for Na^+ transportation. The feature of 3D sodium ions pathways conductivity gives NASICON other applications besides SWBs, such as CO_2 sensors [4]. The structure of NASICON´s phases and the Na^+ pathways are illustrated in Figure 2.8.

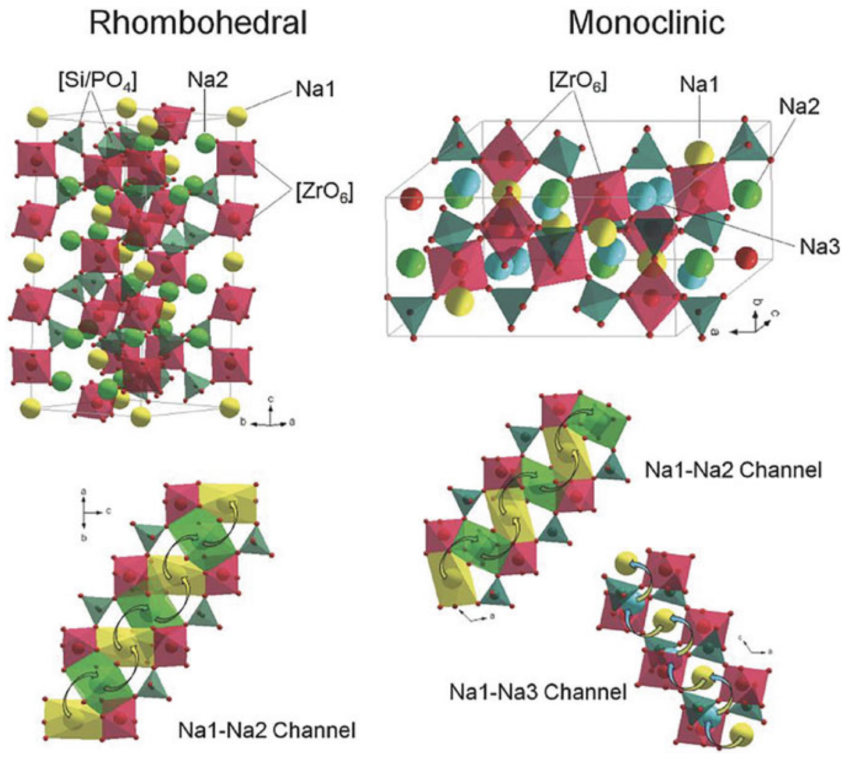

FIGURE 2.8: Crystal structures of NASICON and corresponding sodium transfer pathways. Figure from reference [17].

NASICON has high ionic conductivity for sodium ions of $10^{-5} - 10^{-3}$ S cm^{-1} at room temperature, determined using electrochemical impedance spectroscopy (EIS). The composition of NASICON with the highest ionic conductivity, measuring between $10^{-4} - 10^{-3}$ S cm^{-1}, is $Na_3Zr_2Si_2PO_{12}$, with x=2 [17]. After several improvements, the coin-type NASICON separator used was acquired from 4TOONE [38], a company based in Republic of Korea with an ionic conductivity of 0.8 mS cm^{-1} and a bulk density of 3.03 g cm^{-3} [1].

To safely store metallic sodium in the anode, the mechanic and physical strength of the separator are very important. The structure stability and electrochemical properties must be maintained during the operation of the SWB. NASICON has poor bending strength when compared to other convectional ceramics, being around 50-200 MPa, although if used carefully it is enough to fulfil the needs of a SWB. The chemical stability of NASICON in seawater was confirmed by immersing it for long periods of time. The structure and morphological analysis showed that, after a period of 60 days in seawater, NASICON maintains its structure without any impurity phases. This is the case for pristine seawater. In the case that the solution is a replication of seawater based on deionised water, the chemical stability worsened. Literature reports that the formation of hydronium (H_3O^+) NASICON phase can occur in deionised water at room temperature. The formation of this compound can occupy sites meant for sodium ions, reducing the ionic conductivity of the separator. But overall, NASICON retains its properties in a seawater environment, which is a must in a SWB [17].

2.2.3 Cathode

SWBs have an open-structure cathode configuration, which means that the only component of the cathode beside the catholyte is the cathode current collector. It must have a large surface area to provide many reaction sites, high electrical conductivity to provide electron paths, good chemical and electrochemical stability and also be cost-effective. Many fibrous carbonaceous materials have been employed in SWB, such as carbon felts, carbon papers, and carbon cloths, as they meet all these requirements. Fibrous carbonaceous materials such as carbon felts (CFs) possess sizing agents and polymers meant for mechanical reinforcement that leave the material less hydrophilic. Since the cathode current collector will be immersed in seawater, the hydrophilicity of the CF surface is an important parameter. In order to make the CF more hydrophilic, an heat treatment must be applied to evaporate the polymer and increase the surface area.

Increasing the surface area of a cathode current collector also means having more active sites available for the reactions to occur. If the surface area is increased significantly another mechanism will arise. Activated carbon felts (ACFs) are used as cathode current collector with very high surface area and high porosity, for this purpose. This type of cathode induces a behaviour similar to an Electrical Double-Layer Capacitor (EDLC). It is a type of capacitor with very high surface area electrodes with an electric double layer

(EDL) between the electrodes and the electrolyte. In general, when there is accumulation of charges at the junction of two materials, an EDL forms in the interface at an atomic distance. The two layers are near each other, increasing the surface area and decreasing the distance between electrodes, enabling EDLC to attain high capacitance. The charge that is accumulated in a capacitor begins to be competitive with that generated in a battery, where the electrode breaks down, by faradaic reactions. An illustration of a EDLC without voltage applied, charging and then discharging can be seen in Figure 2.9.

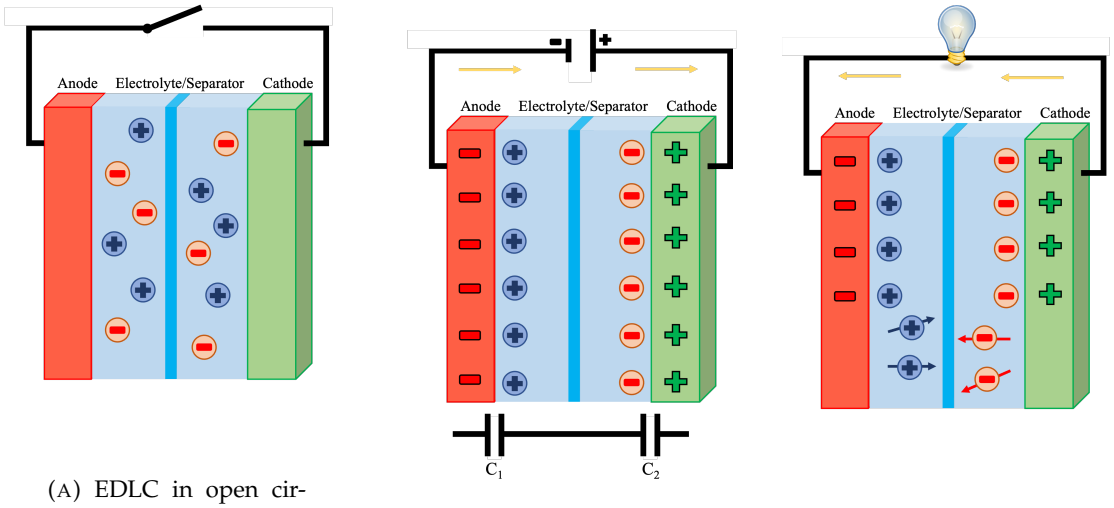

(A) EDLC in open circuit.

(B) EDLC charging.

(C) EDLC discharging

FIGURE 2.9: Typical EDLC and representation of EDL formation.

Without voltage applied, there are positive and negative charged particles distributed randomly through the electrolyte. The charged electrodes will attract the charged particles present in the electrolyte with the opposite charge. The alignment of positive and negative charges in the interface between the electrodes and the electrolyte corresponds to the formation of the electric double-layer and is the responsible for the storage of electrical charge. There are two EDLCs formed that are equivalent to two capacitors connected in series, which results in one equivalent capacitor. The capacitance of a capacitor follows:

$$C = \frac{\epsilon_0 \epsilon_r a}{d}, \tag{2.6}$$

where C is the capacitance, ϵ_0 and ϵ_r are the absolute permittivity for air and the dielectric medium, respectively, a is the area of the electrodes and d is the distance between electrodes. With Equation 2.6 we can see that if the electrodes have a large surface area and a small distance between them, the capacitance is higher. The choice of materials

employed greatly influences the performance of the device. Activated carbon material is common choice for electrodes having low density and being fabricated with a big exposed surface area [3].

This increase in capacitance can also be used in rechargeable batteries, improving its performance. We can achieve it by using a battery-type electrode as the anode and a supercapacitor-type electrode as the cathode. This is only possible if the cathode is immersed in an electrolyte, which is the case for rechargeable seawater batteries [39]. With a normal cathode current collector the main mechanism at work is the electrochemical activity of OER/ORR, which has very slow kinetics and leads to low voltage efficiency, high voltage gaps and a high activation polarisation effect, having a quick plateau formation. The OER/ORR reactions are described in the next section. The charge transport via EDL is much faster than the OER/ORR reactions and other faradaic process. SWBs with ACFs are capable of storing ions via EDL formation. While one electrode is storing ions on the surface, EDL, the other electrode (i.e. battery-type) is storing charges via redox or faradaic reactions, through intercalation/deintercalation or conversion. Capacitive cathodes increase the overall capacity and voltage efficiency, and reduce the voltage gap and the activation polarisation effect. The improvements stated can be observed in Figure 2.10, where two cycles are compared between a normal CF and an ACF.

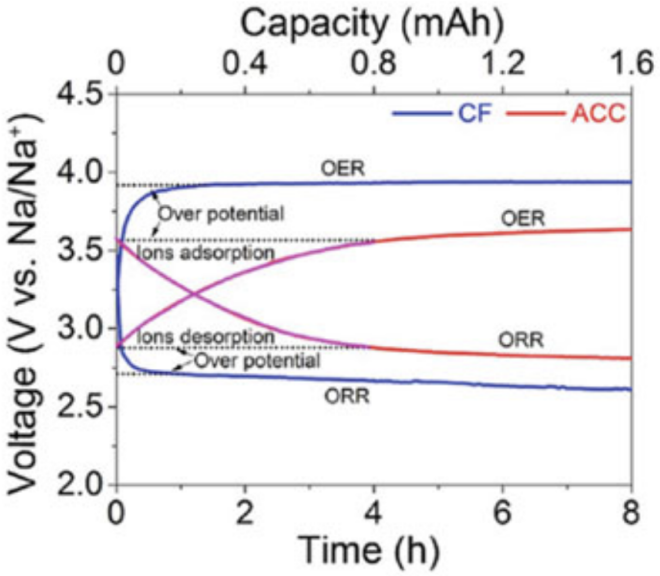

FIGURE 2.10: Comparison between CF and ACF. Figure from reference [39].

Another way to improve SWB performance by altering the cathode current collector is by adding electrocatalysts, which was further explored in section 2.1.5.

2.2.4 Seawater battery working principle

The working principle of a SWB is based on the redox reactions of the active material. The major difference between a common battery and a SWB is the fact that it is not done in a closed system. The seawater in a SWB has the role of supplying sodium ions but also to replace the reaction products that will be carried away, maintaining a constant concentration of reactants. The anode of a SWB uses sodium as the active material while the cathode uses dissolved oxygen (DO).

The ions with the higher concentration in seawater are Na^+ and Cl^-, appearing together in the form of sodium chloride, NaCl. The oxygen evolution/reduction reaction (OER/ORR) is thermodynamically preferred over the chlorine evolution/reduction reaction (ClER/ClRR). However, the proportion of the two reactions depends on the operating conditions close to the cathode current collector [40]. Considering the oxygen partial pressure at 100% from ambient air, the reactions OER/ORR will be preferential. In other words, the OER/ORR will be preferred if the amount of dissolved oxygen present near the SWB is large.

Assuming a typical concentration of Na+ ions in seawater, the half-cells reactions of the OER/ORR and (ClER/ClRR) activity, the redox reaction of the sodium ion and the overall reaction that characterises the operation of a seawater battery are, respectively [1]:

$$DO(aq) + 2H_2O + 4e^- \leftrightarrow 4OH^-, \qquad e^0 = 0.75 \;\; V \quad (vs \;\; SHE), \tag{2.7}$$

$$OCl^-(aq) + H_2O + 2e^- \leftrightarrow Cl^-(aq) + 2OH^-, \qquad e^0 = 1.24 \;\; V \quad (vs \;\; SHE), \tag{2.8}$$

$$Na^+ + e^- \leftrightarrow Na, \qquad e^0 = -2.73 \;\; V \quad (vs \;\; SHE) \tag{2.9}$$

and

$$4Na(s) + DO(aq) + 2H_2O \underset{\text{discharge}}{\overset{\text{charge}}{\rightleftharpoons}} NaOH(aq), \;\; E^0 = 3.48 \;\; V \;\; (vs \;\; Na^+/Na). \tag{2.10}$$

During the charging process, the generation of sodium ions and electrons takes place. Potential difference is applied to the electrodes, inducing the migration of the produced electrons from the cathode to the anode through an external circuit and Na^+ to travel to

the anode via the NASICON and the liquid electrolyte. When both species meet, they will be reduced, leading to the deposition of sodium metal. The non-aqueous liquid electrolyte ensures that the deposition/stripping of the Na metal is a stable and reversible process. The oxidation of both DO and Cl can happen at the cathode, but they result in slightly different formation voltages. As stated before, the OER/ORR is thermodynamically preferred when compared to the evolution of Cl_2 because ideally the amount of DO is larger than that of Cl_2 and the potential is lower for OER/ORR so it is expected that the obtained voltages in the charging process (Figure 2.11a) will be $\sim$ 3.48 V [1, 41].

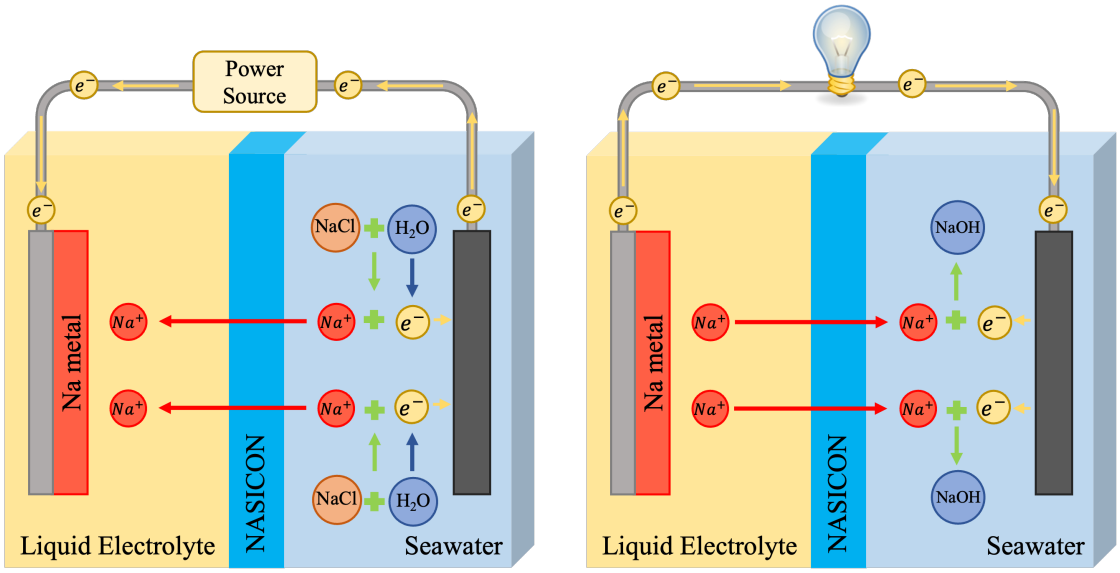

(A) Charging process of a SWB cell.

(B) Discharging process of a SWB cell.

FIGURE 2.11: Scheme of a SWB cell operation.

When the SWB starts to discharge (Figure 2.11b), similar processes occur but in opposite directions. The device that is being loaded by the SWB induces the migration of electrons from the anode to the cathode, creating the current that charges it. For this to happen, the sodium metal is oxidised producing Na^+ and electrons. Both species travel the same paths as in the charge process, but in opposite directions meeting again in the cathode, where they are reduced into sodium hydroxide (NaOH). The products of all the reactions happening at the cathode will be taken away by seawater, replacing them with new reactants allowing for another charging process to take place.

2.3 Seawater as a natural resource

Due to the importance of the composition and properties of seawater to SWBs, a brief introduction of its characteristics will be done. There has been proof of the existence of more than 5000 planets outside of our solar system, but, to the best of our knowledge, Earth remains unique [42]. The presence of water in its liquid state is made possible by this nearly ideal distance to the sun. Earth is a water-rich planet, making up roughly 71% of its surface. Water can be divided into two types: fresh water and seawater, depending on the amount of salt present. The bulk (97.5%) of the water on Earth is seawater, with fresh water making up only about 2.5% of the total volume (Figure 2.12). Just 1% of the available fresh water can be used by humans, so it is clear that seawater is a significant resource at our disposal if handled properly [43].

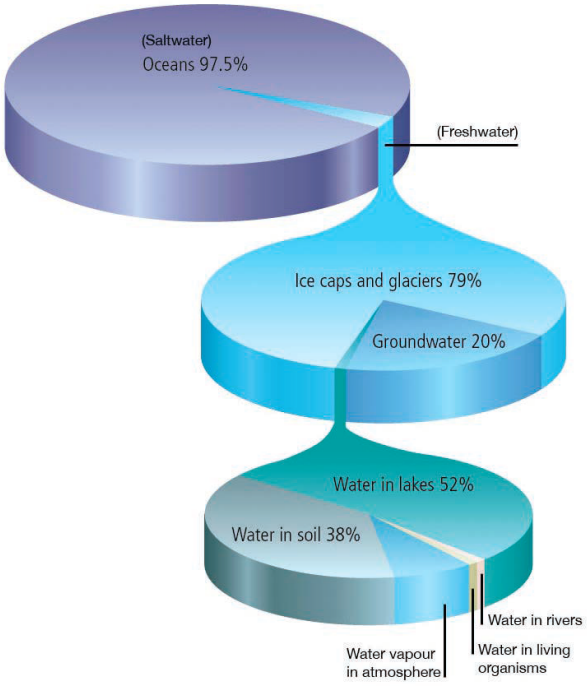

FIGURE 2.12: Global water distribution. Figure from reference [43].

2.3.1 Components of seawater

The majority of the aqueous solution that makes up seawater is sodium chloride (NaCl). Water with salinity of 0.05% or less is considered to be freshwater. Seawater is a combination of water (around 96.5%) and salt, whose concentration varies from 3.3 to 3.7%, which means that seawater contains 70 times more salt than the ordinary freshwater. Salinity is

the salt content in seawater and is denoted by the symbol S, which represents the mass unit gram of the dried salt residue contained in 1 kg of seawater. The physical and chemical properties of seawater are determined by its density, temperature and electrical properties, meaning that seawater's salinity can be estimated by its temperature and electrical conductivity.

Even though, the seawater's salinity may vary, the proportion of its main elements has a rather constant value. This can be explained because the speed of dissolution in water that maintains the inorganic salt composition is faster than the speed of changing seawater's salinity. The salt responsible for the seawater's salinity is comprised of dissolved ions, being the main cations Sodium (Na^+), Magnesium (Mg^{2+}), Calcium (Ca^{2+}), Potassium (K^+) and Strontium (Sr^{2+}) ions. The main anions are Chloride (Cl^-), Sulphate (SO_4^{2-}), Bicarbonate (HCO_3^-), Bromide (Br^-), Borate (BO_3^{2-}) and Fluoride (F^-) ions. The percentage of each ion in a sample of seawater and their concentrations are listed in Table 2.2 [44], where we see that sodium and chloride ions are the dominant components in seawater, comprising about 85% of all salt content.

Ions	Percentage in a salt sample (%)	Concentration (ppm) g/kg
Cl^-	55.0	19.345
Na^+	30.6	10.752
SO_4^{2-}	7.6	2.701
Mg^{2+}	3.7	1.195
Ca^{2+}	1.2	0.416
K^+	1.1	0.390
HCO_3^-	0.4	0.145
Br^-	0.2	0.066
BO_3^{2-}	0.08	0.027
Sr^{2+}	0.04	0.013
F^-	0.003	0.001

TABLE 2.2: Composition of dissolved ions in standard seawater [44].

2.3.2 Physical properties of seawater

Seawater is similar to fresh water in terms of physical properties because is an aqueous solution, differing only in its salinity. Some of the main physical characteristics of water in general are the temperature distribution, density, acoustics, pressure and optics.

Density is a physical property of a substance ascribed to the amount of mass per unit of volume, such as grams per cubic meter (kg m^{-3}). Overall, salt ions are heavier than water molecules making seawater denser than freshwater, ranging from 1024 to 1030 kg m^{-3}, whereas for freshwater is 1000 kg m^{-3} at 20ºC. Reduced temperature, increased salinity, or higher pressure can all increase density, with temperature having the biggest impact [45].

2.3.3 Chemical properties of seawater

As an aqueous solution, seawater is characterised by different chemical features such as pH, ionic conductivity and dissolved gases in seawater. Some of these properties will be discussed in detail hereafter.

2.3.3.1 pH

Potential of hydrogen (pH) is a scale used to state the acidity and basicity of an aqueous solution [44], being associated to the relative activity of hydrogen ions in a solution [46]. A high concentration of H^+ leads to a low pH and acidic condition, while a low concentration of H^+ leads to a high pH and basic condition [45]. The pH scale ranges from 0 (indicating a very strong acid) to 14 (indicating highly basic conditions) [45]. Typically, the pH of seawater ranges from 7.5 to 8.5, being usually around 8.1, which is somewhat more basic than freshwater that is neutral (pH $\approx$ 7), due to the presence of ions, especially carbonate ones, that can influence the pH of water. Among the existing dissolved gases in water, carbon dioxide and other carbon compounds play an important role in buffering the pH of the ocean [45].

2.3.3.2 Ionic conductivity

Ionic conductivity is the electrical conductivity that arises from the motion of electrons. Electrical conductivity is the reciprocal quantity of electrical resistivity and measures a material's ability to conduct electrical current [47]. When addressing the oceans, it is a

fundamental parameter in the electrodynamics of the Earth system because it influences electrodynamic processes and the observable electromagnetic fields within the oceans but also throughout the rest of the planet, extending from the interior to the upper atmosphere [48].

The electrical conductivity of seawater depends on factors such as temperature, salinity and pressure. The mobility of ions is correlated with the temperature of their environment, so the conductivity increases with higher temperatures.

The dissolved ions responsible for the seawater's salinity migrate in the presence of an electric field producing an electrical current, therefore the conductivity increases with the concentration of dissolved ions present. Seawater conductivity has also been widely used to measure and study its salinity [49], indicating the amount of salt, ions or impurities present in a sample, so the purer the water the lower the conductivity [47]. At a constant temperature of 25 °C, Table 2.3 shows the values of resistivity and conductivity for various types of water. We can see that seawater has a ionic conductivity much higher than the other kinds of water mentioned due to its high dissolved ions concentration, such as Na^+ and Cl^-.

Types of water	Resistivity ($\omega \cdot cm$)	Conductivity ($\mu S \cdot cm^-1$)
Pure	20000000	0.05
Distilled	500000	2
Rain	20000	50
Tap	1000-5000	200-1000
River (typical)	2500	400
River (Brackish)	200	5000
Seawater (shore)	30	33000
Seawater (off shore)	20-25	40000-50000

TABLE 2.3: Resistivity and conductivity of various types of water [47].

This indicates that seawater, as an electrolyte, has a lower equivalent series resistance (ESR) than freshwater [44]. ESR represents the loss of useful energy in an electronic circuit consisting of a resistor and an ideal capacitor.

Seawater can therefore be utilised in electrochemical cells and water electrolysis because it can function as a good ionic conductor electrolyte. Nonetheless, one should keep

in mind that temperature and salinity are the key determinants of seawater's conductivity.

2.3.3.3 Dissolved gases in seawater

In seawater, there are other substances dissolved besides ions such as a variety of gases like nitrogen (N_2), oxygen (O_2) and carbon dioxide (CO_2), that are vital to living organisms. They can be found in the atmosphere and can enter the ocean by dissolving into its surface, occurring an exchange between the oceans and the atmosphere that is kept in equilibrium. The process of dissolving the gases at the surface is facilitated by the stirring of the surface water layer due to the wind and the waves [44]. Even so, the amount of each gas in the ocean is very different from the amount in the surrounding atmosphere, as Table 2.4 shows [45].

Gas	Air	Ocean	
		Total	Surface
N2	78%	11%	48%
O2	21%	6%	36%
CO2	0.04%	83%	15%

TABLE 2.4: Percentages of total gases in each place [45].

The solubility and saturation of each gas in water determine the amount of each gas that can be dissolved in the ocean. A gas becomes more soluble with higher pressures, lower temperatures, and lower salinity. The ocean is saturated with the majority of atmospheric gases, except O_2 and CO_2 because they are quickly used by living organisms [45].

The percentage of dissolved oxygen plays a vital role in the operation of a seawater battery and it is particularly important for its performance. At the surface is where oxygen content is the highest because it is where the atmospheric oxygen is dissolved and it is also where some living organisms produce oxygen through photosynthesis. Even with these two mechanisms, there is still far less oxygen dissolved than in the air surrounding. With increasing depth, the dissolved oxygen content decreases a lot because the two mechanisms mentioned before can no longer operate. At higher depth, the water is too far away from the atmosphere to exchange oxygen and the lack of natural light makes the

production of oxygen through photosynthesis negligible, so there is little or any oxygen added to the water far away from the surface.

This behaviour is only seen until the oxygen minimum layer is reached. This layer is located a few 1000 m below the surface. At depths greater than this layer there is often an increase in dissolved oxygen levels. As said before, there is an increase in solubility at lower temperatures and higher pressure and these are the conditions in which the deep water bellow this layer is. This is one of the reasons that explain the increase in oxygen content in deep waters, being the other to do with the way water circulates throughout the deep ocean. The ocean surface absorbs a lot more oxygen in cooler climates due to the exothermic nature of the solvation process by which the gas is dissolved [44]. Due to its high density, this oxygen-rich water sinks to the ocean floor where it will spend the next thousand years spreading throughout the oceans as it moves over the seafloor. This deep-water circulation is the primary source of oxygen for deep marine life [45]. The oxygen richest zones are the best places to have a working seawater battery, being at the surface or in deep ocean, where some primary batteries are located.

2.4 Applications

SWBs are suitable as main or auxiliary power sources for a wide range of maritime sectors and typical energy storage applications because of their unique characteristic of being charged and discharged using natural seawater as the active material. The scope of possible applications can be divided in three categories, being small ($<$1 kWh), medium (1-10 kWh) and large ($>$1 MWh) scales. Examples of small scale are life jackets integrated with GPS and light buoys, where SWBs would store energy generated by solar power. As for medium scale, SWBs could function as a provider of electric power for small autonomous machines, such as exploration robots and drones, and also as an auxiliary power source for boats and other water vessels. Lastly, it is expected that SWBs will act as large-scale, stationary EES systems with energy capacities above 1 MWh, storing electrical energy produced by renewable power plants, such as solar panels and wind turbines, installed near the ocean, acting as independent energy systems [1].

Seawater have also been coupled with important technologies such as energy production and desalination. Waves and tides are produced by the movement of seawater in seas/oceans. While tides are produced by the gravitational forces of the Earth and its interaction with the Moon and Sun, waves are created by the action of winds on the

sea's surface. This movement allows the generation of power, so wave and tidal energy technologies have been developed and commercialised over the years. These technologies are considered as renewable and green energy sources, similar to wind and solar power technologies, because there is no greenhouse gases emission (such as CO_2). In addition, a number of other renewable energy technologies have been studied and used in many coastal regions, including marine current energy, ocean thermal energy, and salinity gradient energy. The ocean thermal gradient can also be used for desalination, cooling and aquaculture, besides the production of electricity [44]. All of these possible ways to produce energy can be coupled with a seawater battery to store said energy, as they are located in a marine environment.

The availability of freshwater is rapidly decreasing worldwide, having some drier areas in the globe already experiencing severe droughts. Hence, it is becoming more urgent to find alternative sources of drinkable water, such as our huge bodies of salt water. The desalination of seawater is a possible solution to this problem, being the technologies of reverse osmosis (RO) and thermal desalination well established and commercialised. Other technologies such as capacitive deionisation (CDI) or electrodialysis, have also been targets of considerable attention, although being still in an earlier development stage [44]. The integration of a seawater battery with a desalination system as already been reported [50].

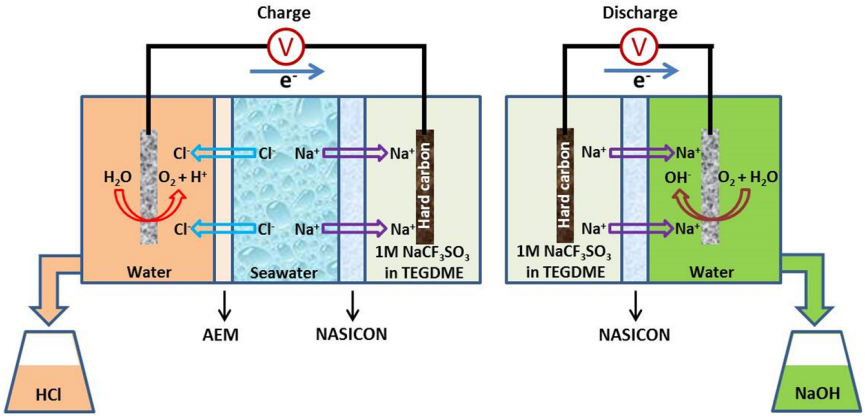

FIGURE 2.13: Schematic of the desalination seawater battery integrated system. Figure from reference [50].

The system shown in Figure 2.13 comprises of a charging and a discharging part. During the charging process, the seawater's Na^+ ions are removed and delivered into the anode side through the NASICON separator, where they are subsequently stored, and

the water's Cl ions are extracted and brought into the cathode side through the anion exchange membrane (AEM), where they are combined with H^+ ions. Na^+ ions held in the hard carbon are transferred to the cathode side during discharge via the NASICON separator, where they combine with OH^- ions forming NaOH. With this system, the design integrates the electrochemical battery, seawater desalination, and acid-alkali production in one system. This work offers a promising technology for the utilisation of natural seawater resources [50].

Chapter 3

Experimental procedures and characterisation techniques

3.1 Experimental procedures and materials

3.1.1 Materials

3.1.1.1 SWB anode compartment

The anode compartment is the coin-cell, that is composed by a bottom, a spring, a spacer with Na metal (with 99.9% purity), a liquid electrolyte that is 1 M NaCF3SO3 in TEGDME (tetraethylene glycol dimethylether), a solid electrolyte that is NASICON, and lastly a cap. All of this components are illustrated in Figure 3.1.

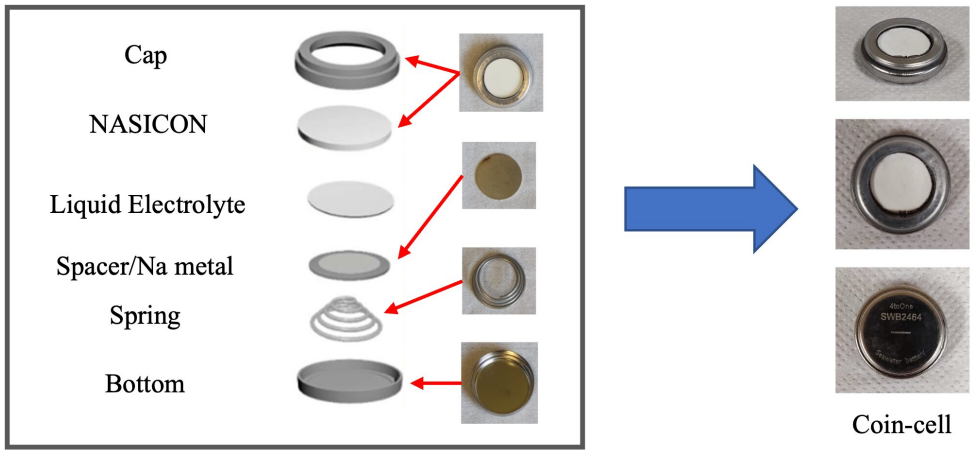

FIGURE 3.1: Constitution of a coin-cell.

The coin-cells and its parts were purchase from a company based in Republic of Korea named 4TOONE [38]. Na metal is isolated from seawater through the NASICON separator, being the only part exposed to do the selective transfer of Na^+ ions between the two electrodes. The NASICON has a round shape with 16 mm for easier manufacturing and more durability. The bottom and cap are made from stainless steel, also with a round shape. The cap was coated with polypropylene to prevent direct electronic contact with the bottom and to protect it from rust caused by seawater. The cap and NASICON are attached using an epoxy glue, that is stable in seawater and in the liquid electrolyte. The assembly process of the coin-cell must be carried out inside a glove box with an Ar environment of high purity (oxygen and water < 1.0 ppm), because of the high reactivity associated with sodium metal. A specially designed pressing machine is needed to seal the coin-cell that only applies pressure on the edges of the cap to ensure that mechanical pressure does not damage the ceramic separator (NASICON) [17, 40]. The anodes used in this thesis were assembled in 4TOONE and we currently have the equipment to assemble them in Portugal.

3.1.1.2 Cathode compartment

The cathode side consists of the catholyte (seawater), a cathode current collector and a titanium string, illustrated in Figure 3.2. The catholyte was synthesised to mimic the composition of natural seawater where the salt concentration is considered to be 0.6 M of NaCl [51]. This was done by dissolving 35 g of commercial marine salt in a litre of water, achieving a concentration of 35 g L^{-1}.

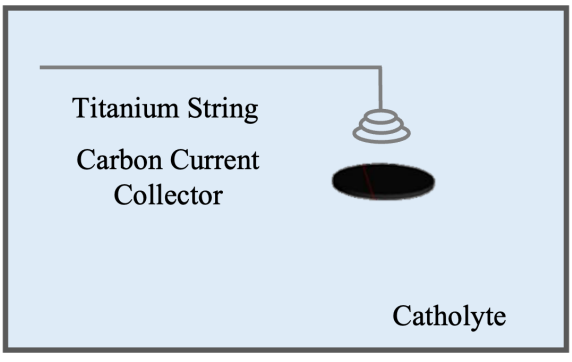

FIGURE 3.2: Constitution of the cathode compartment.

The cathode current collector must have good electronic conductivity, good chemical and electrochemical stability, a large surface area and be cost-effective. Two types of carbon felts that fulfil these requirements were employed, a commercial carbon felt and a

activated carbon felt, whose characterisation will be done in Section 3.1.2.

Commercial carbon felts (CCF) have been extensively used in fuel cells and redox flow batteries [40]. The commercial carbon felt used was purchased from Alfa Aesar [52] and can be seen in Figure 3.3 (A and B). It was processed at a temperature of 1400ºC and has a thickness of 1.90 mm, a surface area of 0.6 m^2 g^{-1} and was cut in a round shape with a diameter of 1.5 cm. CCFs possess sizing agents for mechanical reinforcement which reduce the surface area and decrease the wettability of the surface. To improve this, a heat treatment was applied to the CCF to make the cathode more hydrophilic and with more surface area accessible. The heat treatment was performed with a tubular furnace (Figure 3.3 (C)) for 2 hours at 500ºC (with ramping rate of 4.2 ºC min^{-1}), where the sample was placed inside a quartz tube.

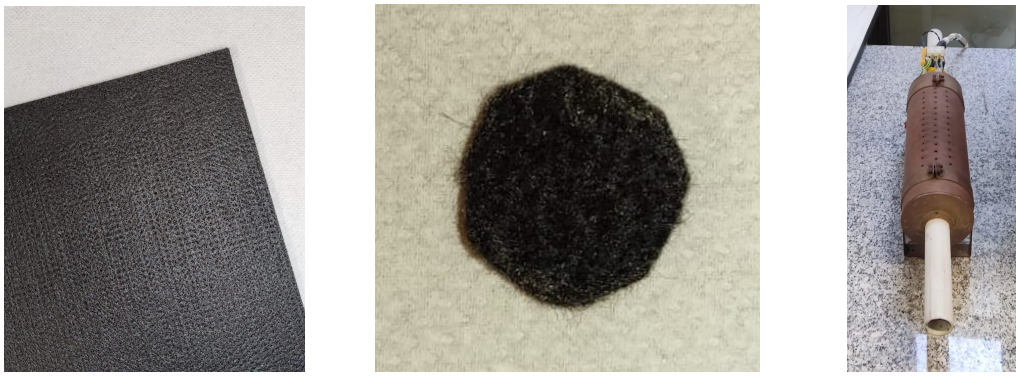

(A) (B) (C)

FIGURE 3.3: Commercial carbon felt (A and B) and the tubular furnace (C) for the heat treatment.

3.1.2 Activated carbon felt synthesis

Commercially available activated carbon felts are commonly produce from carbon fibres with a thermal treatment in a oxidant atmosphere at temperatures between 700 and 1000 ºC, whose surface is organised and with uniformly distributed fibres as shown in Figure 3.4 [53].

The activated carbon fibres are widely used as absorbents because of their defined pore structure surface that provide high and fast absorption capacity. However, due to their high brittleness and lack of mechanical resilience, they cannot be used in commonly employed textile processes. Consequently, it is difficult to transform activated carbon fibres in activated carbon felts, in their textile form. Jossano Macuzzo's team from Faculty of Technology of São Paulo (IFIMUP collaboration team) developed the utilised activated

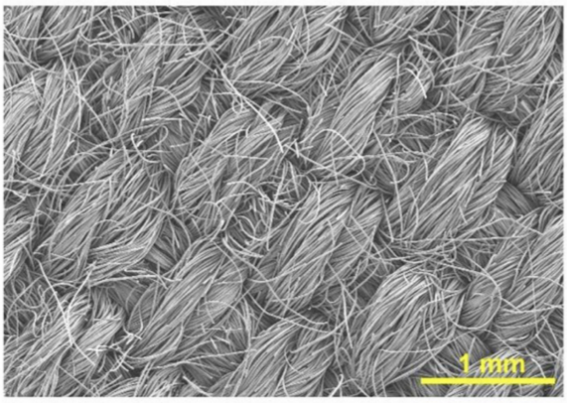

FIGURE 3.4: SEM image of a regular commercial activated carbon felt. Figure from reference [39].

carbon felt. The production of this ACF uses commercially available textile PAN fibres that are oxidised and then transformed into oxidised PAN fibre felt, before the activation process [53].

The process performed by Jossano Macuzzo team starts with the oxidation of textile PAN fibres in a laboratory scale oven and then it was transformed in felt. The next step was the carbonisation done in an electrical furnace with an inert atmosphere of pure argon and a final temperature of 900 ºC (with ramping rate of 30 ºC min^{-1}), where the oxidised PAN lost about half of their mass. Right after, the activation process starts by changing the argon inert atmosphere to carbon dioxide and increasing the temperature to 1000 ºC for 50 minutes. At the end, the inert atmosphere with argon was used again and the furnace was turned off and cooled off to room temperature. The activated carbon felts achieved a relatively high surface specific area of 1.300 m^2 g^{-1} [53] with a thickness of 0.72 mm. In the electrochemical tests, three layers of activated carbon felt were used to achieve a thickness similar to CCF and HCCF, and also ensure electrical contact.

This method of producing ACF solves the difficulty of transforming activated carbon fibres in felts because this transformation is done prior to the carbonisation and activation processes. Another advantage is the fact that this procedure skips some steps of the manufacturing process of commercially available activated carbon felt in terms of surface organisation and fibre distribution, with advantages for the process carbon footprint. The fact that these ACFs have non-uniform fibre distribution is an advantage to their application in SWB because it increases the porosity, surface area and fibre density of the carbon felt when compared to the commercial ones (Figure 3.4). The utilised activated carbon felt is shown in Figure 3.5, where the ACF cathode current collector has a diameter of 1.5 mm.

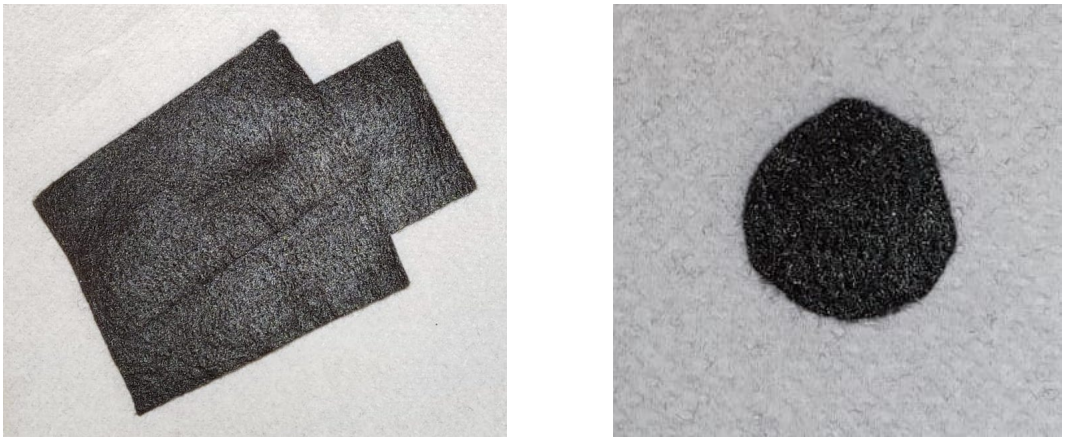

FIGURE 3.5: Activated carbon felt produced by Jossano Macuzzo team.

3.1.3 Peanut shell coated carbon felt synthesis

In the long run, sustainable biomass can supplement or even replace conventional carbon precursors in the making of next-generation electrode materials [34]. The sustainability of the seawater battery is a very important parameter to have in consideration, if large scales are to be considered. To this end, the goal was to develop an electrocatalyst that improved the performance of a SWB and was made from a waste biomass. Biomass has been considered a suitable precursor for creating activated carbons because it is an abundant, green, and renewable source of carbon with a natural biological structure for the development of porous nanostructures. The raw biomass precursor and the activation process influences the microstructure and chemical properties of the activated carbon [9]. Peanut shells are a good raw biomass precursor because of their high carbon content and natural multichannel skeleton that provides an intricate net of connected channels which can improve the performance of a seawater battery.

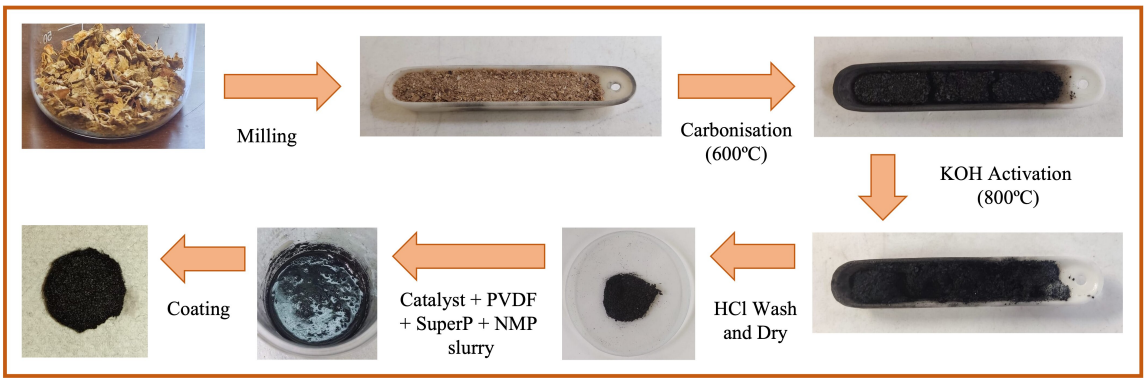

FIGURE 3.6: Schematic of the peanut shell electrode synthesis.

The peanut shell electrocatalyst synthesis is schematised in Figure 3.6 and started with the crushing of the peanut shells with a blender. Around 5g of crushed peanut shells were washed with deionised water and filtered with a funnel and a filter paper. This process was repeated three times and it is an important part because ensures that any residual pesticides or other elements used in the treatment of commercial peanuts are removed. The washed product was then dried in a heating chamber for 24 hours at 105 ºC.

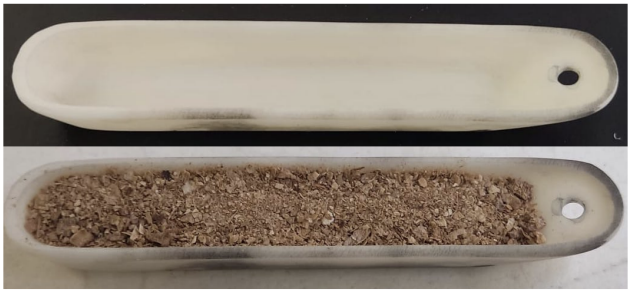

FIGURE 3.7: Ceramic boat empty and full of washed and filtered peanut shells.

The next phase is the carbonisation of the peanut shells. It starts by placing the crushed and washed peanut shells (PS) in a ceramic boat (Figure 3.7). The PS mass before carbonisation was 1.4466 g. The carbonisation was done using a furnace with argon inert atmosphere (Figure 3.8). The ceramic boat was placed inside a quartz tube that was then put inside the furnace with the PS in the middle of the chamber. The PS were carbonised for 3 hours at 600ºC (with ramping rate of 5 ºC min^{-1}) with an inert atmosphere of argon. The argon flow had a pressure of 2 mbar and was controlled by a flow meter at around 140 mL min^{-1}. The carbonised peanut shells (CPS) had a mass of 0.3372 g, having lost about 77% of the initial mass (Figure 3.9 A).

The next step is the activation of the CPS, where firstly the CPS is crushed again using a mortar and pestle reducing it to dust. Potassium hydroxide (KOH) activation has been extensively used to modify pore properties, increase surface area, and introduce functional groups as a means to produce biomass-derived carbon composites with improved features for energy storage [34]. So, we used KOH in the activation process because is the activating agent that presents good electrochemical, a three-dimensional porous hierarchical structure with a high surface area, good micro-mesopore ratio and a relatively high degree of graphitization [9]. The CPS were mixed with KOH with a mass ratio of 1:4, being used 1.3574 g of KOH. They were mixed together and a few drops of deionised water were added to ensure uniformity and sufficient mixing. The mixture was transferred to the ceramic boat and was dried for 30 minutes at 80ºC in a heating chamber before going

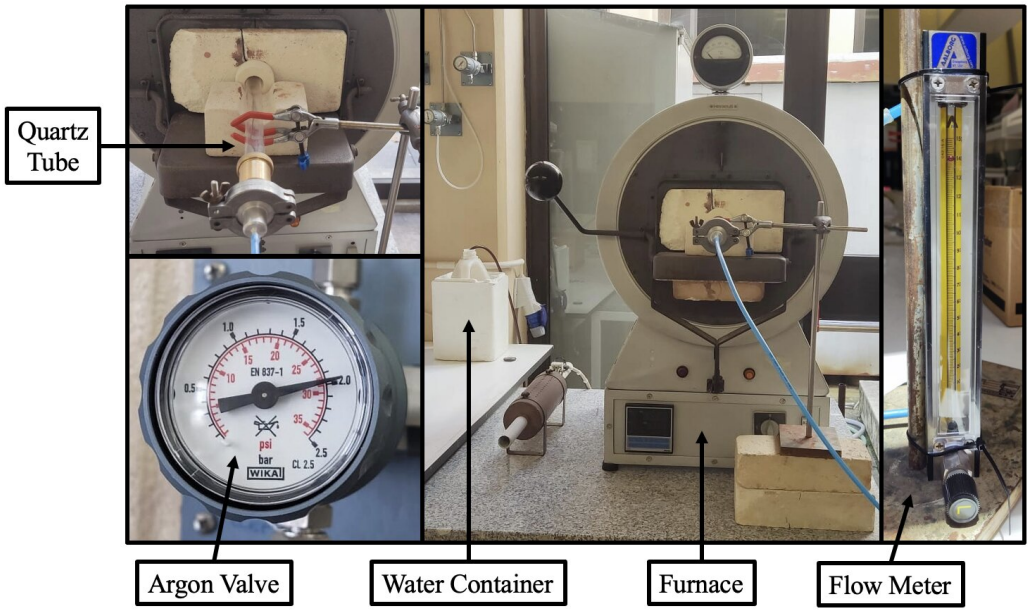

FIGURE 3.8: Furnace used in carbonisation and activation and its components.

inside the furnace once again. The CPS were activated for 2 hours at 800ºC (with ramping rate of 4.7 ºC min^{-1}) with an inert atmosphere of argon. The argon flow had a pressure of 2 mbar and was controlled by a flow meter at around 140 mL min^{-1}.

FIGURE 3.9: Ceramic boat with carbonised PS (A) and with activated PS (B).

The activated and carbonised peanut shells (ACPS) (Figure 3.9 B) were crushed again and transferred to a goblet. The ACPS were dispersed in a 1M HCl solution of 200 mL to remove the residual chemicals. The HCl (hydrogen chloride) used had a concentration of 37%, so 16.4 mL was used and added to the goblet with the ACPS and then filled with deionised water making the 200 mL solution. The dispersed ACPS was stirred with a magnetic hot plate for 2 hours at 60 ºC. At the end, the solution was filtered to remove the HCl and then rinsed with deionised water and filtered twice. The final biochar of ACPS was obtained after it was dried overnight at 105 ºC in a heating chamber, and then it was

scrapped from the filter paper with a spatula (Figure 3.10). The activated and carbonised peanut shell carbon weighed 0.2165 g, having lost 85% of the total initial mass.

FIGURE 3.10: Final peanut shell biochar.

The final step was the coating of the peanut shell electrocatalyst. The chosen substrate was the heated commercial carbon felt (HCCF) because from the carbon felts available was the one with more abundance and that was promising. The coating consists of 80wt% peanut shell catalyst (ACPS), 10wt% carbon black SuperP, 10wt% of poly (vinylidene) fluoride (PVDF) and the solvent N-methyl-2-pyrrolidone (NMP). PVDF is a binder that is naturally an insulator, being this the reason for the addition of SuperP, that is a conductive agent, in the same amount. The amounts of the slurry components were varied and two sets of concentrations were tested. Both had the same amount of catalyst (80wt%), but on the first set the amount of PVDF and carbon black SuperP were doubled (20wt% each), and on the second set they were tripled (30wt% each). The PVDF and carbon black SuperP quantities were always maintained equal to ensure that the insulating nature of PVDF was compensated by the high conductivity of carbon black SuperP. After the obtained electrodes were tested, the concentrations that showed better results were 10wt% of PVDF and carbon black SuperP, so this was the concentrations used throughout the rest of the work. Firstly, 0.0287 g of PVDF and 2 mL of NMP were mixed until homogeneity was achieved. Only then, 0.2165g of ACPS and 0.0282 of SuperP were added and mixed together [7]. After sufficient mixing, a black slurry like it is seen in Figure 3.11a was obtained.

The slurry was coated onto the surface of a preheated HCCF using a spatula and then 2 drops of NMP were added to each peanut shell coated carbon felt (PSCF) to homogenise the coating even further. Finally, the coated electrode was dried in a heating chamber at 80 ºC overnight. With the presented amounts of materials, there was enough slurry

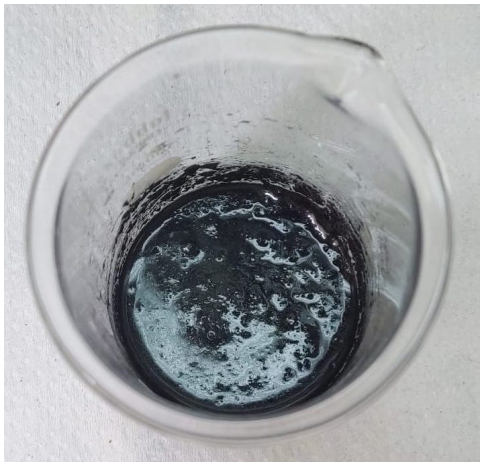

(A) Black slurry of the electrocatalyst coating.

(B) Peanut shell coated carbon felt.

FIGURE 3.11: Peanut shell electrocatalyst coating and a finalised peanut shell coated carbon felt.

to coat three HCCFs. The HCCF before coating had a mass of 0.0375 g and with the coating the mass increased to 0.0687 g, almost doubling it. The thickness also increased 38%, becoming 2.62 mm. Figure 3.11b shows a picture of a finalised peanut shell coated cathode current collector.

3.1.4 Experimental apparatus

The anode and cathode compartment are joined together in a testing setup (Figure 3.12 A and B) also bought in 4TOONE [38]. It is made of polycarbonate because it prevents seawater corrosion [40]. The cathode current collector is immersed in the seawater that is placed in the tank and the coin-cell is blocked from seawater, having the NASICON in direct contact with the carbon current collector. A screw and titanium string are connected to the coin-cell and the cathode current collector, respectively, and function as conductive wires. The potentiostat is connected to these wires allowing for electrochemical tests to be performed to the seawater cell, and it was purchased from Gamry Instruments [54].

The connection used was a two-electrode configuration. The working and the working sense connect to the positive electrode that is the cathode, the counter and counter sense are connected to the negative electrode that is the anode. The experiments performed were done using the Na metal in the anode as the reference, so the reference cable was also connected to the negative electrode. The connections can be seen in Figure 3.12 (C). It is important to point out that a three-electrode connection would be the most appropriate experimental procedure for the cathode electrochemical measurements. This procedure

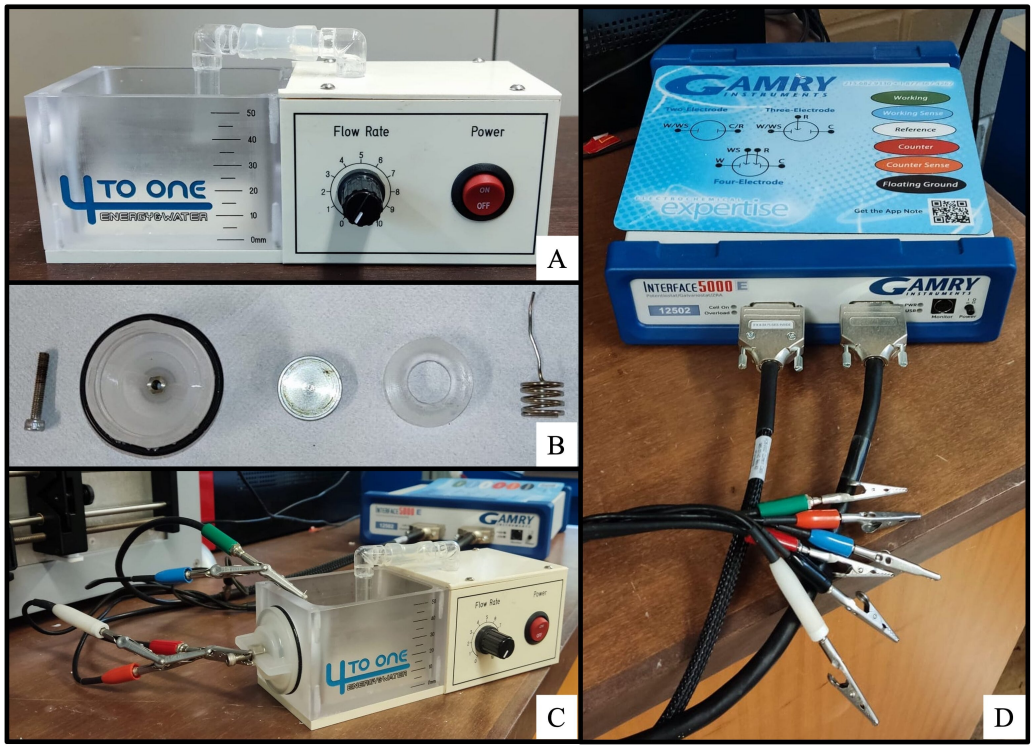

FIGURE 3.12: Experimental apparatus which includes the testing kit (A), the parts to join the anode and the cathode compartments (B) and the potentiostat (D), being all connected like it is seen in (C).

will be carried out shortly. It was not possible to perform it in time due to a problem with the reference electrode existing in the laboratory.

3.2 Structural and chemical characterisation

The morphological and chemical characterisation of the different cathode current collectors' surface was done with various characterisation techniques, such as scanning electron microscopy (SEM) to see the surface distribution and organisation and the size of the fibres, energy dispersive X-ray spectroscopy (EDS) to identify some of the chemical elements present at the surface, and lastly the wettability of each cathode current collector was measured. In a near future, we intend to perform N_2 absorption-desorption isotherms to evaluate specific surface area and porosity of the CCCs, specially PSCF, and the estimation of pore size distribution by density functional theory (DFT) method.

3.2.1 Scanning Electron Microscopy (SEM)

Scanning electron microscopy (SEM) is a technique that has been used worldwide as an effective method in analysis of organic and inorganic materials at a nanometer (nm) or micrometer (μm) scale. With a high magnification that can reach 300000x and even 1000000x (in some recent models), SEM creates very detailed and exact gray-scale images of a variety of materials, including metals and polymers. SEM analysis depends upon electron emission, consisting of a variable pressure system with the ability to hold any samples (wet or samples with minimal preparation). The apparatus enables the analysis of samples with a diameter of up to 200 mm and an 80 mm height [55]. A general SEM device is comprised by six main components, presented in Figure 3.13.

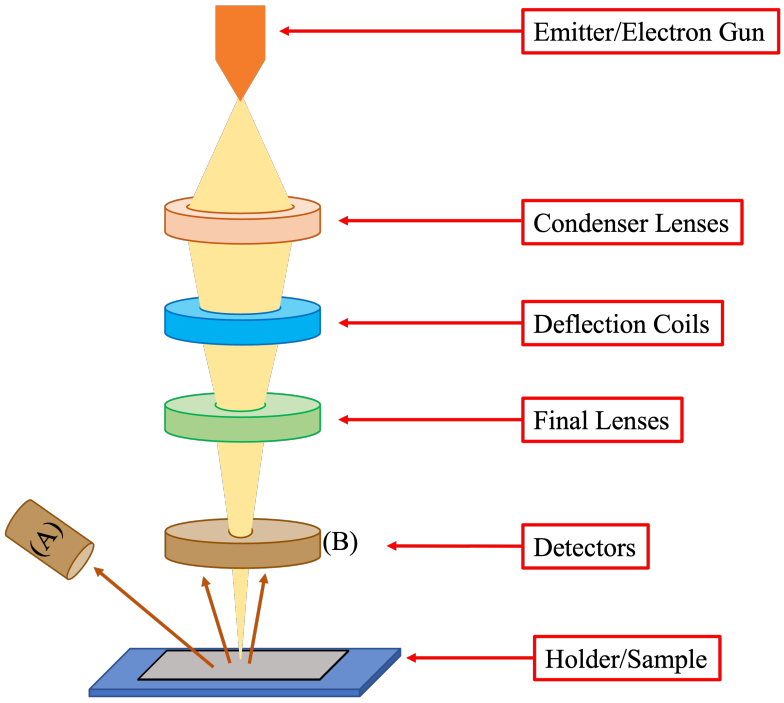

FIGURE 3.13: Schematic of the main components of a SEM device with (A) being a secondary electron detector and (B) being a back-scattered electron detector.

The main components of a SEM machine are [12]:

- Electron gun: emits high energy electrons and the source of electrons can be a Tungsten (W) electron filament that is heated resistively to produce electrons, a Lanthanum hexaboride (LaB6) or Cerium hexaboride (CeB6) that is a thermionic emission gun, and a field emission gun (FEG) that is a tungsten wire with a very sharp tip that produces an electron beam with field electron emission.

- Lenses: there are a series of condenser lenses that focus the electron beam down the column.
- Detectors: they collect the electrons emitted from the sample. They could be secondary electrons [(A) in Figure 3.13] that are low energy electrons produced from the k-orbitals of the atoms in the sample when hit by the beam, and back-scattered electrons [(B) in Figure 3.13] that are high energy electrons elastically back-scattered by the atoms of the sample.
- Scanning coil: they deflect the focused beam in the X and Y axes so that it examines the sample's surface in a raster approach.
- Sample holder: that fixates the sample and includes translation, tilt and rotation devices and other that can assist the analysis of the sample.

The device is connected to a computer system that controls the electron beam and displays the scanned images. The working mechanism of a SEM device consists of electrons being produced and accelerated through the column becoming a focused beam that interacts with the atoms of the sample. Both the column and the holder are in vacuum by a combination of pumps to ensure that the electrons only interact with the atoms of the sample and not with air particles. The interaction generates various signals that are detected. These signals contain information about the sample's surface morphology and composition, crystalline structure and materials orientation, because the beam only penetrates the sample to a depth of a few micrometers [12, 56]. Conductive samples allow for scanning images with better quality. The device is usually equipped with other detectors to perform energy dispersive X-ray spectroscopy (EDS).

3.2.2 Energy Dispersive X-ray Spectroscopy (EDS)

EDS is an analytical method for identifying a sample's chemical makeup or elemental composition. From the interaction of the electron beam with the sample, besides the secondary and back-scattered electrons, X-rays are also generated. This happens because when the electrons enter the coulomb field of an element they will decelerate and the loss of energy is emitted as a photon. The energy of such photons is unique to the specific elements and because each element has a unique atomic structure, we will have a unique set of peaks on the spectrum. So, we can incorporate an X-ray detector on the SEM device

that is responsible for the separation of the various characteristics X-rays into an energy spectrum. The software for the EDS system will then analyse the spectrum to determine the amplitude of a particular element, having the photon energy converted into electrical signals. Finally, we can obtain the chemical composition of the sample, both qualitative and quantitative [55, 56].

3.2.3 Wettability

Wettability measures the ability of a liquid to spread over a surface [57]. It quantifies the degree of wetness when solid and liquid phases interact [58]. The measurement is done with the contact angle between the surface of the material to be analysed and the tangent to the surface of the liquid's drop. The contact angle was determined by the sessile drop method whose experimental apparatus consists of a stage with adjustable height and a high-magnification camera pointed at the stage, as it can be seen in Figure 3.14. The drops where released with a pipette. The contact angles were measured in different sections of the substrate and with their arithmetic average we obtained the wettability of the substrate.

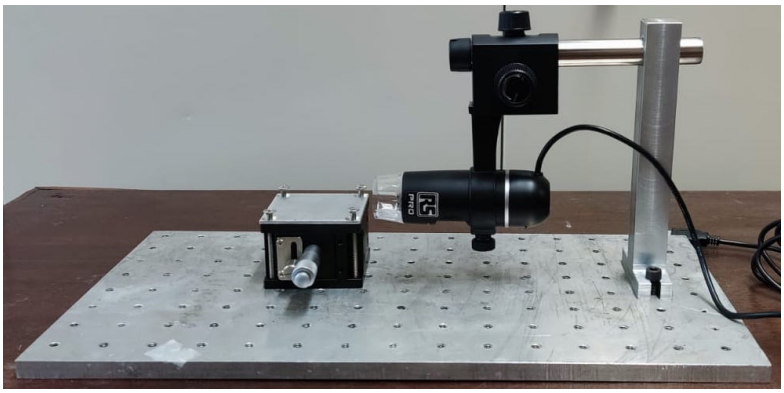

FIGURE 3.14: Experimental apparatus of the sessile drop method to measure the contact angle.

This setup allows for a versatile and low-cost way to measure wettability with precision. The camera records the drop, and the images were analysed with Imagej software and Plugin Drop analysis, where the program determines the contact angle through a polynomial fit curve that is mainly determined by the user. After analysing the operation parameters in a known substrate that was aluminium, the ideal parameters were a drop volume of 6 to 10 μL and a height difference between the substrate and the pipette's

tip less than 8 mm. This experimental apparatus allows for the determination of another experimental parameter that was the absorption time of the drop.

A material is considered to have a good wettability if the contact angle is bellow 90º, being hydrophilic, and a poor wetting ability if the contact angle is higher than 90º, being hydrophobic, as it is schematised in Figure 3.15. If the contact angle is close to 0º, the substrate presents excellent wettability.

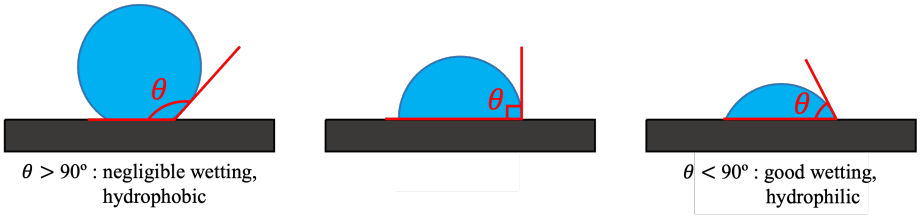

FIGURE 3.15: Scheme of the wettability as a function of the contact angle.

3.3 Electrochemical characterisation

The seawater full cell was electrochemically characterised mainly through galvanostic cyclic charge/discharge voltage profiles and cyclic voltammetries.

3.3.1 Galvanostic charge/discharge cycles

Galvanostic cycling is one of the most used characterisation technique in battery research, where a constant positive/negative current is applied/drawn from the electrodes, respectively, while the voltage values are registered. Typically, low currents are used for capacity tests and high currents are used to study properties such as ion diffusion and electrical conductivity. This electrochemical test is done with a voltage window to safeguard the battery that is being tested, in a way that if the charging process exceeds a certain voltage or if the discharging process goes below a certain voltage the test is stopped. This ensures that the coin-cell is working within safe voltage values, preventing its damage [59].

A galvanostic cycle is illustrated in Figure 3.16. The voltage gap of a cycle is the difference between the final voltage of the charge and the discharge profiles. The plateau is a voltage value associated with the electrochemical reaction that is predominant in the charge or discharge profile [60].

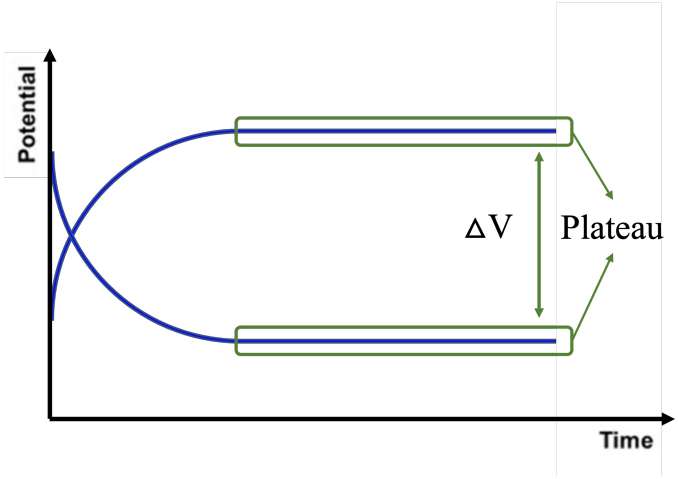

FIGURE 3.16: Possible galvanostic cycle of a battery.

The three different kinetics effects for polarisation that can be considered in a charge/discharge profile are the activation polarisation, the ohmic polarisation and the concentration polarisation. They are illustrated in Figure 3.17.

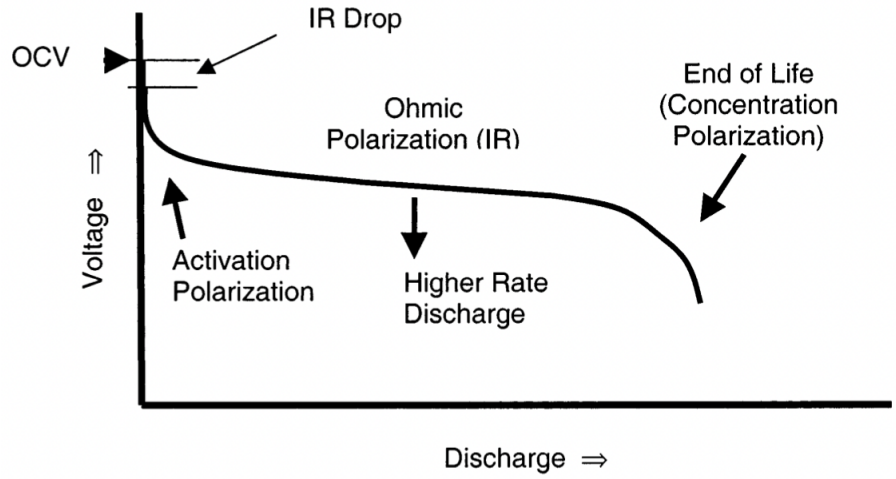

FIGURE 3.17: Typical discharge profile of a cell, with the different polarisation effects identified. Figure from reference [61].

The activation polarisation is ascribed to the kinetics of the electrochemical redox reactions taking place at the electrode/electrolyte interfaces of anode and cathode [61]. It is the potential difference above the equilibrium potential necessary to overcome the activation energy of the cell reaction in order to create a specific current and could be associated to an electron accumulation on the surface of the electrode that produces an energy barrier [62] or to the formation of an EDLC. In other words, it is the slope in the charge and discharge profiles before the plateau is reached. The ohmic polarisation refers to the resistance of individual cell components and it is associated with the plateau previously

mentioned. The concentration polarisation arises from limited mass transport capabilities because the availability of the active species at the electrode/electrolyte interface changes, as the redox reactions take place [61].

The galvanostic cycle presented in Figure 3.17 corresponds to a cell with a discharge profile that is predominantly faradaic. In the case of a EES device with relevant capacitive behaviour, Figures 3.18a and 3.18c present in a more general way the typical galvanostic cycles of an ideal capacitor and a capacitor-like EES device.

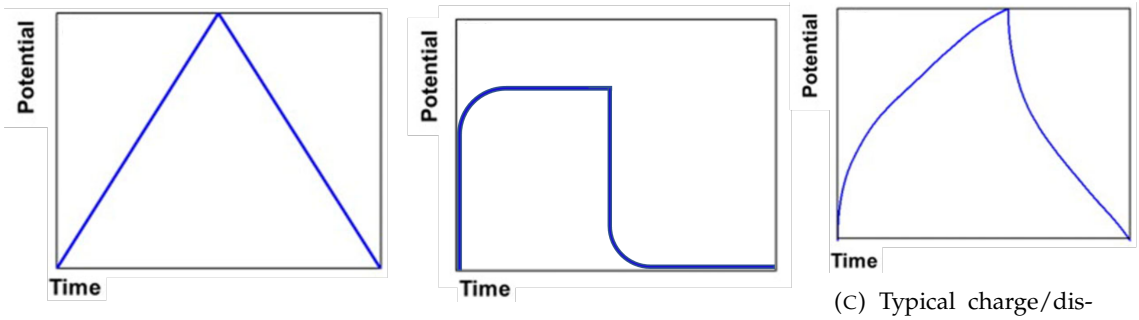

(A) Typical charge/discharge cycle of an ideal supercapacitor.

(B) Typical charge/discharge cycle with faradaic mechanisms.

(C) Typical charge/discharge cycle with distortion due to faradaic reactions.

FIGURE 3.18: Typical charge/discharge cycle curves. Figure from reference [63].

3.3.2 Cyclic voltammetry

Cyclic voltammetry (CV) is an important analytical tool that can detect the electrochemical activity of the electrode materials such as electron transfer kinetics, the presence of reversible and irreversible reactions [56], and also allows to identify faradaic and non-faradaic behaviours. Generally, a CV experiment is done with the scanning of the working electrode potential with a specific sweep rate, which in our case is the cathode current collector, while the current is registered.

Figure 3.19 illustrates a cyclic voltammetry. The initial and final voltages of a CV are called vertex potentials. With a CV we can distinguish reversible reactions from irreversible ones. A reversible redox reaction appears as two peaks, one associated with the cathode and the other with the anode, generally with the same peak amplitude. If an increase in current is observed and only one peak is formed, the reaction that caused it is irreversible. A CV also allows for the identification of the electrochemical stability window (ESW) that starts and ends at the potential values where the electrolyte starts to decompose, having the peaks at the beginning and end of the voltage window being caused by that decomposition [59]. Another information provided by a CV is the current

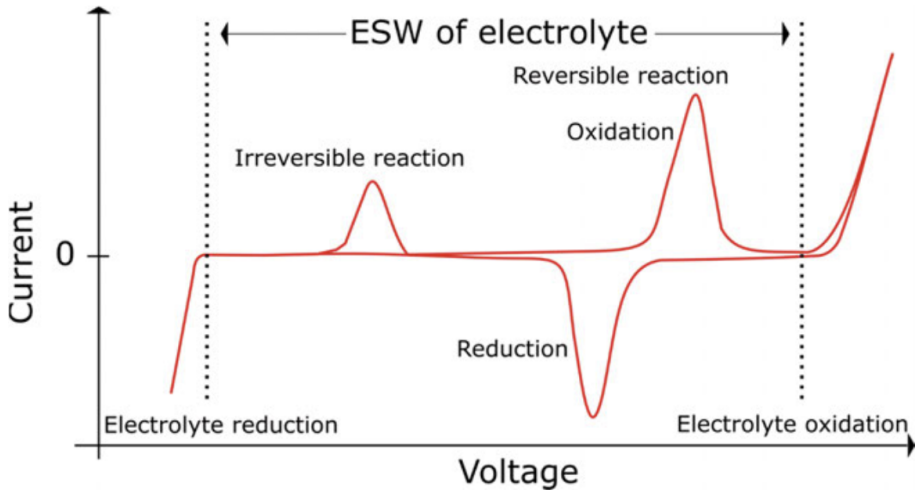

FIGURE 3.19: Possible CV of a battery. Figure from reference [59].

area caused by the EDL formation, if a relevant capacitive behaviour is present. This area can be used to calculate the capacitance associated with the working electrode. The presented CV is for EES devices that operate mainly with faradaic reactions. In the case that an EES device is closer to a capacitor, Figures 3.20a and 3.20c present typical CVs of an ideal capacitor and a capacitor-like EES device. Figure 3.20b represents a non-faradaic CV with an extra resistance component.

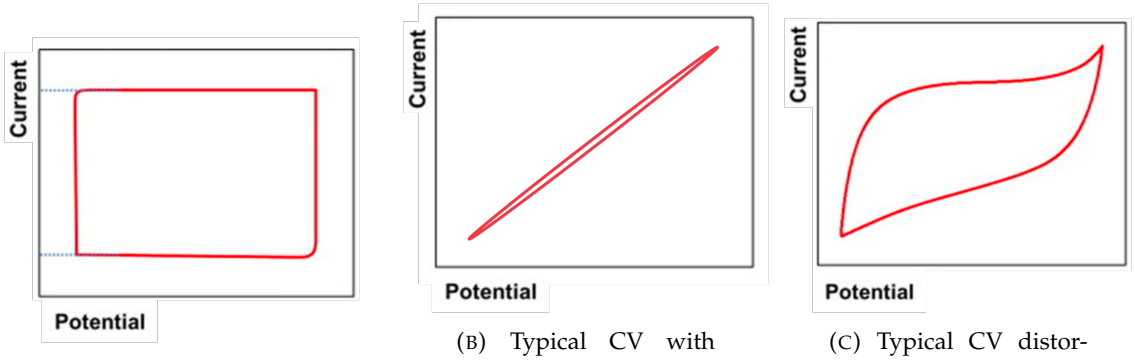

(A) Typical CV of an ideal supercapacitor.

(B) Typical CV with a main resistive behaviour.

(C) Typical CV distortion due to Faradaic reactions.

FIGURE 3.20: Typical cyclic voltammetry (CV) curves. Figure from reference [63].

The experimental setup can be done with two or three electrode connections, being the third a reference electrode. In our case, the CVs were all performed in a two-electrode system, where the active material present in the anode acts as the reference, as previously mentioned.

Chapter 4

Seawater batteries with carbonaceous materials: characterisation and performance

The performance of a seawater cell was studied by varying the cathode. Four were studied, a commercial, a heated and an activated carbon felts and a peanut shell bio-waste carbon electrode. Their performance was evaluated through galvanostic charge and discharge cycles and cyclic voltammetries. The surface morphology was analysed by scanning electron microscopy (SEM), energy dispersive X-ray spectroscopy (EDS) and the wettability was measured.

4.1 Morphological and chemical characterisation

The surface morphology of the different cathode current collectors (CCC) was analysed through scanning electron microscopy (SEM) and energy dispersive X-ray spectroscopy (EDS) to evaluate fibre distribution and deposition of materials. In the morphological characterisation, two situations will be analysed, before and after cell operation.

4.1.1 Commercial carbon felt (CCF)

Figures 4.1a and 4.1b show the fibrous surface of the commercial carbon felt (CCF) with two magnifications.

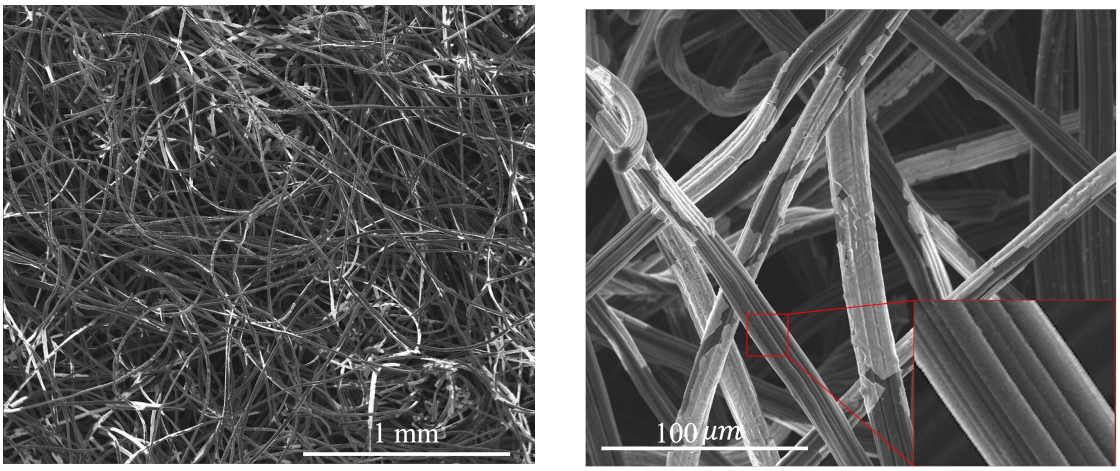

(A) CCF surface with 1 mm magnification. (B) CCF surface with 100 μm magnification.

FIGURE 4.1: SEM images of the commercial carbon felt surface with two magnifications.

The surface of a CCF is composed by a large number of microfibres randomly distributed. The microfibres have a diameter of 15 to 20 μm, displaying a slit-shaped pore structure on their surface, as can be seen in Figure 4.1b.

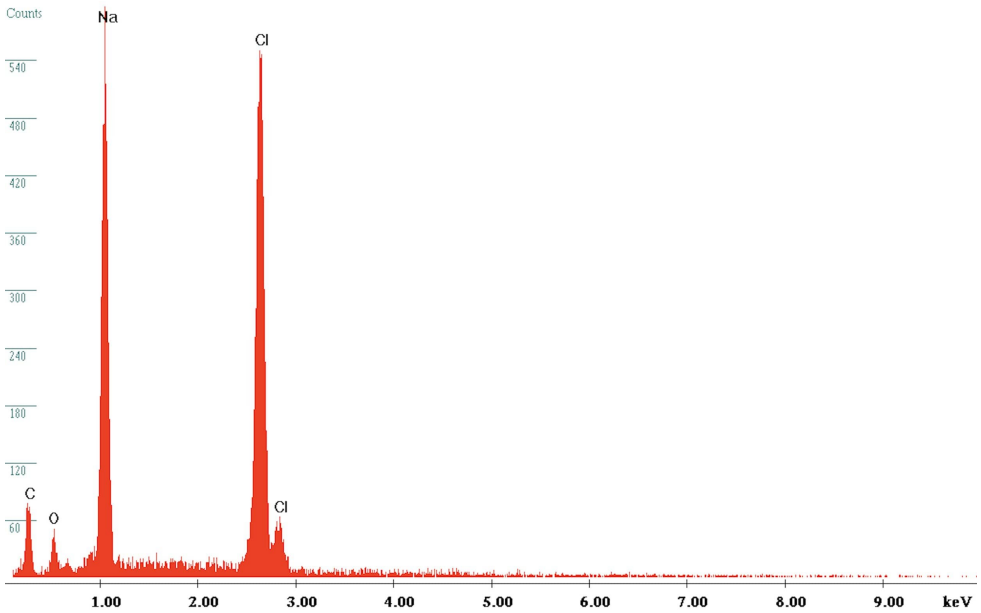

FIGURE 4.2: EDS analysis of the CCF surface

The CCF that was analysed by SEM had already been immersed in the catholyte and it was observed that NaCl was deposited in the microfibres during cell operation, through EDS analysis. NaCl is a very abundant salt in the synthesised seawater (35 g L^{-1} of NaCl).

4.1.2 Heated commercial carbon felt (HCCF)

Figure 4.3 shows a heated commercial carbon felt (HCCF) before and after it being used in electrochemical tests.

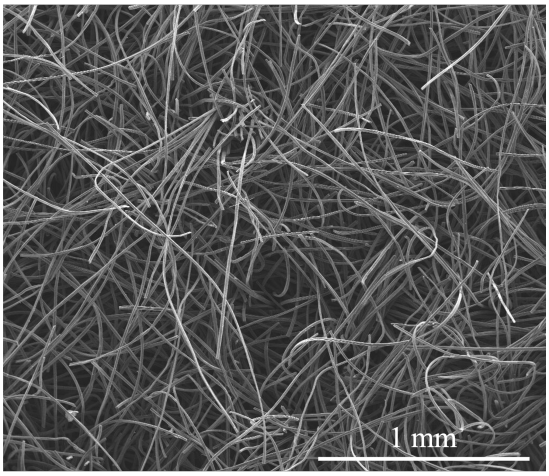

(A) Unused HCCF surface with 1 mm magnification.

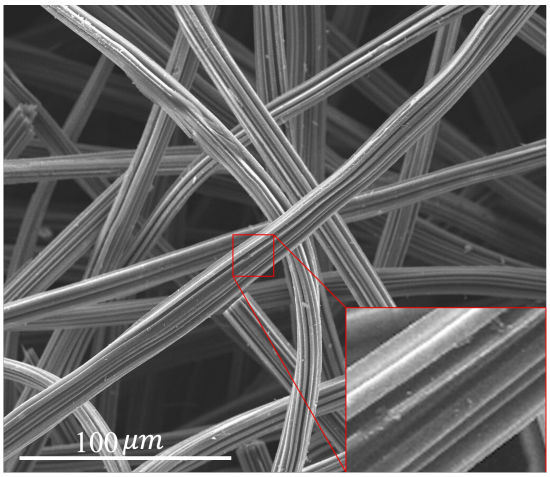

(B) Unused HCCF surface with 100 μm magnification.

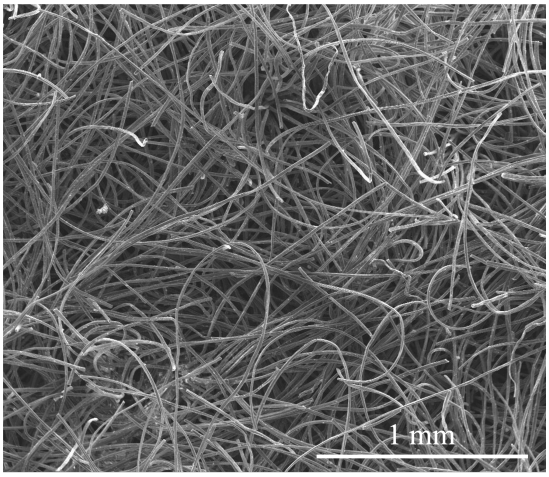

(C) Used HCCF surface with 1 mm magnification.

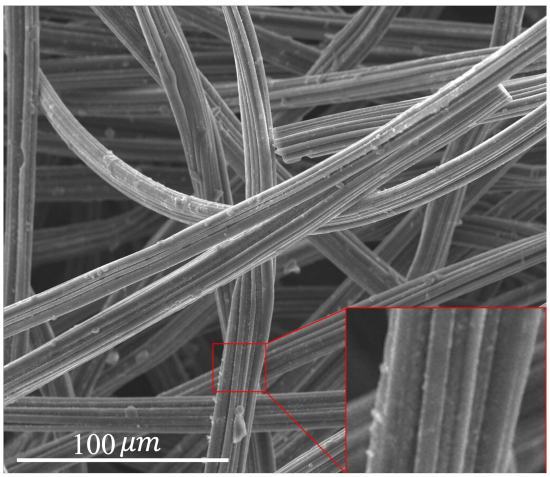

(D) Used HCCF surface with 100 μm magnification.

FIGURE 4.3: SEM images of the heated commercial carbon felt surface with two magnifications, before and after utilisation.

The HCCF presents microfibres randomly distributed but with a lighter colour. Comparing Figure 4.1 with Figure 4.3, the CCF fibres have a darker colour that corresponds to the polymer used in its manufacturing to ensure mechanical strength. With the polymer evaporated with the heat treatment, the fibres take a lighter shade. The SEM analysis shows that the amount of NaCl deposited was much less in the HCCF. The fact that the deposition of NaCl decreased in the fibres without the polymer suggests that NaCl has good affinity with the polymer, making its deposition easier. The absence of the polymer

in the HCCF is probably the reason why the same carbon felt exhibits two distinct NaCl deposition behaviours. The fibres possess the same diameter range and non-uniform distribution like in CCF, but the slit-shaped pore structures are more exposed in the HCCF (Figures 4.1b and 4.3d). This increase in available porosity leads to the increasing of the surface area and the hydrophilic behaviour of the carbon felt.

4.1.3 Activated carbon felt (ACF)

Figure 4.4 shows the surface of the activated carbon felt (ACF) with the same two magnifications, after utilisation.

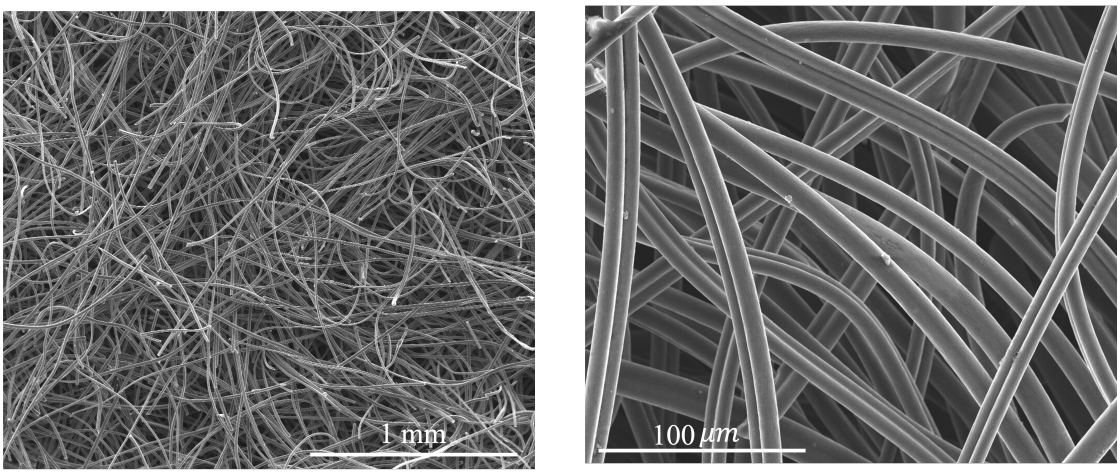

(A) ACF surface with 1 mm magnification.

(B) ACF surface with 100 μm magnification.

FIGURE 4.4: SEM images of the activated carbon felt surface with two magnifications.

Unlike usual commercial activated carbon felts whose surface is comprised of organised fibres like seen in Figure 3.4, the used activated carbon felt has a non-uniform microfibre distribution, whose manufacturing process was explained in section 3.1.2, much like CCF and HCCF. Commercial activated carbon felts usually have an organised surface to provide mechanical strength, an unnecessary characteristic in our case. The ACF used in this thesis has smaller microfibres with diameters ranging from 8 to 11 μm and it is observed in Figure 4.4a an increase in fibre content. The synthesis process of this particular ACF has been previously dictated. The decrease of fibre diameter, when compared to CCF and HCCF, results in a much higher surface area and porosity. The ACF already used in electrochemical tests had a negligible amount of NaCl deposited in the fibres, meaning that the fibre diameter and surface porosity also influence the deposition of NaCl. Besides, the lack of deposited NaCl could also be caused by the absence of the

polymer in the ACF's fibres, further suggesting that the polymer is the main prompter for the deposition of NaCl in CCF.

4.1.4 Peanut shell coated carbon felt

The fourth cathode current collector was the peanut shell coated heated commercial carbon felt (PSCF), whose morphological and chemical characterisation was performed during all synthesis steps. The peanut shell cathode results are currently being summarized in a paper in preparation [64].

4.1.4.1 Synthesis process analysis

The synthesis process of the peanut shell electrocatalyst has three main phases that are the carbonisation, the activation and the final cleaning process of the activated KOH peanut shells, as previously dictated. Figure 4.5a shows the morphology of peanut shells after being crushed and washed, and its EDS analysis.

Through EDS analysis (Figure 4.5b) we can see that the main components of peanut shells are carbon (C) and oxygen (O), having residual traces of magnesium (Mg), silicon (Si), sulphur (S), potassium (K) and calcium (Ca), which may be some of residual components that were not completely removed in the washing and filtering process. The SEM image of the peanut shells (Figure 4.5a) shows pore-like structures all over the surface of the material that continue inwards and connect with each other. The quality of this image is lower than the rest because the sample is less conductive, reducing the quality of the images. The improvement in image quality can be seen in Figure 4.5c, where the carbonised peanut shells presented are more conductive. The pore-like structure was maintained throughout the carbonisation process and the oxygen was almost completely consumed as it can be seen in the EDS analysis in Figure 4.5d. If the carbonisation step is done at low temperatures, the biomass can have an unstable or fragile structure that is going to be excessively etched during the following activation phase. This results in meso-/macropores formation in excess. Even though this benefits ions transport and charge accumulation, it severely reduces the particle density and conductivity of the activated carbon material [34]. That said, the carbonisation temperature used was 600ºC, which is higher than the temperature considered low by the literature, that is 500ºC. This was performed in order to have many meso-/macropores formation but also to safeguard the conductivity of the material [34]. The next phase is the activation process with potassium hydroxide (KOH),

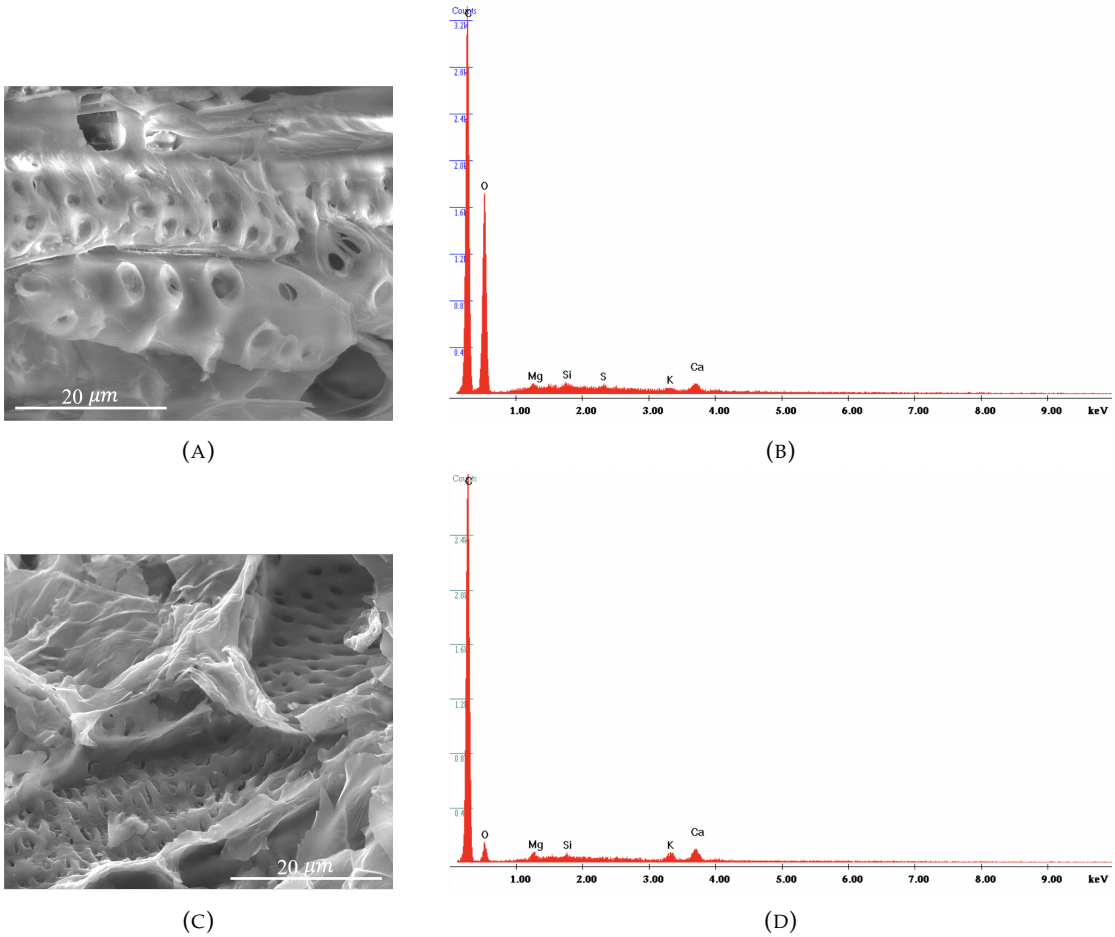

(A) (B)

(C) (D)

FIGURE 4.5: SEM images of the surface of washed and crushed peanut shells (A) and carbonised (C) with 20 μm magnification and its EDS analysis (B) and (D), respectively.

which will increase the surface area accessible to the ions in the electrolyte by opening meso- and macropores and introducing abundant micropores. In addition, KOH activation also modifies the chemical and electronic properties of the peanut shells to further minimise the resistance associated with ion transport [34]. The following equations describe what occurs in the activation process:

$$6KOH + 2C \longrightarrow 2K + 3H_2 + 2K_2CO_3, \tag{4.1}$$

$$2K_2CO_3 + C \longrightarrow K_2O + 2CO, \tag{4.2}$$

$$2K_2CO_3 \longrightarrow K_2O + CO_2, \tag{4.3}$$

$$2K + CO_2 \longrightarrow K_2O + CO. \tag{4.4}$$

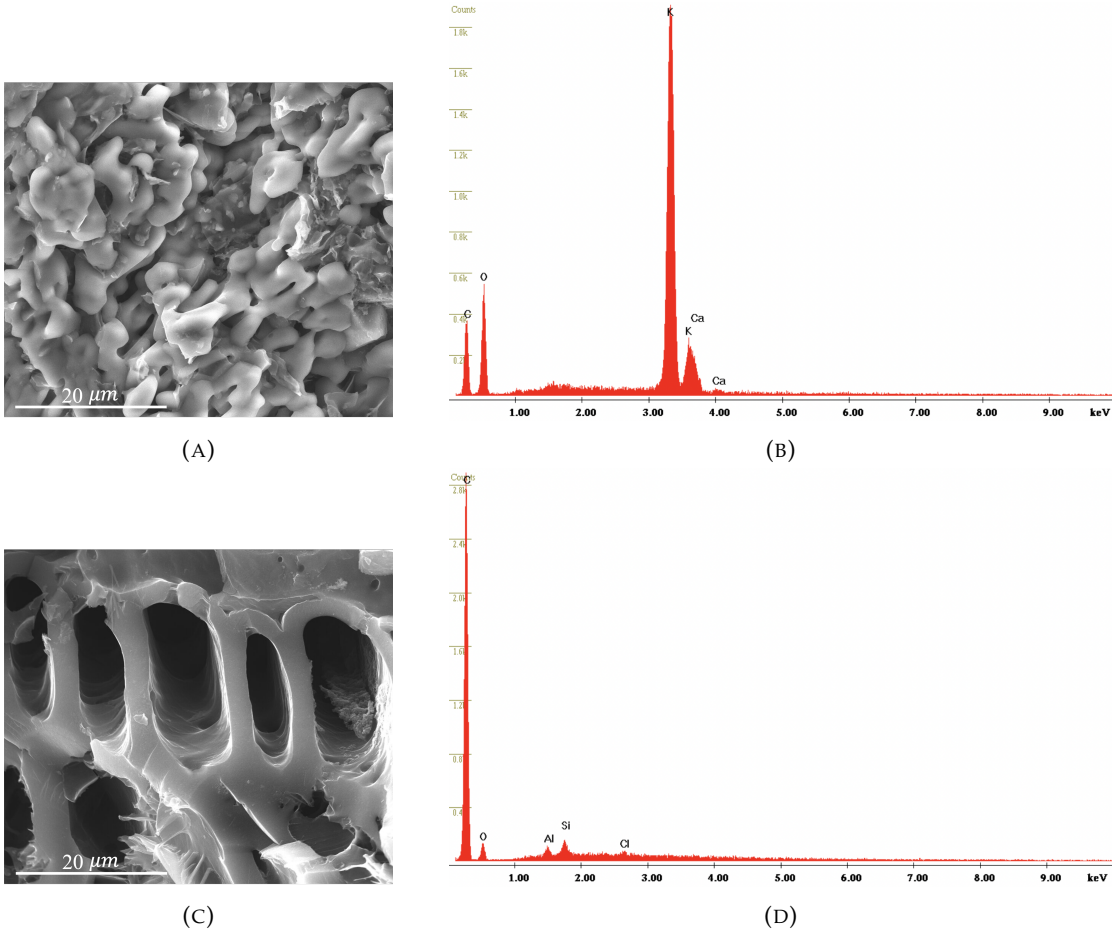

(A) (B)

(C) (D)

FIGURE 4.6: SEM images of the activated peanut shells surface before being washed and filtered (A) and after (C) with 20 μm magnification and its EDS analysis (B) and (D), respectively.

Through Figures 4.6a and 4.6b, we can see that the surface of the activated peanut shells is completely covered with potassium (K). Carbon (C), that was before the most abundant element was surpassed by oxygen (O), as it is one of the reaction products that arise from the activation process with KOH in the form of potassium carbonate (K_2CO_3), potassium oxide (K_2O), carbon monoxide (CO) and carbon dioxide (CO_2). The released hydrogen (H_2) (Equation 4.1) is a very light element that was taken away by the argon flow present during the activation process and it was not identified by EDS analysis. The cleaning and filtering process with the HCl solution removed the potassium almost completely from the surface as it can be seen in Figure 4.6c where the pore-like structure is shown once again and in Figure 4.6d, where the EDS analysis reveals carbon (C) as the main component at the surface of the peanut shell electrocatalyst.

4.1.4.2 PSCF morphology

After the coating process, the finalised cathode current collector was analysed before and after electrochemical tests were applied and similar to ACF, no NaCl deposition is observed on the surface of PSCF during cell operation.

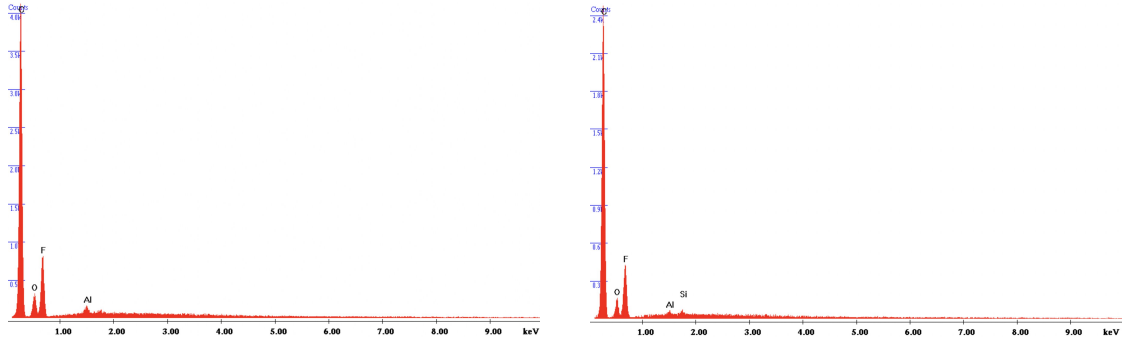

(A) PSCF before electrochemical tests. (B) PSCF after electrochemical tests.

FIGURE 4.7: EDS analysis of the peanut shell coated carbon felt before and after utilisation.

In Figure 4.7, we see that no NaCl is present, neither before or after. This supports that the increase in surface area and porosity influences the superficial NaCl deposition. Except for the element Silicon (Si), the composition is the same before and after the electrochemical tests. The appearance of Si is most likely due to the site of EDS analysis being different in the two samples. Initially, Si was thought to come from the solid electrolyte NASICON, whose composition is $Na_3Zr_2Si_2PO_{12}$, and Si was released and attached to the surface of PSCF indicating the degradation of the NASICON. However, Si is also found in the EDS analysis of samples from the synthesising process of the PSCF (Figures 4.5b, 4.5d and 4.6d), before the peanut shell electrocatalyst was in contact with NASICON, meaning that the Si present comes from the pristine peanut shells used. The amount of silicon (Si) present in the targeted area of the PSCF's EDS analysis after cell operation was probably too small to be detected.

Figure 4.8 shows that the PSCF surface is the electrocatalyst, being the fibres underneath. The analysed cathode was at the final stage, meaning that the natural multiple channel structure characteristic of peanut shells was maintained throughout the carbonisation and activation processes. The peanut shell electrocatalyst has many larger pores whose diameter can vary from 3 to 15 μm, as it can be seen in Figure 4.8c. These larger channels have internal sub pores that connect the various larger pores [65], forming an

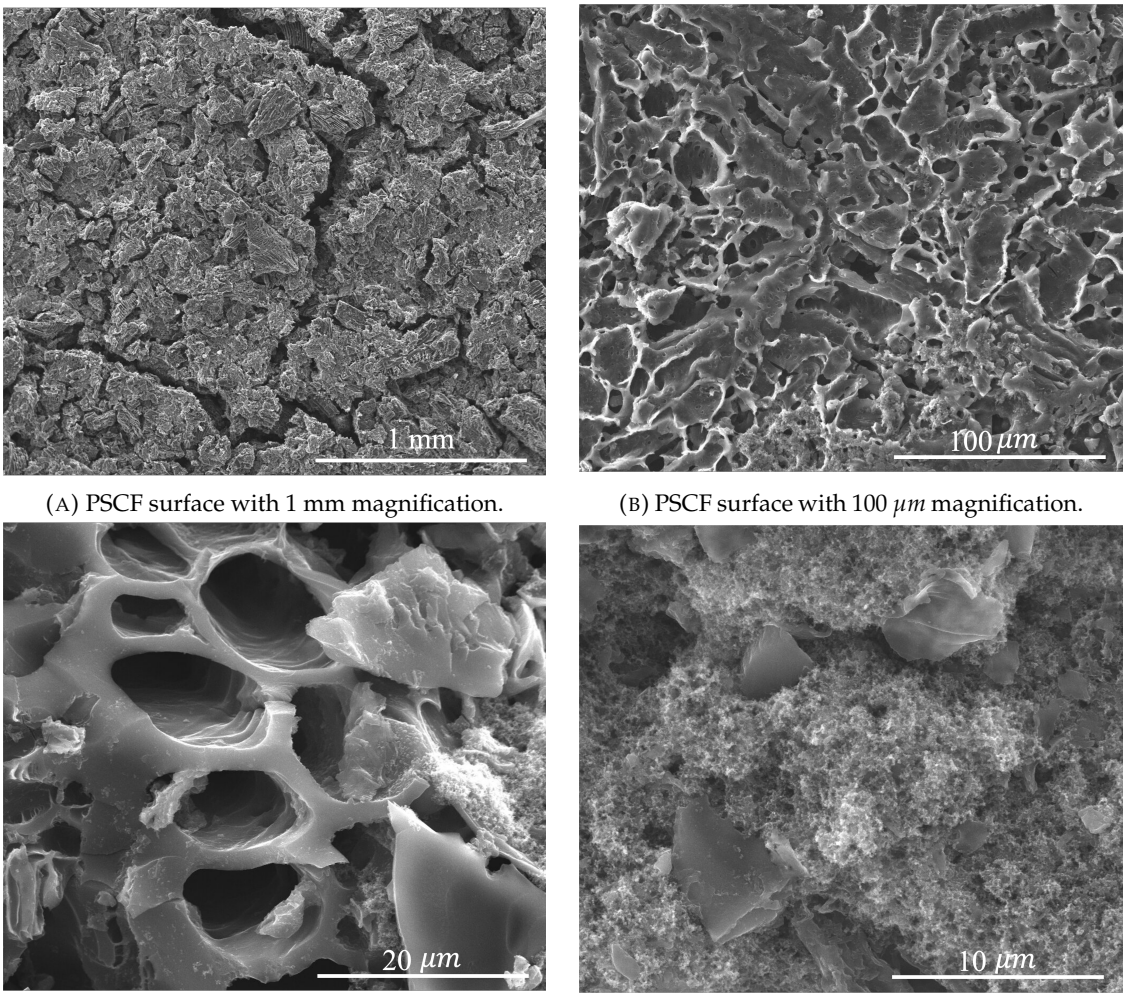

(A) PSCF surface with 1 mm magnification.

(B) PSCF surface with 100 μm magnification.

(C) PSCF surface with 20 μm magnification.

(D) PSCF surface with 10 μm magnification.

FIGURE 4.8: SEM images of the peanut shell coated carbon felt surface with four magnifications.

intricate network of micro channels that connect with the HCCF fibres where the electrocatalyst is deposited. This allows the movement of ions and electrons as well as the accumulation of charges that contribute to the EDL formation in the cathode current collector. According to [33], most of the porous carbon materials possess micropores due to the burn-off of non-carbon elements, such as oxygen, nitrogen and hydrogen, and carbon containing compounds during the process of carbonisation, so that inside the bigger pores seen in the SEM images there are multiple macro-, meso- and micropores. As stated before, these micropores will contribute has sites for ion storage and charge transfer reactions during the charge/discharge processes, with high ion accessible surface area. The mesopores will provide fast mass transport pathways and the macropores can act as ion-buffer reservoirs that minimise the diffusion paths. This is the hierarchical porosity behaviour widely studied in the literature [33]. With all of these characteristics, it is believed

that the peanut shell electrocatalyst will lead to a good SWB performance.

4.2 Wettability analysis

The wettability of the cathode current collectors is a parameter that can influence the performance of a seawater cell. The degree of three-dimensional penetration of the ions and the volumetric capacitance [34] of the material used are also important parameters to characterise the volumetric accessibility of active sites. Because no volume and particle density measures where performed, the measurement of wettability is the best approximation to a 3D notion that we could have. The wettability is measured with the contact angle between the surface of the material and the tangent of the drop, as illustrated in Figure 4.9, and the absorption time.

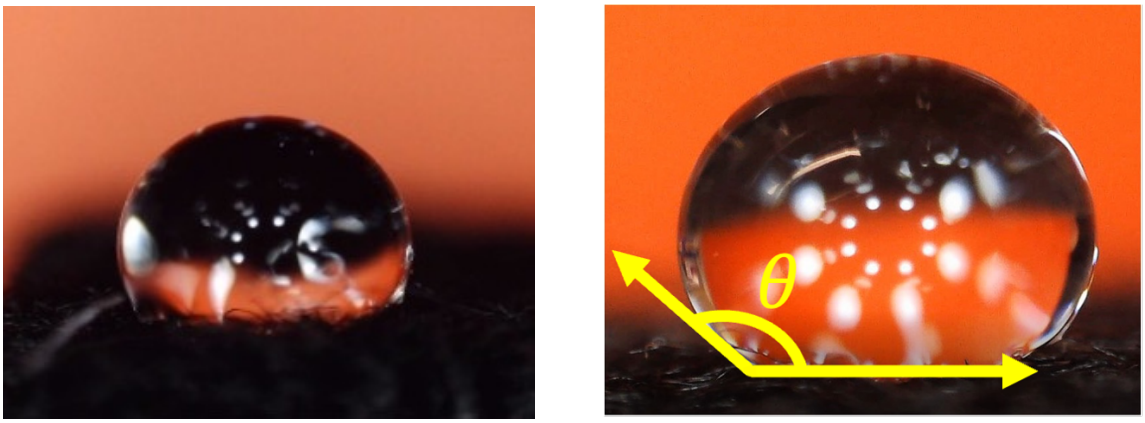

(A) Measure of HCCF wettability. (B) Contact angle schematic in a ACF.

FIGURE 4.9: Wettability measure with synthesised seawater.

The measurement of the wettability of the cathode current collector surface was performed before and after the application of electrochemical tests, allowing to see if the hydrophobic or hydrophilic behaviour changes. The obtained measures are displayed in Table 4.1.

A carbon felt has good wettability when the contact angle is smaller than 90°. All of the analysed cathode current collectors have poor wettability before their utilisation, being the CCF the worst because of the mechanical reinforcement polymer. A heat treatment was applied for polymer evaporation and an improvement of the hydrophilic nature of the commercial carbon felt by 20° was achieved. Before the heat treatment there was no absorption of the drop and after the drop was absorbed in under 3 seconds. Heat treatments have been reported to populate carbon felts with surface-active oxygen functional

Cathode Current Collector		Contact Angle (°)	Absorption Time (s)
CCF	Unused	141.9	No absorption
	Used	Unmeasurable	0.25
HCCF	Unused	121.4	2.97
	Used	Unmeasurable	0.1
ACF	Unused	133.1	137.6
	Used	134.9	42.4
PSCF	Unused	91.3	8.6
	Used	81.6 - 125.6 (inconsistent)	<3 (inconsistent)

TABLE 4.1: Contact angle and absorption time of each cathode current collector before and after utilisation, where unmeasurable means that the drop was absorbed to fast to be measure.

groups that improve the wettability of the carbon felt [66]. After electrochemical tests were applied, the wettability was measured once more revealing that it improved significantly having an unmeasurable contact angle. This means that the absorption of the drop was so fast (0.25 s for CCF and 0.1 s for HCCF) that the software was unable to capture a frame in time to measure the contact angle.

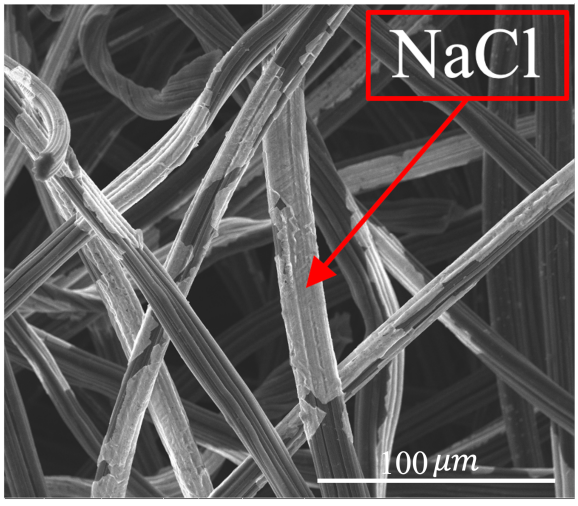

FIGURE 4.10: CCF surface with NaCl deposited at 100 μm magnification

This significant increase in wettability may be due to the deposition of NaCl in the fibrous surface of the CCF and HCCF that was seen in the SEM images (Figure 4.10). NaCl is a wetting agent that can reduce the surface tension and, consequently, improve

the wettability. When NaCl is present on the surface of the carbon felt, the counter ion in the salt neutralises a portion of the hydrophobic group charges in the surface, lowering the surface tension. Young's equation describes the relationship between the contact angle and the surface tension of solid-liquid, liquid-gas, and solid-gas when a drop of liquid falls onto a solid surface and finds equilibrium [67]:

$$\gamma_{SG} - \gamma_{SL} = \gamma_{LG} \cos\theta, \tag{4.5}$$

where γ_{SG}, γ_{SL} and γ_{LG} are the surface tension of gas-solid, solid-liquid and gas-liquid, respectively, and θ is the contact angle. When the surface tension decreases, the shrinkage tendency of the liquid surface is weakened resulting in an increase of the contact area at the interface between liquid and solid and the decrease of the contact angle [67]. Therefore the CCF and HCCF become significantly more hydrophilic with NaCl deposited as a wetting agent. The same does not apply to the activated carbon felt. ACF is hydrophobic before and long after electrochemical tests applied, having only a decrease in absorption time of 95.2 s. This supports the SEM analysis (Figure 4.4) where no deposited NaCl was observed in the fibrous surface of the cathode current collector, maintaining its hydrophobic behaviour. The increase in ACF surface area could be large enough to induce a loss in volumetric capacitance that is, in other words, the ion insertion capacity, resulting in poor wettability.

The PSCF presents a different behaviour from the other three CCCs. As stated before, heat treatments on carbonaceous surfaces lead to an increase in the amount of surface-active oxygen functional groups which results in an increase of wettability [66]. The wettability improvement due to the increase of functional groups available was already seen in the heated carbon felt (heat treatment performed at 500ºC). In the PSCF case, during the carbonisation in an inert atmosphere the majority of oxygen and hydrogen is removed in the form of different gases. Defective carbon atoms are produced on graphene-like sheets while the remaining carbon atoms self-organise into a group and form aromatic sheets. Because some of these defective carbon atoms have unpaired electrons or unsaturated valences, they can interact with other heteroatoms (such as oxygen and hydrogen) to form different types of surface functional groups [7, 34]. Thus, the activation process generates more surface-active oxygen functional groups. This is the main reason for the good wettability of PSCF, both before and after cell operation. The peanut shell electrocatalyst

coating, when dried at the final stage, has cracks on its surface, as it is highlighted in Figure 4.11. The adhesion of electrocatalyst will be a focus of optimisation in the future to decrease crack formation.

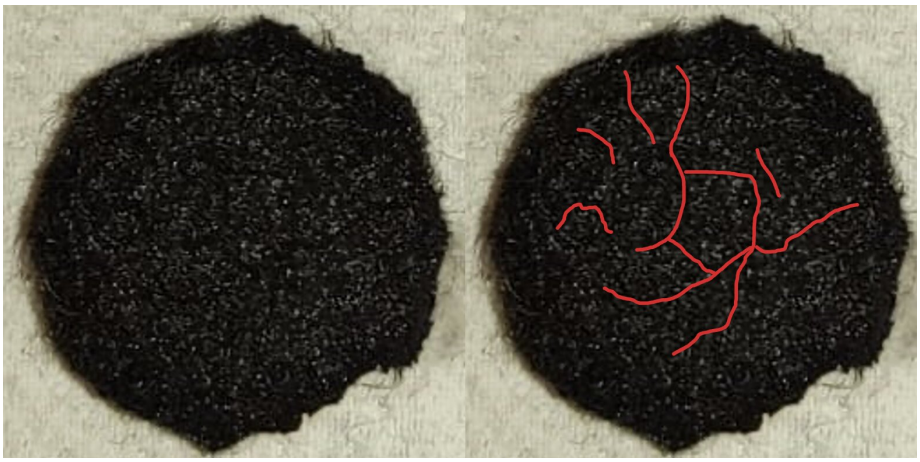

FIGURE 4.11: PSCF with highlighted cracks on the coating.

These cracks are probably responsible for the inconsistent behaviour seen in the used PSCF, which had to be moved and handled causing the coating to crack and even have some of the surface of the carbon felt eroded. The used PSCF has different contact angles and absorption times depending on the section measured, having the contact angle range from 81.6° to 125.6°. The highest values of contact angle were measured on the sections that were more cracked and worn out. The similarity between the high contact angles of the PSCF and the contact angles associated with the unused HCCF suggests that the thinner coating on those sections causes the increased wettability. The lower contact angles were taken from sections that were more preserved, presenting good wettability due to the amount of surface-active oxygen functional groups. The unused PSCF presented a more consistent behaviour because it was less handled and moved, conserving the coating on the surface of the carbon felt. It has good wettability with a contact angle of 91.3° and an absorption time of 8.6 s due to the presence of surface-active oxygen functional groups.

4.3 Simulated seawater

A synthesised catholyte was made from the dissolution of marine salt in ultra-pure water, making a salt water solution with a concentration of 35 g L^{-1}. To safely use the synthesised solution throughout the electrochemical experiments, a comparison between the

seawater sample and the saltwater solution was performed by comparing two galvanostic charge and discharge cyclic voltage profiles in the same conditions, only changing the catholyte. Both cycles can be seen in Figure 4.12.

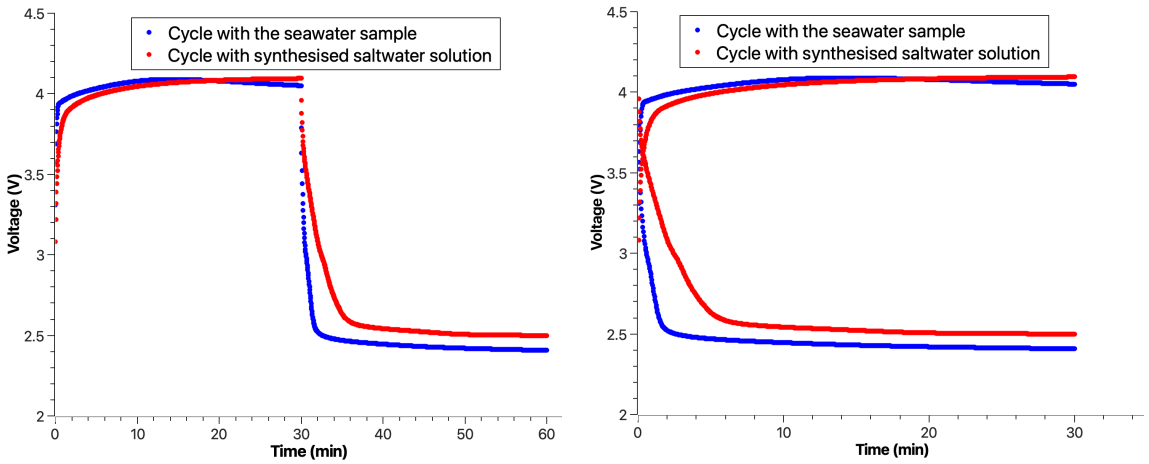

FIGURE 4.12: Galvanostic cyclic voltage of both catholytes at a current of 0.05 mA performed with a commercial carbon felt as the cathode current collector.

By comparing the two voltage profiles we can see that the performance of the SWB is similar, being slightly better when considering the synthesised salt water as the catholyte. The charge profile of the two catholytes is identical, but the discharge profile of the saltwater solution has a final voltage (2.50 V) slightly higher than that of the seawater (2.40 V), and the plateau is not reached as fast. This difference in the discharge profile means that the charge/discharge cycle with the saltwater solution has lower voltage gap, Δ V=1.6 V, and activation polarisation effect. Even though, the voltage gap decrease is very small having only a difference of 0.04V, since the voltage gap of the profile with seawater is Δ V=1.64 V. With this comparison, it is possible to conclude that the synthesised saltwater solution induces the same performance as the seawater and can be used as the catholyte for the following electrochemical tests.

4.4 SWB stability

The stability of the cyclic performance of the SWB was examined with a CCF by galvanostic charge/discharge cycling at a current of 0.05 mA with 10 hour cycles. The 25 cycles are shown in Figure 4.13.

Figure 4.13 shows that the stability is maintained throughout the 250 hours of continuous cycling. Figure 4.14 presents the voltage gaps for each cycle.

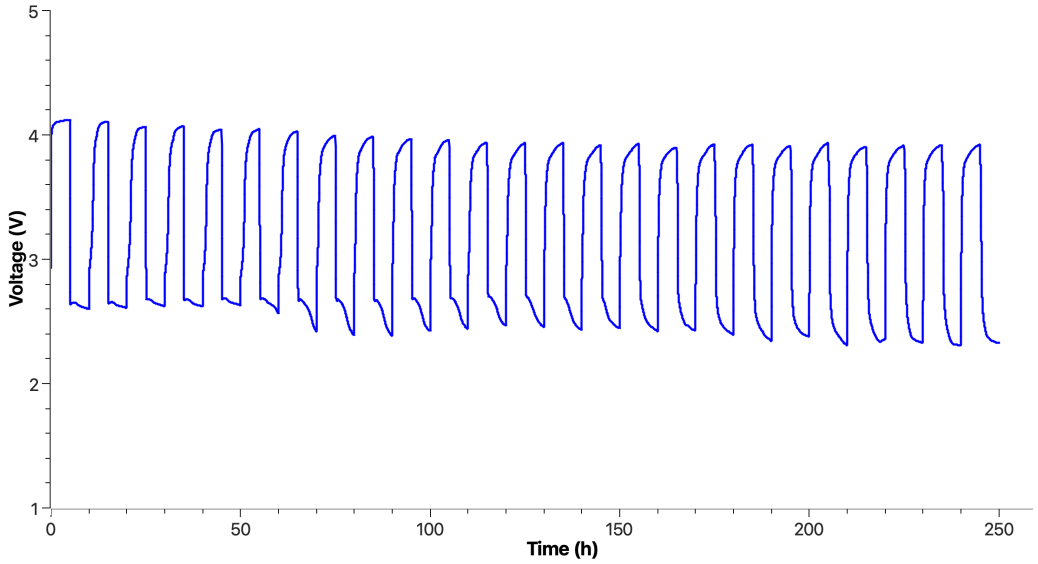

FIGURE 4.13: Galvanostic voltage profiles of 25 cycles for 250 hours, at a current of 0.05 mA with the commercial carbon felt.

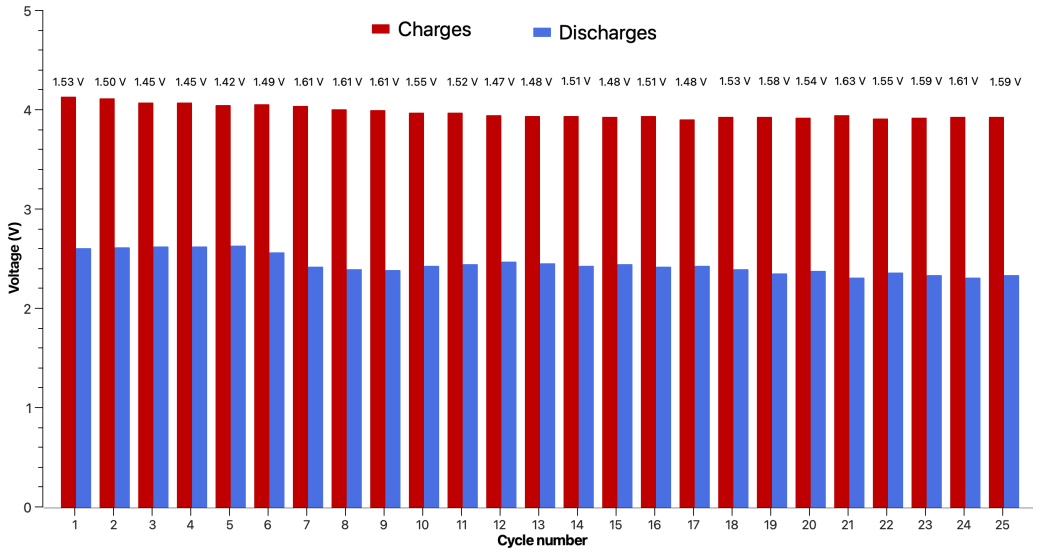

FIGURE 4.14: Final voltages of charge and discharge from each cycle, and respective voltage gap of CCF.

Even though Figure 4.14 shows a slight increase of the voltage gap, this increase is very small. The first cycle has a voltage gap of 1.53 V whereas the last has a voltage gap of 1.59 V. The voltage gap increased by only 0.03 V between the 1st and the 25th cycle, however this amount does not accurately reflect the voltage gap variation over the 250 hours because the voltage gap increase did not have a linear behaviour. The highest voltage gap measured was 1.63 V on the 21st cycle, and the lowest was 1.42 V on the 5th cycle, having a total voltage gap variation of 0.21 V, which is a small variation when considering the continuous cycling over 250 hours and that the cathode current collector

(CCC) used was a simple commercial carbon felt without any further treatment. Figure 4.15 shows the calculated energy efficiency for each cycle.

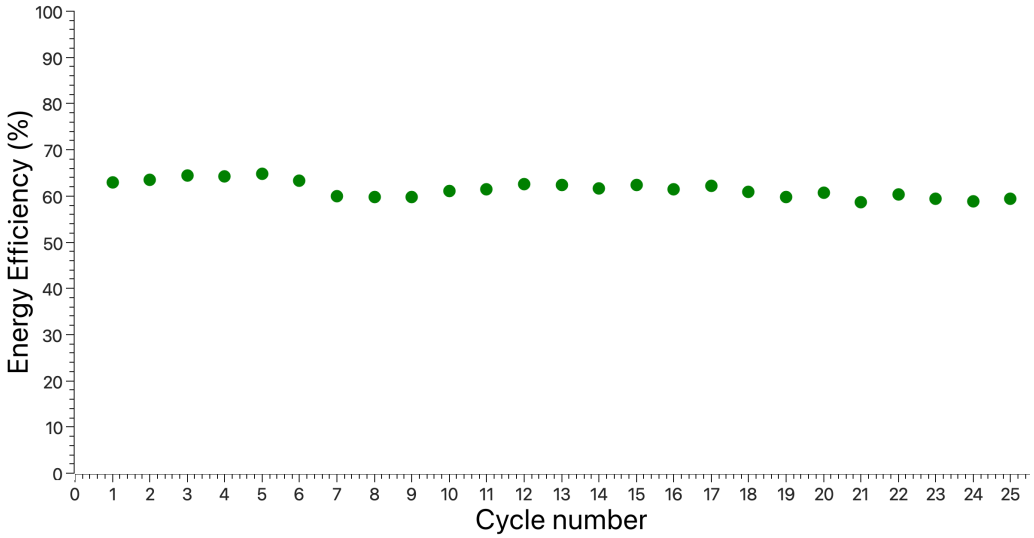

FIGURE 4.15: Energy efficiency during the 25 cycles of CCF.

The energy efficiency was calculated using:

$$EE(\%) = \frac{DFV}{CFV} \times 100, \tag{4.6}$$

where DFV is the discharge final voltage and CFV is the charge final voltage. The SWB with a commercial carbon felt as a carbon current collector has a nonlinear energy efficiency behaviour, having its highest value in the 5th cycle of 65% and its lowest of 59% on the 21st cycle, which agrees with what was stated about the limits of the voltage gap. The average energy efficiency is around 61% for a commercial carbon felt as the CCC, being consistent with the available literature [39].

These results allow us to draw the conclusion that a SWB has a stable performance over a 250-hour period, with voltage gaps and energy efficiencies that can be enhanced by altering the CCF properties.

4.5 Capacitive behaviour in different cathode current collectors

By changing the properties of the CCC, such as increasing its hydrophilic behaviour, increasing the surface area, and depositing an electrocatalyst that enhances the surface porosity, the performance of a SWB can be improved. All of these modifications will increase the CCC's surface area, which will increase the number of active sites available

for redox reactions to take place. They will also create the necessary conditions for the emergence of an EDL formation, which will result in an increase of the capacitive behaviour and an improvement of the overall SWB's performance. Some electrochemical experiments, such as galvanostic cyclic charge/discharge profiles and cyclic voltammetries, are carried out to assess the impact of the resistive and capacitive behaviours on the performance.

4.5.1 Galvanostic cyclic voltage profiles

In this work, four CCCs were studied: a commercial carbon felt (CCF), a heated commercial carbon felt (HCCF), an activated carbon felt (ACF) and a peanut-shell coated heated commercial carbon felt (PSCF). Figure 4.16 presents the galvanostic voltage profile of the full cell with CCF as the CCC.

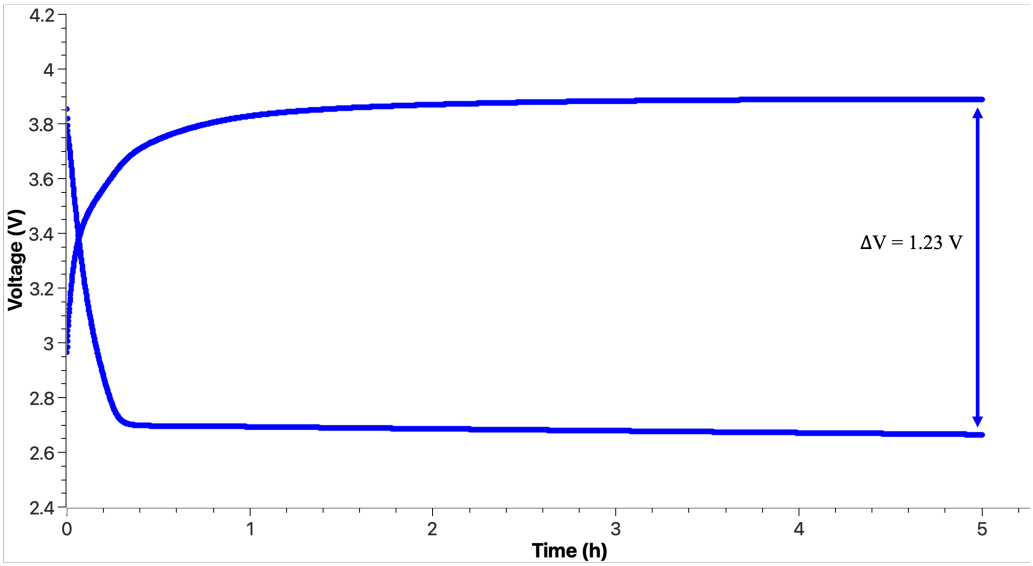

FIGURE 4.16: Galvanostic charge-discharge cycle of a SWB with CCF, at a current of 0.025 mA with a 5 hour duration.

CCF has a very small surface area of 0.6 $m^2\ g^{-1}$ and is coated with a polymer for mechanical reinforcement that covers some of the available active sites for the redox reactions and makes the surface of the material more hydrophobic. Figure 4.16 shows a voltage profile with a large voltage gap (1.23 V). In this profile, the plateau is reached very fast, both in charge and discharge, having a very high activation polarisation effect which is due to the kinetics of the electrochemical redox reactions. The plateau of a voltage profile can be described by the Ohm law when the resistance of the equivalent circuit becomes constant and it is associated with the ohmic polarisation effect, described in section 3.3.1.

The redox reactions taking place at the electrodes are the main working mechanism operating. The charging voltage profile ends at a voltage of 3.89 V, whereas the discharging one ends at 2.66 V. From section 2.2.4, we can conclude that the main reaction occurring during the charging process is the oxygen evolution reaction (OER, Equation 2.10) with a theoretical electrochemical potential of 3.48 V and with an overpotential of 0.41 V. The discharging process ends at 2.66 V. When compared to the theoretical value of the ORR reaction (Equation 2.10), we have an overpotential of 0.82 V, which is higher than that of the charge profile. It is common to observe a larger overpotential in the discharge profile when compared to the charge profile. The measured charge voltage was smaller than the theoretical ClER potential (3.94 V) suggesting that it did not take place.

CCC surface area can be greatly increased with a heat treatment that evaporates the mechanical reinforcement polymer. With the polymer gone, more active reaction sites will be available for the redox reactions to take place, but this increase of surface area can also result in the EDL formation, adding a capacitive behaviour to the performance of the SWB. The galvanostic voltage profile of the full cell with a heated commercial carbon felt (HCCF) is shown in Figure 4.17.

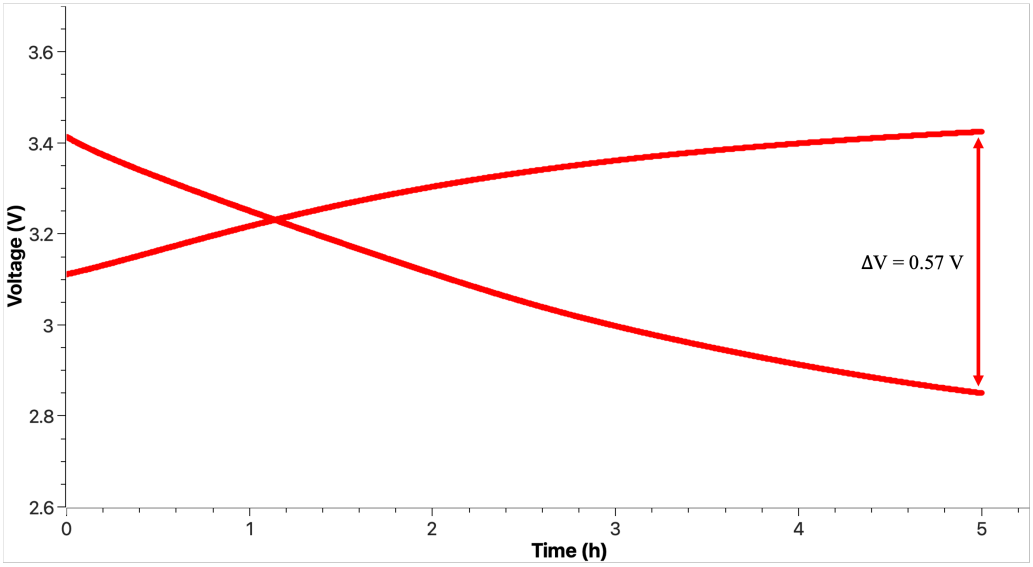

FIGURE 4.17: Galvanostic charge-discharge cycle of a SWB with HCCF, at a current of 0.025 mA with a 5 hour duration.

With the cycle in Figure 4.17 we can see that, improving the hydrophilicity of the cathode, improves its performance since it shows a much lower voltage gap (0.57 V) that is less than half of the one for CCF. The reduction of the hydrophobic behaviour of the CCC leads to the increase of its surface area, which means that more active sites will be

available for the redox reactions to take place. This improvement reduces the resistance of the CCC and, consequently, mitigates the slowness of the redox reactions which is verified when compared with Figure 4.16. With HCCF, the plateau did not fully form within the 5 hour charge. The charge profile ends at 5 hours with a voltage of 3.42 V whereas the discharge one ends with 2.85 V. From section 2.2.4 we can again conclude that the main reaction occurring during the charging process is the oxygen evolution reaction (Equation 2.10) with an electrochemical potential of 3.48 V, but this time our final charge voltage is smaller (3.42 V). Because of this, no overpotential can be calculated, and the reason for the final voltage of the charge profile being smaller than the theoretical one is that the plateau was not fully reached within the 5 hour charge. Once again, the obtained final voltage suggests that ClER did not take place during charge, as it is well below its theoretical value (3.94 V). The discharging process ends at 2.85 V. When compared to the ORR reaction (Equation 2.10), we have a overpotential of 0.63 V, which is lower than the overpotential observed in the discharge profile with CCF as the cathode current collector. The delay in plateau formation seen with HCCF could be due to the emergence of another working mechanism that complements the redox reactions and induces even further the reduction of the voltage gap and activation polarisation effect. This mechanism is due to the increase of the specific surface area that results in an added contribution of the EDL formation. With the two working mechanisms combined, the slowness of the redox reactions will be further mitigated by the storage of charges between the ions in the liquid and the surface of the CCC, forming the EDL. The slope associated with the activation effect when the capacitive behaviour is strong can be described by:

$$V = \frac{Q}{C} = \frac{1}{C}\int idt = \frac{I}{C}\cdot t, \tag{4.7}$$

where Q is the charge, C is the capacitance of the capacitor, and I is the current. We see that the voltage increases with time with a slope equal to I/C. The bigger the capacitive behaviour, the smaller the slope associated with the activation polarisation effect. So far, we are able to conclude that the combination of resistive and capacitive behaviours improve the performance of the battery.

The next cathode current collector is the activated carbon felt (ACF), which possesses very high surface area ($\sim 1300\ m^2\ g^{-1}$). This significant increase will result in even more active sites available for the redox reactions to take place and the EDL formation will

have a larger contribution in the performance. The profile of the full cell with a activated carbon felt (ACF) as the CCC is shown in Figure 4.18.

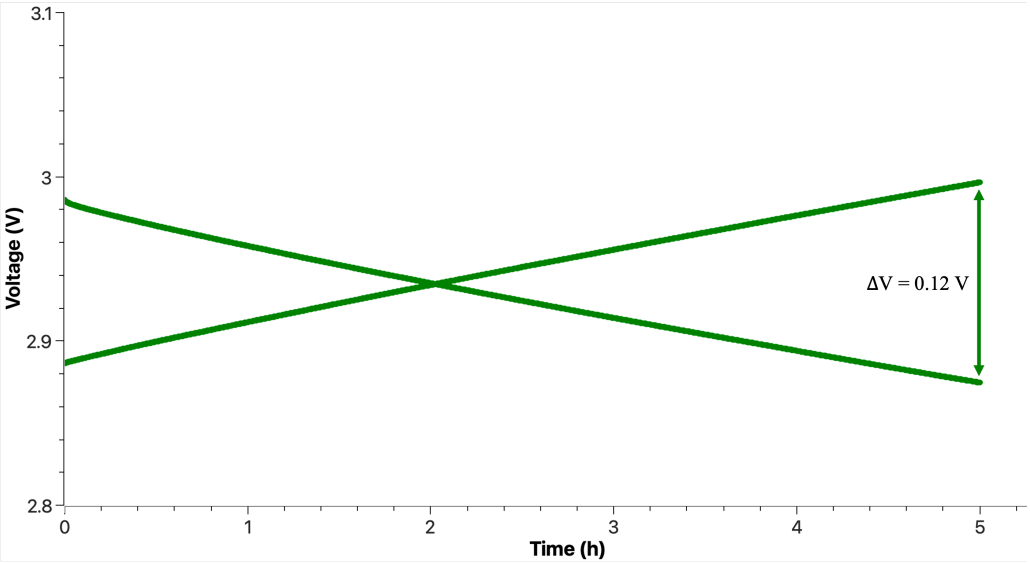

FIGURE 4.18: Galvanostic charge-discharge cycle of a SWB with ACF, at a current of 0.025 mA with a 5 hour duration.

The increase in surface area mitigates the sluggishness of the redox reactions because there are many more active sites available for them to take place, so there less accumulation of reactants on the surface of the CCC waiting to be able to react just because all the spaces are full. This enables the CCC to have many redox reactions taking place simultaneously, which improves the performance. This improvement is seen in the voltage profile of Figure 4.18, where we have a very small voltage gap of 0.13 V, that is about 10% of the CCF and 23% of the HCCF. The contribution of the EDL formation is bigger with a smaller slope (Equation 4.7) because of a higher capacitance of the equivalent capacitor. This indicates that the capacitive behaviour is more significant when using ACF. It is important to notice that we have chosen the same 10h charge and discharge time for all the cathodes. This is the appropriate choice to envisage the contribution of capacitive behaviour but not to analyse the final equilibrium potentials. The voltage gap calculated after 10h in all cells allows for the comparison of the contribution of the involved cell performance phenomena. The plateau formation is delayed not being seen within the 10 hour cycle. Although OER and ORR reactions are taking place, the strong capacitive effect impedes the comparison of the 10h final voltage with theoretical values since the cell starts the discharge and ends the charge before any plateau has been reached. Nevertheless, the charge profile ends at a voltage of 3.00 V, whereas the discharge one ends at 2.87 V.

The final voltage value ascribed to the discharge is similar to the obtained with the HCCF. The fact that the final charge voltage value is further bellow the theoretical than that of HCCF is another indication that there is a bigger capacitive behaviour present, delaying more the plateau formation. The final charge profile voltage of the cycle with ACF is even further away from the theoretical potential associated with ClER (3.94 V), so it is assumed that this reaction did not take place within the 5 hour charge that is being analysed.

Lastly, the fourth CCC studied was HCCF coated with an electrocatalyst made from peanut shells (PSCF). The peanut shell electrocatalyst was made and coated onto the surface of a heated commercial carbon felt. The galvanostic voltage profile of the full cell with PSCF as the CCC is in Figure 4.19. The peanut shell cathode results are currently being summarized in a paper in preparation [64].

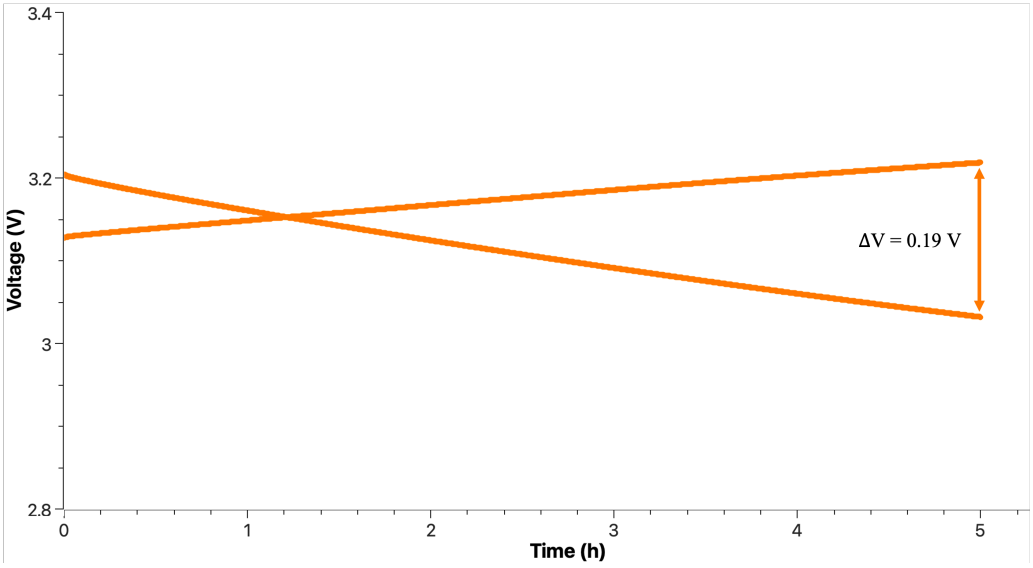

FIGURE 4.19: Galvanostic charge-discharge cycle of a SWB with PSCF, at a current of 0.025 mA with a 5 hour duration.

As we can see, the performance is improved just by adding a coating of carbonised and activated peanut shells onto a heated commercial carbon felt. When compared, the voltage gap of PSCF (ΔV = 0.19 V) is 67% smaller than that of HCCF (ΔV = 0.57 V), revealing an improvement in OER/ORR catalytic activity [7]. PSCF's voltage gap is comparable to that of ACF. The reduction of the voltage gap, in relation to HCCF, is due to the high porosity and abundance in surface-active oxygen functional groups that characterise the peanut shell electrocatalyst, which leads to an increase in surface area and in available active sites designated for the redox reactions to take place. Figure 4.20 illustrates the

manufacturing process of PSCF. During the carbonisation in an inert atmosphere the majority of oxygen and hydrogen is removed and defective carbon atoms are produced on aromatic (graphene-like) sheets while the remaining carbon atoms self-organise into a group and form aromatic sheets. Because some of these defective carbon atoms have unpaired electrons or unsaturated valences, they can interact with other heteroatoms (such as oxygen and hydrogen) to form different types of surface functional groups [34]. These abundant oxygen functional groups and defective carbon atoms can act as active sites for OER/ORR reactions [7]. The carbonised and activated peanut shell electrocatalyst possesses a micro-mesoporous structure that promotes ion absorption and transportation [9]. The electrocatalyst excellent ion transportability with a lower transfer resistance also leads to a strong contribution of the EDL formation, improving the performance of the SWB by increasing the capacitive behaviour. Another reason for this improvement is the fact that the electrocatalyst has a relatively high degree of graphitization and an ordered carbon structure that can shorten the diffusion path of ions at the electrode/electrolyte interface, promoting fast ion transfer [9]. The improvement of the electrochemical activity of OER/ORR because of the abundant oxygen functional groups and the defective carbon atoms plus the contribution of the EDL formation lead to the improvement of the performance of a SWB cell that uses PSCF [7].

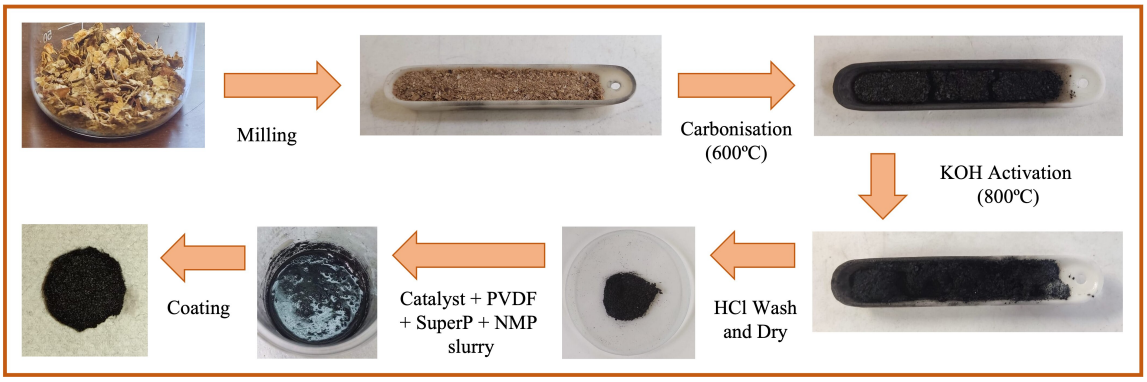

FIGURE 4.20: Schematic of the manufacturing process of the peanut shell electrode.

The charge profile ends at a voltage of 3.22 V, whereas the discharge one ends at 3.03 V. Because the final charge voltage value is less than 3.48, we can conclude that once again the plateau was not formed within the 5 hour charge. The fact that this value falls in the middle between the final charge voltage value associated with HCCF and ACF indicates that the delay of the plateau formation in the cycle with PSCF is larger than that of HCCF, but smaller than that of ACF. This suggests that the contribution of the EDL

formation that causes the delay of the plateau formation is smaller with PSCF than with ACF. The peanut-shell electrocatalyst improved the efficiency of the ORR reaction. All of these working mechanisms combined explain the reduced voltage gap and activation polarisation effect when compared to the HCCF, and the similar good performance in relation to ACF. In summary, Figure 4.21 shows all four galvanostic cycles for a more visual voltage gap and activation polarisation effects comparison.

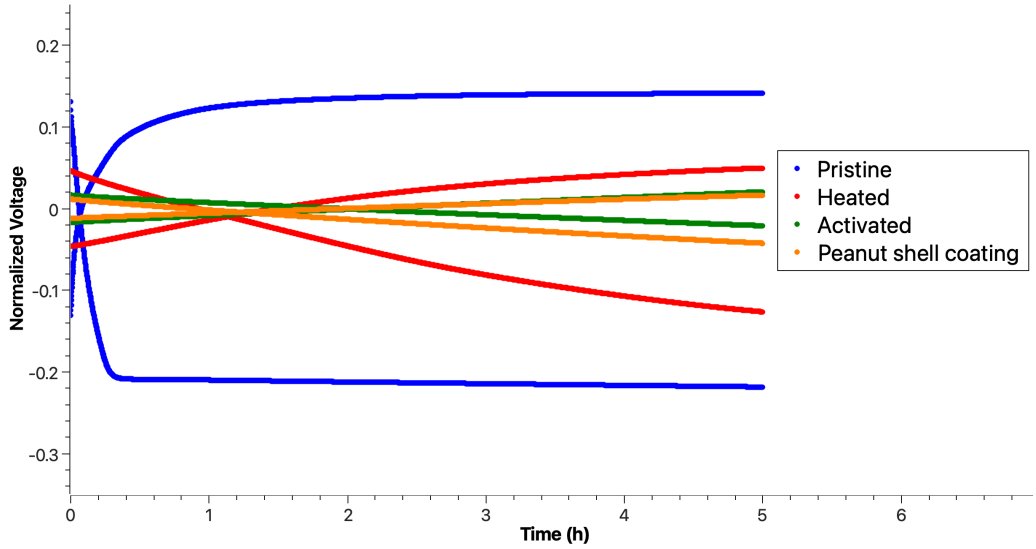

FIGURE 4.21: Galvanostic charge-discharge cycles of a SWB with the different CCCs, at a current of 0.025 mA with a 5 hour duration.

One clearly observes that there are differences in SWB performance between the four CCCs. The peanut shell electrocatalyst coated carbon felt shows a very good performance, being a promising candidate for seawater batteries as a replacement for the regular electrocatalysts that comprise expensive materials, such as Pt/C, RuO_2 and IrO_2 (mentioned in section 2.1.5), and presenting enhanced electrochemical performance, low activation polarisation effect, and low voltage gap [7].This can also be confirmed in Figure 4.22.

The shape of the continuous charge and discharge cycle can be an indicator of the electrochemical reversibility and capacitive behaviour during the SWB operation. The closer the shape of the cycle is to a symmetric triangle the better the electrochemical reversibility is, and its performance is closer to that of an ideal supercapacitor displaying good capacitive behaviour [6]. In a capacitor, the capacitance is constant meaning a constant slope in Equation 4.7 which explains the triangular shape characteristic of a capacitor cycle. Figure 4.22 shows the galvanostic charge-discharge cycles of a SWB with the different CCCs mentioned over the 10 hours.

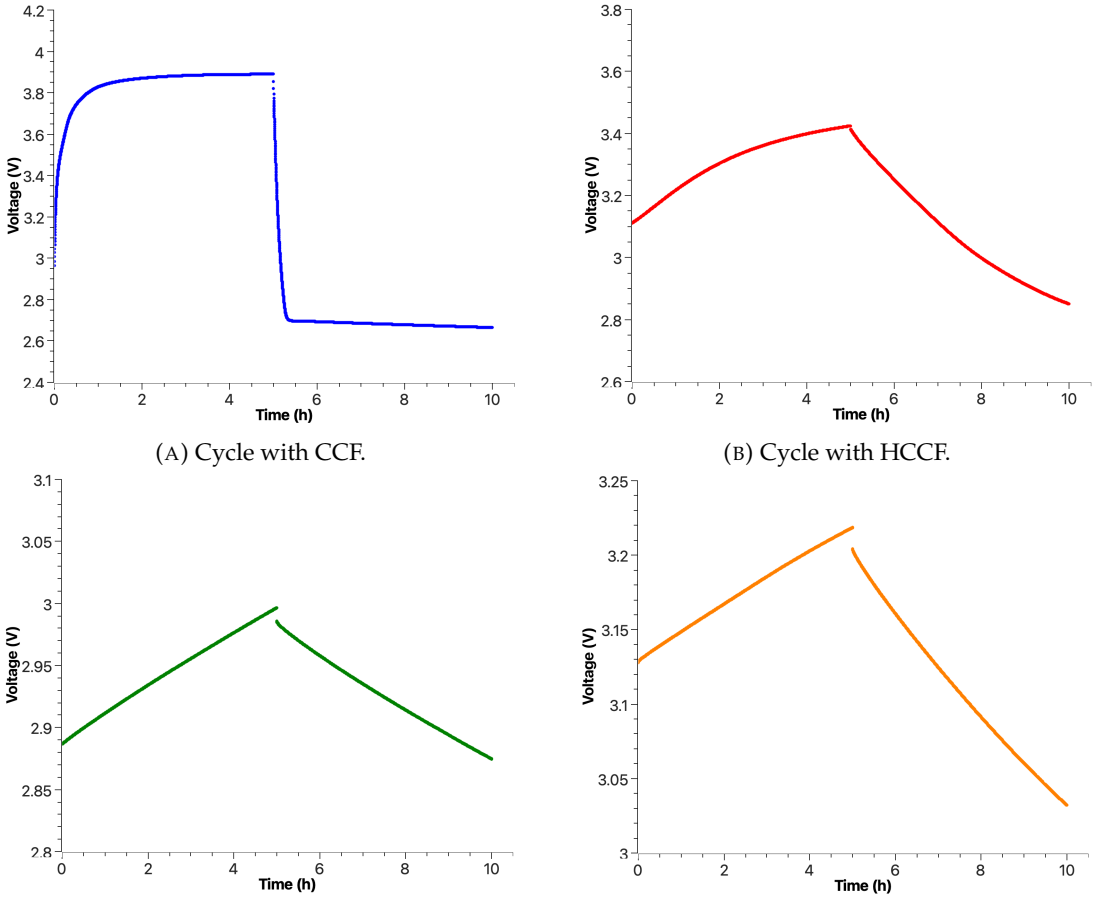

(A) Cycle with CCF.

(B) Cycle with HCCF.

(C) Cycle with ACF.

(D) Cycle with PSCF.

FIGURE 4.22: Galvanostic charge-discharge cycles of a SWB with the different CCCs, at a current of 0.025 mA over the 10 hour duration.

CCF (Figure 4.22a) is the one with a cycle shape further from a triangle and closer to the shape of a EES device with a predominant resistive behaviour (Figure 3.18b). The HCCF cycle is very similar to a cycle of a supercapacitor with distortion due to faradaic reactions (Figure 3.18c), indicating once more that HCCF is a combination of the two behaviours. Both ACF and PSCF present cycles with good electrochemical reversibility and big capacitive behaviour, as they have triangular-shaped cycles. This is in agreement with what has been observed so far, being that the ACF and PSCF are the ones with the larger capacitive behaviour.

4.5.2 Study on current variation

To further investigate the performance of a SWB with the different CCCs, galvanostic charge and discharge cycles were performed varying the current from 0.025 mA to 0.2 mA. This study was performed leaving out the commercial carbon felt without additional

treatment because its voltage gap is already large with the lower current applied. Figure 4.23 presents the results of the current variation in the SWB with the three different cathode current collectors. This study should be done sequentially from the smallest to the highest current in order to see the behaviour correctly like it is observed with HCCF (Figure 4.23a) and PSCF (Figure 4.23c), but unfortunately not with ACF. This was the first study performed and the currents were not applied sequentially, so in order to see the behaviour with ACF we normalised the cycles (Figures 4.23b and 4.23d). The normalisation is described by:

$$NV = \frac{V - AFV}{AFV}, \tag{4.8}$$

where NV is the normalised voltage, V is each voltage value and AFV is the average final voltage between the charge and discharge cycle.

Here, we have the expected behaviour in all three CCCs, where higher current results in an increase of the voltage gap and activation polarisation effect. It is also possible to observe in all three CCCs at a current of 0.2 mA, a plateau starts to form within the 5 hour charge/discharge, which was absent in lower currents. This behaviour is due to the increase of the resistance with current. As stated before, the redox reactions are a slow process and, with low currents, the reactions have more time to occur. When the current is increased, the time needed for the redox reactions to occur is the same but there is a much higher demand of electrons. Since the amount of active sites is the same with higher currents, there will be an accumulation of ions in the carbon matrix at higher current densities which results in the increase of the CCC's resistance [8]. The increase in the resistive behaviour is responsible for the increase of the voltage gap, the activation polarisation effect and the initial formation of the plateau within the 5 hour charge/discharge.

The SWB cell with HCCF starts to form a plateau in the charge within the 5 hours cycle after the current 0.1 mA, although being only at an early stage. The final charge voltages of all the applied currents are above the theoretical potential of 3.48, having an increasing overpotential with its biggest value at 0.2 mA. This charge ends at 3.79 V, having an overpotential of 0.31 V. The plateau formation is absent in the discharge profiles, where, at the highest current, there is no clear plateau formed. The same behaviour is overall observed, where all the discharges have a final voltage well below the theoretical value of 3.48 V. As it was seen before, the overpotential associated with the discharge is higher

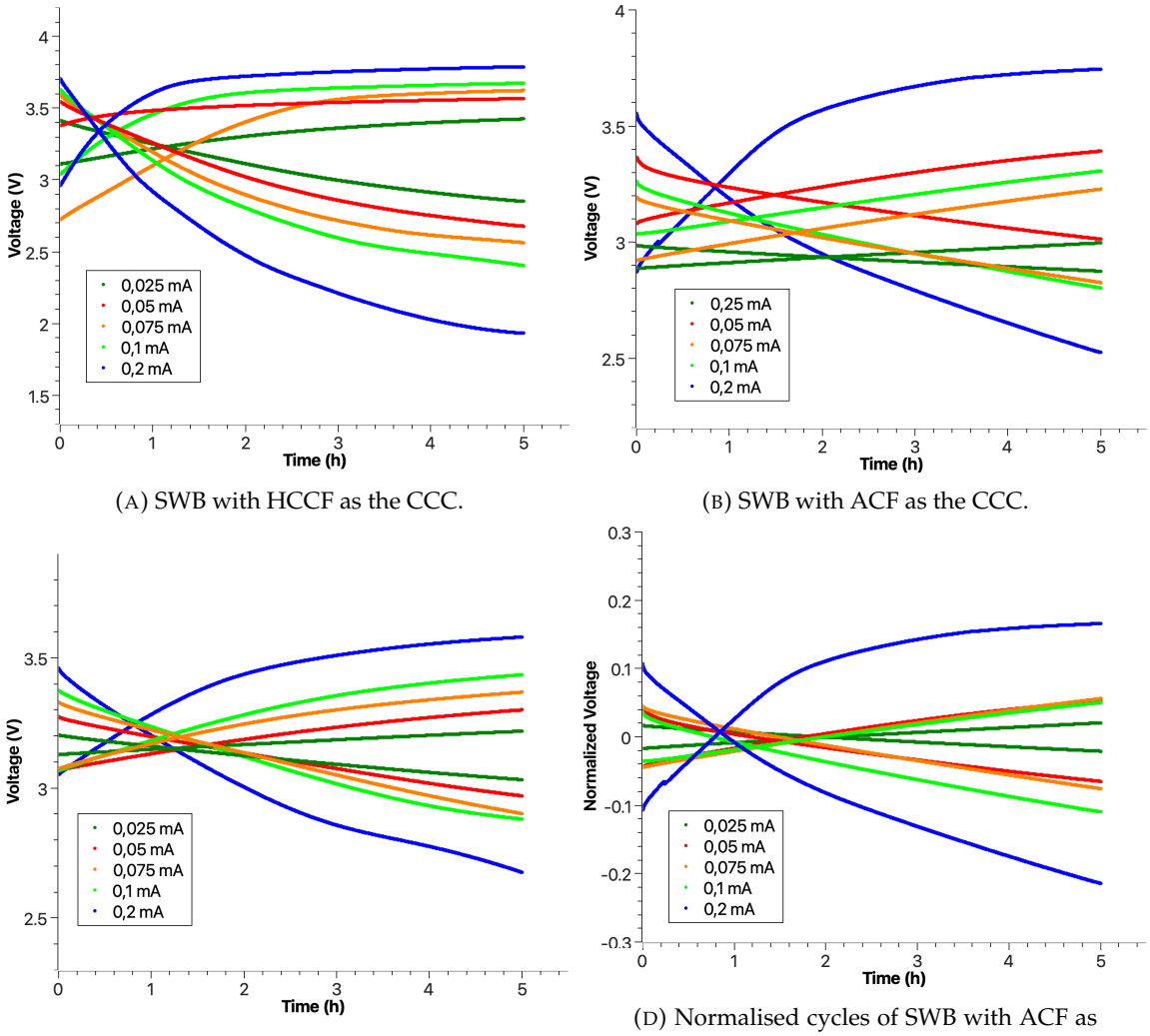

(A) SWB with HCCF as the CCC.

(B) SWB with ACF as the CCC.

(C) SWB with PSCF as the CCC.

(D) Normalised cycles of SWB with ACF as the CCC.

FIGURE 4.23: Galvanostic charge-discharge profiles of a SWB with the different CCCs at various currents over the 5 hour duration.

than the charge ones, also increasing with current, reaching its highest value at 0.2 mA. This discharge ends at 1.93 V with an overpotential of 1.55 V, being 80% higher than that of the charge.

The SWB cell with ACF starts to form a plateau in the charge within the 5 hours cycle only at the current 0.2 mA, although being only at an early stage. Unlike with HCCF, all the final charge voltage values, besides for 0.2 mA, are below the theoretical value of 3.48 V, needing more time to fully reach the plateau. The only cycle whose overpotential can be determined in the charge is the one with 0.2 mA, which ends at 3.75 V, having a similar overpotential of 0.27 V when compared to HCCF. Unlike with HCCF, all of the cycles, expect the one at 0.2 mA, have similar activation polarisation effects in charge and discharge. Nevertheless, all discharge profiles end at the 5 hour mark bellow the

theoretical value of 3.48, having the highest overpotential at 0.2 mA, where the discharge ends at 2.52 V with an overpotential of 0.96 V. The voltage value one cycle ends influences the voltage value where the next cycle begins and thus where it will end after 5 hours. In ACF the current variation study was not performed sequentially. For this reason, it is harder to clearly see the cycle evolution that can be seen with the other two CCCs. A normalised current was calculated for comparison reasons (Figure 4.23d).

Finally, we have the SWB cell with PSCF that only has one cycle with the plateau formation within the 5 hours at a current of 0.2 mA, much like ACF. The other cycles have the plateau formation more delayed. Similar to ACF, all of the cycles, expect the one for 0.2 mA, have similar activation polarisation effects both in charge and discharge. The charge for the cycle at 0.2 mA ends at 3.58 V, having an overpotential of 0.1 V. This is the smallest overpotential value for the charge of all three CCCs at 0.2 mA, but Figure 4.23c suggests that the plateau is not fully formed meaning that this value would increase if the charge duration was longer. Nonetheless, at the same time and current, the PSCF has the lowest overpotential. The same can be said for the discharge that ends at 2.68 V, having an overpotential of 0.83 V that it is also the lowest one when compared to the other two CCCs. But the discharge for 0.2 mA does not appear to have any plateau formation at the end of the 5 hour period, indicating that this overpotential value will increase if more time was given until the plateau was fully formed.

In order to further compare these three CCCs, a voltage gap comparison for the same 5h charge/discharge was performed (Figure 4.24).

The ACF and PSCF voltage gaps are always in the same order of magnitude except for the last current value (0.2 mA), where the voltage gap for PSCF (0.90 V) is considerably lower than that of the ACF (1.22 V). Even though this voltage gap does not correspond to the final voltage values of the plateaus fully formed, they allow to make a good comparison of the performance of the SWB cell with each CCC at a certain point in time that is the 5 hour mark. So far, these results confirm what was prior mentioned, that ACF and PSCF improve the SWB's performance.

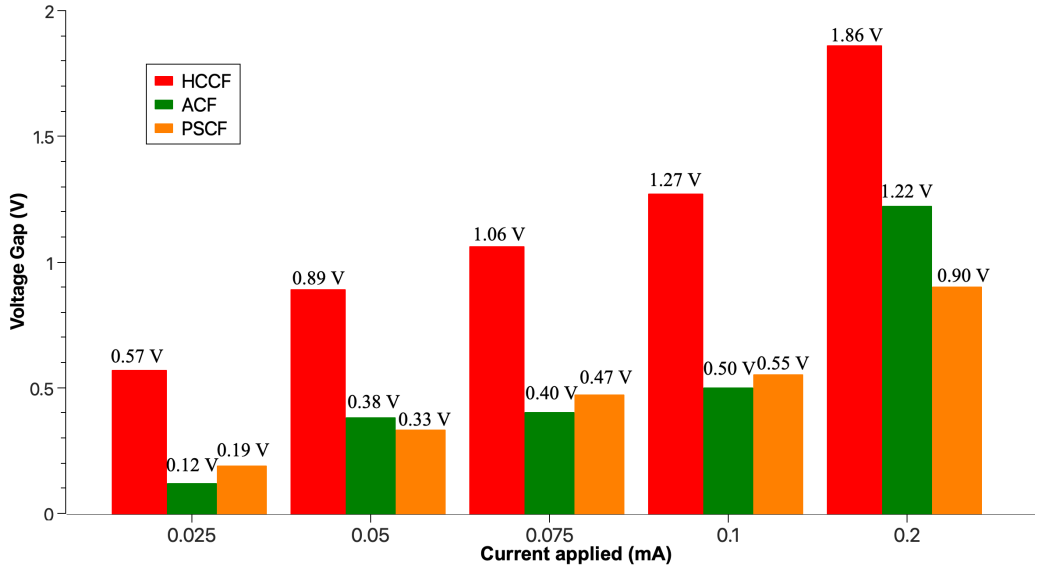

FIGURE 4.24: Voltage gap comparison of the SWB with the three CCCs charge/discharge cycles in Figure 4.23.

4.5.3 Cyclic voltammetry

Cyclic Voltammetry (CV) is a very powerful analytic tool that allows the analysis of complex electrochemical reactions, dynamics and behaviours. The cathodes capacitance analysis, limited to the full cell cyclic voltammetries and galvanostic charge cycles, is incomplete. It should be noted that there was a problem with the reference electrode which prevented us from performing impedance spectroscopy measurements on a three-electrode connection, in order to determine the equivalent circuit for the cathode and confirm the relative values of resistance and capacitance. These experiments are planned to be carried out soon. The capacitance analysis from cyclic voltammetries was carried out within the expected limitations. A CV was performed for each of the available options for the cathode current collector in a full cell configuration with the coin-cell as the reference. The CVs were all performed with the same parameters to facilitate the comparison between them, with a scan rate of 1.5 mV s^{-1} and a potential window from 2.5 to 4.0 V. Current density unit is presented, which is the current divided by the amount of active material in the coin-cell (36 mg of Na metal). Different potential windows should have been used in some cases, but for the sake of comparison, and since it was not possible to use a standard reference electrode for each cathode, we decided to keep the same potential window in the four cathodes. Figure 4.25 shows the CV for the SWB with a commercial carbon felt (CCF).

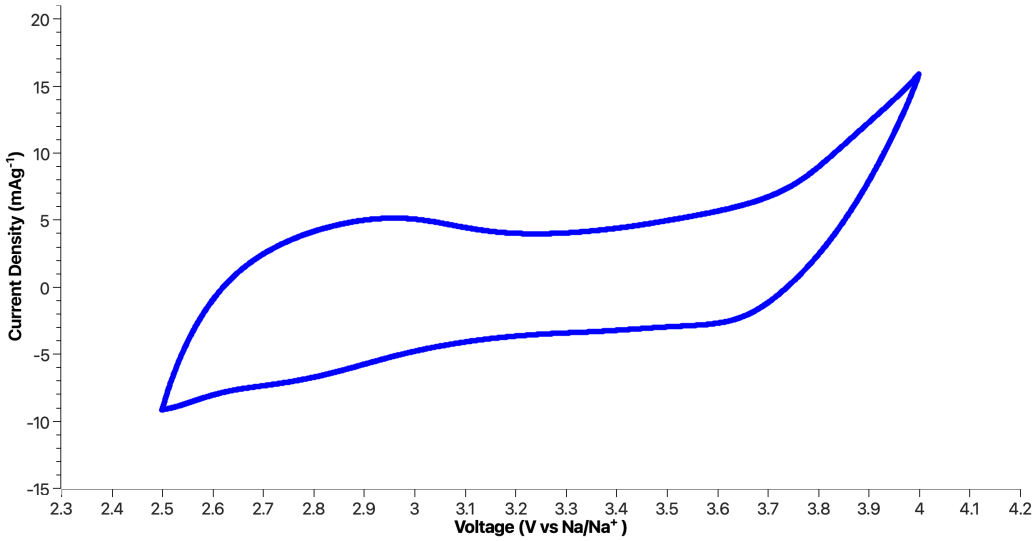

FIGURE 4.25: Electrochemical cyclic voltammetry of a SWB with CCF, at a scan rate of 1.5 mV s^{-1}.

During SWB battery operation we have faradaic and non-faradaic processes. The faradaic processes are the redox reactions OER/ORR, mainly. On the other hand, the non-faradaic processes can be due to the EDL formation, associated to the capacitive effect, or to resistance behaviours. In a faradaic process the charge transfer moves towards a constant value of voltage and composition, whereas in non-faradaic processes the charge is stored progressively [68]. With Figure 4.25 is possible to see that there are no main redox reactions within the electrochemical stability window (ESW). This window is delimited by the onset potentials associated with the OER/ORR reactions. The onset potential is the threshold where a large current increase is measured once the voltage passes a certain value. In other words, over this specific applied voltage, the electrochemical reaction is driven at a higher rate [69]. Outside of the ESW, the catholyte starts to decompose, which corresponds to the OER/ORR reactions. A SWB with a CCF as the carbon current collector possesses a very small current area within the ESW. This area could be due to small redox reaction peaks with low intensity, making harder to identify them, or to a very small contribution of an EDL formation. Possibly, the small current area within ESW is due to a combination of both because of the analysis performed to the galvanostic charge/discharge cycle of a SWB cell with CCF (Figure 4.16), where a negligible capacitive behaviour was observed. The main working mechanism is the OER/ORR reactions whose onset potentials are 3.75 V and 2.7 V, respectively. The CV of CCF can be seen as a combination of a typical resistive CV (Figure 3.20b) and a typical CV of a supercapacitor with faradaic reactions (Figure 3.20c), having a very small capacitive effect, being mainly resistive, which

once again is in agreement with the galvanostic charge-discharge cycles. The CV associated with CCF reaches very low current densities, being the potential window limits -9.1 mA g^{-1} at 2.5 V and 15.9 mA g^{-1} at 4.0 V, which further indicates a strong resistive behaviour because high potential and resistance values mean low current density.

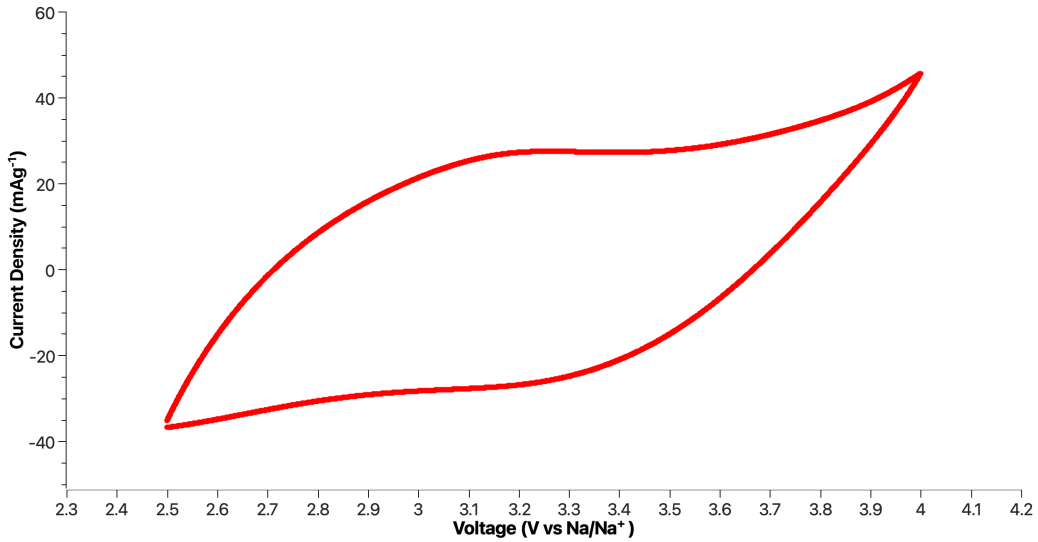

FIGURE 4.26: Electrochemical cyclic voltammetry of a SWB with HCCF, at a scan rate of 1.5 mV s^{-1}.

The CV for the SWB with the same cathode current collector but with the additional heat treatment applied (HCCF) is shown in Figure 4.26 and presents a similar behaviour to that of CCF but augmented. The HCCF presents a hybrid behaviour, combining capacitive and resistive alike. Here we have a strong contribution of the OER/ORR activity and a strong contribution of the EDL formation. Besides the OER/ORR reactions, we are mainly dealing with non-faradaic processes as no reversible or irreversible reaction peaks are observed. In this CV the onset potentials that delimited the ESW and indicate the start of the decomposition of the catholyte through OER/ORR reactions are harder to identify, when compared to the previous CV. In order to better identity them a smaller voltage window is needed, but the CV suggests that the onset potentials for OER/ORR are 3.3 V and 3.1 V, respectively. The onset potentials decreased when compared to CCF which could indicate an improvement of the electrochemical activities towards the OER/ORR. This behaviour is very similar to that of a supercapacitor distorted with faradaic reactions (Figure 3.20c). With just an additional heat treatment, it is already noticeable a big difference in terms of the obtained current density range. The CV for a SWB with HCCF (Figure 4.26) presents a large current area, ranging from 27.8 to -27.8 mA g^{-1}. This increase in the current area is caused by the increase of the specific surface area that led to an increase in

available active sites, promoting the EDL formation and the efficiency of the OER/ORR activity. The initial and final peaks associated with the catholyte decomposition are also higher, where the peak associated with ORR reaches -36.1 mA g^{-1} at 2.5 V and the peak associated with OER reaches 44.4 mA g^{-1} at 4.0 V. This indicates a decrease in the resistive behaviour when compared to CCF because, at the same potential values, the current density is higher. The CV with HCCF allows to conclude that this CCC facilitates the combination of the electrochemical processes of EDL formation and OER/ORR activity resulting in the improvement of the SWB's performance due to its hybrid energy storage system behaviour [39].

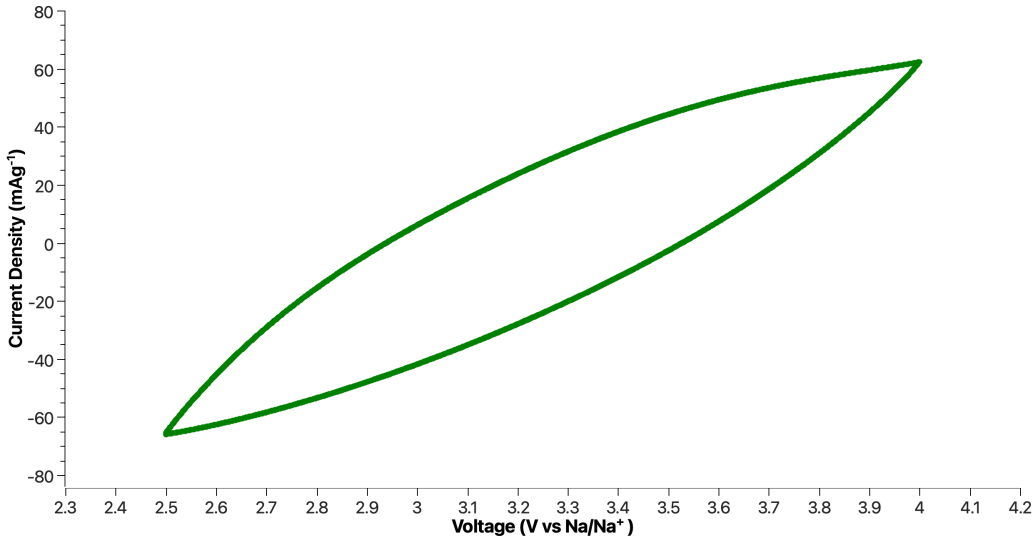

FIGURE 4.27: Electrochemical cyclic voltammetry of a SWB with ACF, at a scan rate of 1.5 mV s^{-1}.

The CV of a SWB using a ACF as the CCC is shown in Figure 4.27. The shape of the ACF's CV is substantially different from the previous two. It was expected that because, of the significant increase of surface area and capacitive behaviour, the CV would be closer to a rectangle, much like Figure 3.20a, being the shape associated to typical supercapacitors. Instead of this, the shape is closer to a resistive CV (Figure 3.20b) but with a much higher current area. In this CV it is even harder to identify the onset potentials associated with the faradaic reactions. This suggests that the increase in the specific surface area was so large that the capacitive behaviour also increased significantly, making it hard to identify the characteristics of the resistive behaviour associated with the OER/ORR activities. Another indication that supports this possibility is the fact that the CV reaches even higher current densities. The CV's extremities are -63.9 mA g^{-1} at 2.5 V and 61.1 mA g^{-1}

at 4.0 V. At the same voltage value, the current density is much higher, indicating that, at those current density values, the resistance due to the OER/ORR activity is lower.

Nonetheless, the pseudo-oval shape of this CV curve indicates that there is in fact an extra resistive component that is not associated with the faradaic activity, besides the capacitive component derived from the EDL formation, which causes the CV to be tilted and smoother, looking like an oval. The presence of this extra resistance that is not observed in the previous two CCCs can have two reasons. The first is the fact that the used activated carbon felt was thinner than the remaining CCCs, so to ensure electrical contact with the titanium string in the testing kit, three layers of activated carbon felt were used reaching a similar thickness to that of CCF and HCCF. This extra two layers increase the resistance of the cathode current collector. The second reason is related to the wettability of the CCC. As mentioned before, the wettability of the ACF remained constant with the cell operation, which did not happen with the CCF and HCCF, who became very hydrophilic after usage. The ACF has poorer wettability when compared to CCF and HCCF, adding an extra resistance component. Although this extra resistive component changes the CV's shape to a pseudo-oval [70], it still presents a significant capacitive contribution that is responsible for the low voltage gaps and activation polarisation effects obtained.

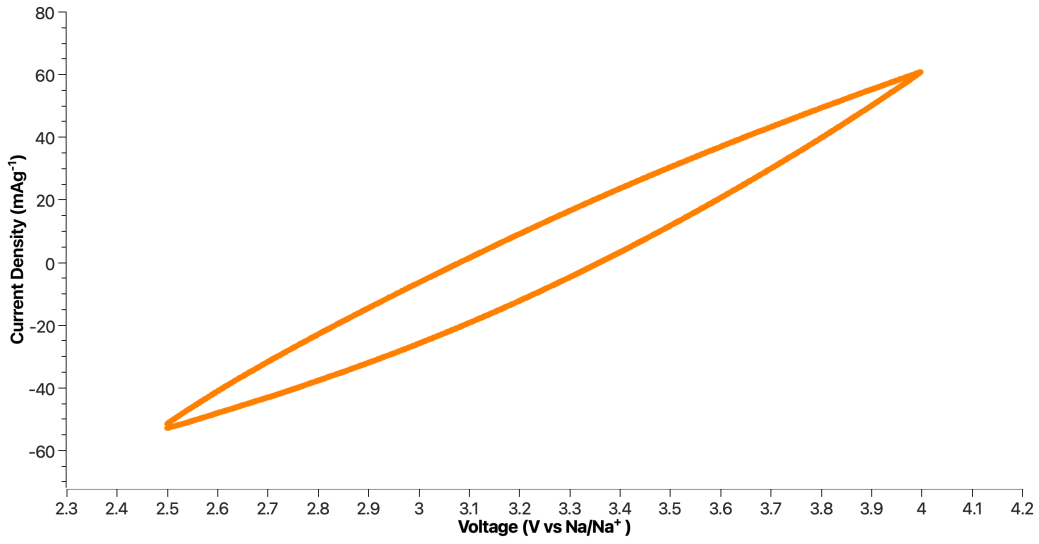

FIGURE 4.28: Electrochemical cyclic voltammetry of a SWB with PSCF, at a scan rate of 1.5 mV s^{-1}.

Finally, Figure 4.28 shows the CV for the SWB with the peanut shell coated carbon felt as the CCC. The CV with the peanut shell cathode carbon collector is similar to that of ACF with the same difficulty in determining the onset potentials that would define the

ESW, differing only by having a smaller current area. The pseudo-oval shape again indicates that a resistive component exists besides the capacitive one. In the case of PSCF such resistive component could be due to four different possible reasons. The first being relative with the electrocatalyst coating itself. Even though the peanut shells were carbonised and activated at high temperatures to ensure a high level of graphitization and a good electrical conductivity, the electrocatalyst has other components that cause its resistance to increase. It was done by mixing the carbonised and activated peanut shells with PVDF, SuperP black carbon and NMP. PVDF is naturally an insulator which increases the resistance of the coating. SuperP black carbon is added to mitigate this increase of resistance. The NMP present in the mixture will be evaporated before the cathode current collector is finalised. Nevertheless, some of the NMP may still remain after the drying process. When a solution of PVDF and NMP comes in contact with water, they transform into a gelatinous, hydrophobic and insulating film. The electrocatalyst manufacturing process tries to make sure that these possibilities are mitigated, but some of them may still remain. The second reason is associated with the (38 %) thickness increase due to the addition of the electrocatalyst to the HCCF, which will decrease the capacitance of the EDL formation, as can be seen in Equation 2.6. The third reason behind the extra resistance component could be the carbonisation temperature of the peanut shell electrocatalyst manufacturing process (600ºC). Literature states that carbonisation temperatures below 500ºC can reduce the conductivity of the activated carbon material, which is what happened with the peanut shell electrocatalyst produced [34]. In order to confirm this hypothesis, a part of the prospective work will be to test the electrochemical performance of the peanut shell electrocatalyst at different carbonisation temperatures. The fourth reason could be related to the interface between the electrocatalytic and the HCCF where it is deposited. One way to minimise the resistance of this interface will be to improve the degree of volumetric mixing in the synthesis process.

The obtained CVs are in agreement with what was stated in section 4.5.2, again indicating that the EDL formation has a strong contribution in galvanostic charge-discharge cycles (Figure 4.23). Figure 4.19 also suggested that the smaller plateau formation delay, when compared to ACF, was due to a smaller contribution of the capacitive effect, which is also corroborated by the PSCF CV's analysis.

In Figure 4.28 we can see that although having a smaller current area when compared to that of ACF, PSCF's CV reaches high current density values, higher than HCCF. This

means that, even though the EDL contribution is smaller, the high surface area and porosity supply enough active sites to decrease the resistance associated with OER/ORR reactions, being the current density limits of -52.8 mA g^{-1} at 2.5 V and 61.1 mA g^{-1} at 4.0 V.

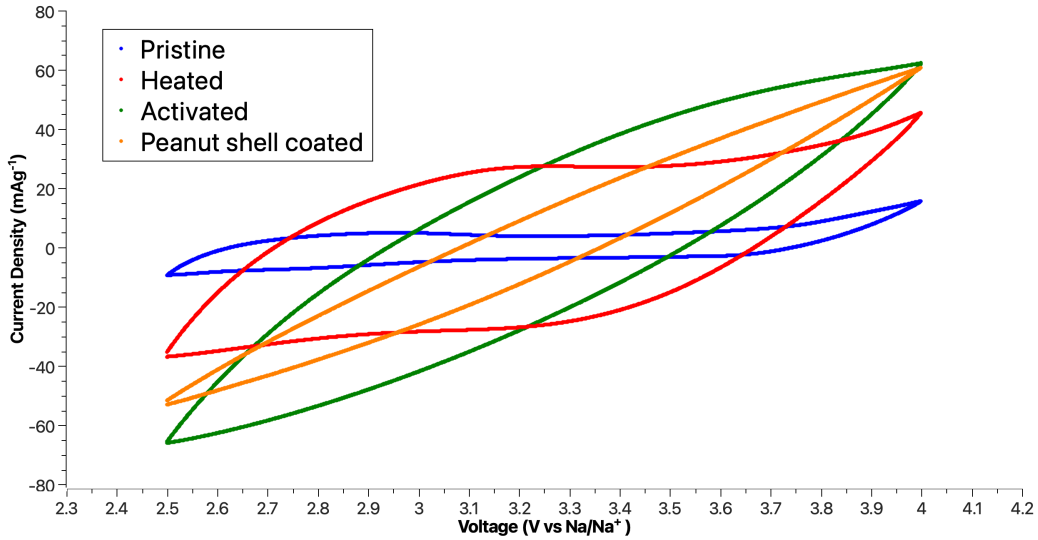

FIGURE 4.29: Comparison of all four CVs.

With all of the CVs presented in Figure 4.29, it is easier to see the significant differences in terms of current area and range. The CV relative to CCF has a current area negligible compared to the areas of the other three. The ACF and PSCF CVs are the ones with the largest current density range, larger than HCCF and much larger than CCF. The analysis of electrochemical behaviour from galvanostic cycles and cyclic voltammetries of the full cells, although limited, allowed to verify the possibility of using a bio-waste carbon with an annual waste of several tons and also demonstrate its good performance.

4.5.3.1 Gravimetric capacitance quantification

From the CVs it is possible to evaluate and compare the gravimetric capacitance. As previously mentioned, this analysis should be done with a three-electrode connection measurements and electrochemical impedance spectroscopic analysis to infer the respective equivalent circuit. Since the ACF and PSCF are the ones that present mainly a capacitive behaviour, this study will only be performed on them. Two methods were applied to quantify the gravimetric capacitance of a CV curve, which can be defined by:

$$C = \frac{Q}{mV}, \tag{4.9}$$

where C is the gravimetric capacitance, Q is the amount of charge, V is the voltage window (1.5 V) and m is the mass of the active material, which in this case is going to be the mass of the metallic sodium in the anode (36 mg), given that the cells were not charged for very long periods in this analysis. The first method is by using the average current level of the CV curve region with higher current area, using the following equation:

$$C = \frac{Q}{mV} = \frac{It}{mV} = \frac{I}{m\frac{dV}{dt}}, \tag{4.10}$$

Cathode Current Collector	ACF	PSCF
Average Current (mA)	1.2112	0.6557

TABLE 4.2: Average currents of the CVs for ACF and PSCF.

where I is the average current level of the higher current area, that is presented in Table 4.2 for ACF and PSCF, and $\frac{dV}{dt}$ is the scan rate used in the cyclic voltammetry (1.5 mV s^{-1}). The second method uses the area within CV with the following equation:

$$C = \frac{Q}{m\Delta V}, \tag{4.11}$$

where ΔV is the voltage window used in the cyclic voltammetries. The amount of charge, Q, is given by the area within the CV curve and can be obtained using Gamry potentiostat analysis. Figure 4.30 shows the areas of ACF and PSCF, and Table 4.30 has each value.

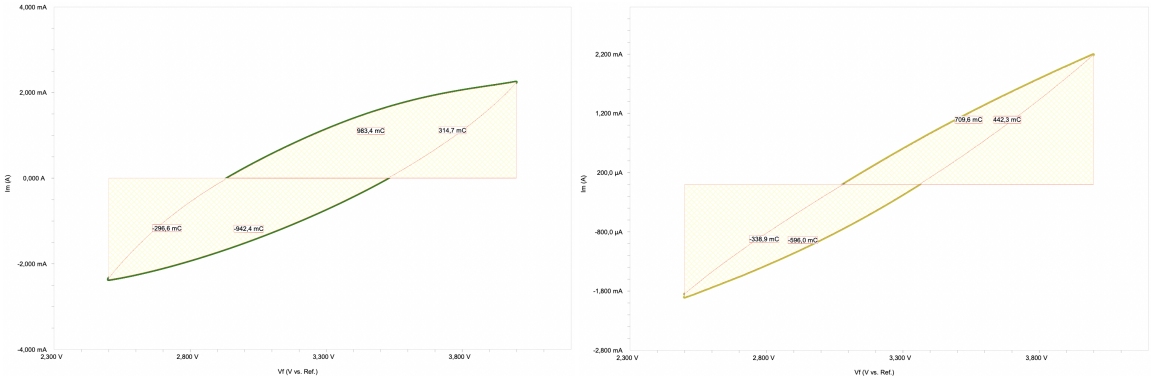

(A) (B)

FIGURE 4.30: Areas associated with ACF (A) and PSCF (B).

By applying the Equations 4.10 and 4.11, the gravimetric capacitance was determined by the two methods. The results are presented in Table 4.4.

Cathode Current Collector	ACF	PSCF
Current Area (mC)	1314.5	524.4

TABLE 4.3: Areas associated with ACF and PSCF.

Cathode Current Collector	Gravimetric Capacitance (Fg^{-1})	
	Average Current	Current Area
ACF	22.43	24.34
PSCF	12.14	9.7

TABLE 4.4: Gravimetric capacitance of the full seawater cell with ACF and PSCF calculated with the two methods.

The obtained values seem low, but they do not represent the specific gravimetric capacitance of the two CCCs but of the full cell, as these CVs were obtained with a two-electrode method. Thus, they can only be used for comparison reasons. The gravimetric capacitance of PSCF is lower than that of ACF in both methods which is in agreement with the analysis made so far of the galvanostic charge and discharge cycles and of the CVs. The ACF has a predominant capacitive behaviour resulting in a good performance of the seawater cell. This comparison indicates that, even though the research process around the application of PSCF in SWB is still in early stages, the synthesised peanut shell electrode achieves a gravimetric capacitance value close to that of ACF, whose manufacturing process has already been optimised. This is also suggested by the good performance seen in the analysis of the galvanostic charge and discharge cycles and CVs with PSCF as the cathode current collector.

Combining all the analysis of the results obtained so far in terms of the SWB performance with the different cathode current collectors, we are able to conclude that the introduction of a capacitive behaviour leads to an improvement of the performance, resulting in lower voltage gaps and activation polarisation effects. The utilisation of a hybrid energy storage system can be done using a cathode current collector already with supercapacitor-like characteristics or by using a normal carbon felt and subjecting it to a heat treatment. We were also able to achieve a very good SWB performance using a waste product as the main material to manufacture a peanut shell electrocatalyst, that, to the best of our knowledge, had not been done in the literature. The possibility to use a waste product to improve the performance of the SWB increases the sustainability of the battery

for large scale applications.

Chapter 5

Conclusions and prospective Work

In this research work, the performance of a seawater cell employing cathode current collectors with different characteristics was studied and analysed. The cathode current collectors used were a commercial carbon felt, pristine and with a heat treatment applied, an activated carbon felt and a peanut shell electrocatalyst carbon felt.

The surface morphology and wettability of each cathode current collector was analysed. The morphological and chemical analysis of the CCCs allowed to know the diameter and distributions of the carbon fibres, being all non-organised. The activated carbon felt has smaller fibres but, in more quantity, when compared to the commercial and heated carbon felts. SEM and EDS analysis allowed to conclude that the evaporation of the polymer meant for mechanical reinforcement present in the commercial carbon felt increased the specific surface area and porosity of the material and that the degree of NaCl deposition on the fibres was dependent on whether the polymer was present. This conclusion was then associated with the wettability analysis, where we were able to conclude that the amount of deposited NaCl influenced the wettability and hydrophilic behaviour of the pristine and heated commercial carbon felts. It was seen that the wettability of the CCF and HCCF improve a lot with their utilisation, which did not happen for the activated carbon felt where the wettability remained constant, being the CCC with the poorest wettability.

The peanut shell electrocatalyst was also analysed in each main phase of the manufacturing process and in the finalised electrode stage. We were able to conclude that the natural structure of the peanut shells was preserved throughout the crushing, carbonisation and activation processes, where the intricate network of channels connected with each other was present in the finalised electrode. This cathode current collector showed

good wettability due to the high amount of surface-active oxygen functional groups that were originated during the activation process.

The commercial carbon felt was used to access the stability of the seawater cell which was confirmed over at least 25 cycles of 10 hours each. A detailed analysis was done of each CCC galvanostic charge and discharge cycles used. The commercial carbon felt was the one with the worst performance, with the highest activation polarisation effect, voltage gap and overpotentials when compared with the theoretical potential of the reaction taking place. It was confirmed that the heat treatment applied improved the performance of the seawater due to the increase in surface area which resulted in lower voltage gaps and activation polarisation effects. The contribution of the EDL formation and the improvement of the OER/ORR activities created a hybrid energy storage system with improved performance. This improvement was more significant with the activated carbon felt, where the specific surface area was much bigger resulting in much lower voltage gaps and activation polarisation effects and an even more delayed plateau formation.

PSCF also showed great performance, with voltage gaps and activation polarisation effects similar to that of ACF. This improved performance is due to the combination of the EDL formation and the enhancement of the OER/ORR efficiencies because of the high specific surface area, porosity, and the abundance of oxygen functional groups and defective carbon atoms. The conclusions stated so far were further confirmed by the current variation study. Cyclic voltammetry analysis was performed for each cathode current collector. The results helped to confirm the analysis made in the galvanostic charge and discharge cycles. The commercial carbon felt presents a mostly resistive behaviour with a small current density area, that was increased by heat treatment. ACF and PSCF showed close gravimetric capacitance. The fact that the PSCF had a lower gravimetric capacitance than ACF confirmed that the small voltage gaps seen in the galvanostic charge/discharge cycles are due to a big contribution of the EDL formation and also to an improvement in the OER/ORR efficiencies related with the abundance of oxygen functional groups and defective carbon atoms.

This research work allowed the comparison of four different cathode current collectors, being the bio-waste PSCF the newly synthesised one. We were able to conclude that the application of a peanut shell electrocatalyst to a seawater battery is possible with good performance. Bio-waste PSCF is a low-cost electrode, with low carbon footprint and facile manufacturing. Nonetheless, the peanut shell coated electrode research is in the

beginning.

Throughout the dissertation, this work was presented in the following meetings and article:

- IJUP'22 - 15th Meeting of Young Researchers of University of Porto, in Porto, Portugal, with oral presentation in the session 'Environment' named "Rechargeable sodium seawater battery with optimised cathode", with abstract printed in book of abstracts.
- ANM'22 - 20th edition of the conference about Advanced Nano Materials, in Aveiro, Portugal, with oral presentation in the session "Alternative Energy Materials (AEM)" named "Capacitive effect in rechargeable sodium seawater batteries", with abstract printed in book of abstracts.
- Física'22 - 23rd National Physics Conference, in Porto, Portugal, with oral presentation in the session "Energy and Applied Physics" named "Capacitive effect in rechargeable sodium seawater batteries", with abstract printed in book of abstracts.
- PRODEF Day'22 - 1st meeting of Engineering Physics Doctoral Program students, in Porto, Portugal, with oral presentation named "High porosity carbon cathodes for seawater batteries".
- "High Porosity High Porosity Bio-waste Electrocatalyst for Seawater Batteries" [64], an article about the results obtained with the peanut shell cathode that it is still in preparation.

5.1 Prospective work

Future work should focus in the optimisation of the manufacturing process of the peanut shell electrocatalyst. One of the ways to achieve this optimisation is by varying the quantities of the components that compose the slurry that will later be coated onto the heated carbon felt and then analyse them to determine the component ratio that produces the best results. This was already done, but with only three sets of different amounts and more variations should be tested. The carbonisation temperature of the peanut shells electrocatalyst manufacturing process should also be varied and studied, since in this work 600ºC

was used and the conductivity of the electrocatalyst was compromised due to it still being a low carbonisation temperature. An optimal carbonisation temperature should be obtained by increasing it and then study the produced performance.

Besides the optimisation, future work should also focus on a more detailed characterisation of the electrochemical performance of the peanut shell electrocatalyst electrode and also the other three carbon felts. A more detailed study of the morphology of the carbon current collectors should be done involving N_2 absorption-desorption isotherms to evaluate specific surface area and porosity of the CCCs, specially PSCF, and the estimation of pore size distribution by density functional theory (DFT) method. This analysis will allow us to better characterise the materials and determine their volumetric capacitance. The performance of the seawater battery with the different cathode current collectors should also be further analysed by employing a three-electrode system to perform cyclic voltammetries and electrochemical impedance spectroscopy and obtain the equivalent circuit of the electrodes. This electrochemical characterisation methods will give us more accurate information about the resistance and capacitance of the cathodes current collectors. Cyclic voltammetries with both two and three electrode systems should be performed varying the scan rate and the potential window.

An additional study should also be done in an economic and environmental point of view, to access the carbon footprint of the seawater battery with the peanut shell coated electrode, its total manufacturing process cost and the recyclability of the materials composing the seawater battery.

5.2 On going work

In parallel to this study, the analysis of carbonaceous cathodes produced by electrospinning was initiated. The cathode optimisation is being done by removing the binder PVDF from the electrocatalyst as it is a natural insulator. In particular we intend to ally electrospinning deposition technique to the peanut shell electrocatalyst. Electrospinning is a quick and inexpensive method to create self-supported webs made of continuous ultrafine carbon fibres using a suitable precursor solution to create polymer fibres with submicron diameter. The conditions in which the electrospinning deposition takes place can be controlled to ensure a wanted outcome. The properties of the precursor solution and the thermal treatment can influence the flexibility, fibre diameter, surface area, porosity, and the electrical conductivity of the electrospun carbon fibre webs [71].

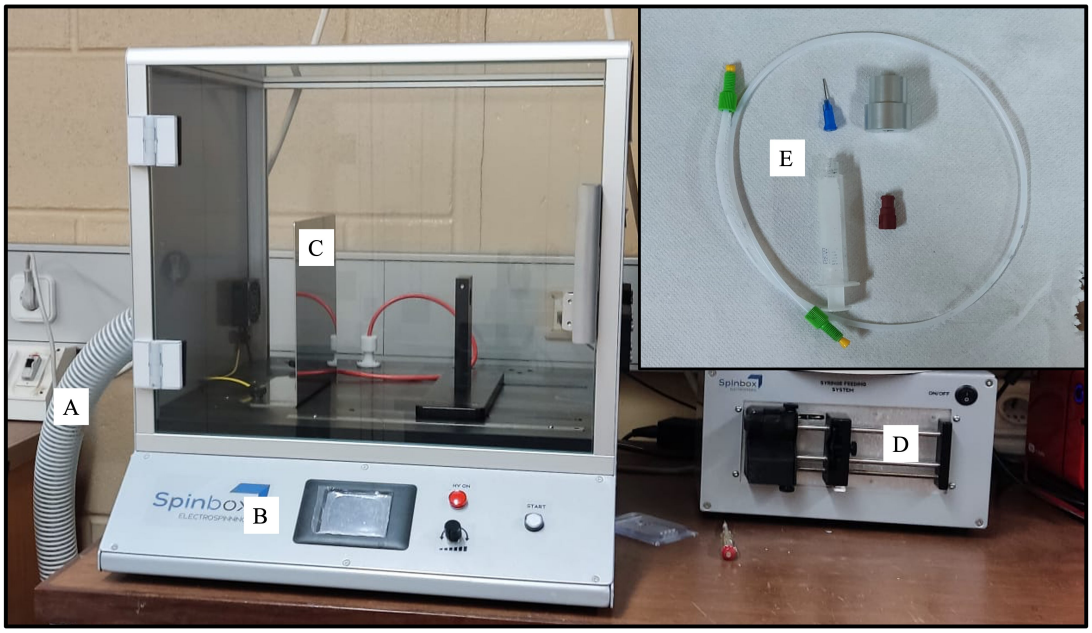

FIGURE 5.1: Electrospinning machine and its components: exhaustion tube (A), control panel (B), collector plate (C), pumping system (D), and solution feeding system (E).

Figure 5.1 shows the three main components of an electrospinning setup, which are a high voltage power supply (B in Figure 5.1) , a syringe and a spinneret (E in Figure 5.1), and a grounded collector (C in Figure 5.1).

The electrospinning technique is based on a drop of polymer solution on the tip of a spinneret being subjected to an electric field. The surface of this drop elongates to take a conical shape known as the Taylor cone as the strength of the electric field increases. The repulsive electrical forces overcome the surface tension of the drop when the applied electric field reaches a critical value, causing a charged jet of the solution to be ejected from the cone's tip and accelerated downfield. Between the tip and the collector, an electrohydrodynamic whipping instability of the jet develops, causing further liquid filament stretching and solvent evaporation to produce solidified continuous, micro- or nanofibres on the grounded collector. Electrospinning has a number of benefits, including ease of operation, effectiveness, affordability, and high yield. The nature of electrospinnable materials, as well as the various fibre assembly and design configurations, are examples of how versatile electrospinning is [71]. The electrospinning machine was purchased about a year ago. The first months of this work consisted in the familiarisation with the operation of the new machine and electrospinning technique.

The initial chosen concentration for the electrospinning solution was 10w/w% of PAN (polyacrylonitrile) in DMF (dimethylformamide), which provided a good combination

of mechanical and morphological properties, according to literature [72]. But with this concentration, the deposition was harder and made the cleaning process of setup very difficult due to the coagulation of the solution in the feeding tube because it was very viscous. To solve this problem, the concentration was reduced to 8w/w% PAN/DMF. The solution is achieved by mixing 8 g of PAN with 10 mL of DMF and magnetically stirring the solution for 1h at 60ºC and 600 rpm [72]. This procedure must be done inside an hotte with extraction due to the toxic nature of DMF. The electrospunned mats obtained were always very thin, not having enough thickness and mechanical resistance to act as the cathode current collector for a seawater cell, so the goal with the electrospinning technique became to coat an electrocatalyst onto the surface of a carbon felt. After some depositions meant for the electrospinning parameters optimisation, we were able to do the deposition shown in Figure 5.2.

(A) PAN deposition.

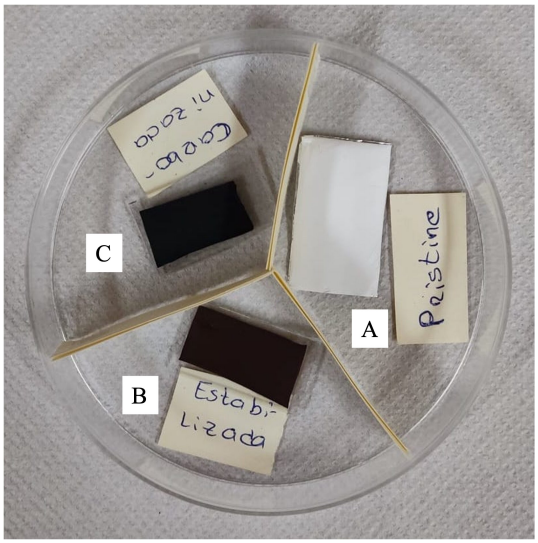

(B) Same PAN deposition in different stages, pristine (A), stabilised (B) and carbonised (C).

FIGURE 5.2: PAN deposition and subsequent treatments.

The deposition in Figure 5.2a was performed for 2h30, at 7-11 kV and with a feeding rate of 2 - 4 μL min^{-1}, onto a aluminium sheet substrate. The parameters changed during the deposition with the given ranges because, from time to time, the Taylor cone changed needing an adjustment of the electrospinning conditions. It is also important to mention that the humidity of the surrounding environment influences the deposition. The sample was then stabilised and carbonised. The stabilisation step was performed in air and resulted in cyclisation and thermally stable aromatic ladder polymer formation, increasing

the chemical and mechanical stability of the electrospunned mat which is essential for the carbonisation step. The stabilisation was performed at 280ºC for 1 hour in air (Figure 5.2b (B)) and the carbonisation was performed at 500ºC for 1 hour in an inert atmosphere of argon (Figure 5.2b (C)) [73]. From Figure 5.2b it is possible to see the darkening of the sample with each step. Because the carbonisation temperature used is close to the aluminium melting temperature, both steps were done on a glass substrate. The resistance of samples measured was extremely high, being in the range of $G\Omega$, which was the expected result because PAN, in most cases, cannot achieve a high degree of graphitization during carbonisation causing low conductivity of the electrospunned mats [71]. The initial conductive additive was MXenes materials, but the available ones were in liquid forms and after many attempts to dry them, the outcome was a very small amount of dried MXenes, not enough to allow the multiple depositions needed to optimise the electrospinning process. The drying process was tried in vacuum and with an inert atmosphere, separately. Since activated carbon derived from peanut shells was already being produced, the goal became to use it instead of MXenes. The stabilisation and carbonisation process induce the shrinking of the electrospunned mats. Because of this, the peanut shell electrocatalyst electrospunned mat needs to be already attached to the carbon felt before these steps are performed. Due to the small-scale laboratory equipment, the peanut shell biochar amount produced each time is low. So before using it, the optimisation depositions were done using black carbon SuperP instead. An electrospinning solution was done by adding 20 w/w% of SuperP to the already known 8w/w% PAN/DMF. To do so, 0.1656g of SuperP were added to 0.8 g of PAN and mixed together in 10 mL of DMF with a magnetic hot plate at 60ºC and 600 rpm overnight [74]. With this solution we were able to achieve the deposition seen in Figure 5.3. The deposition with the conductive additive SuperP already decrease the resistance of the electrospunned mats to the range of $k\Omega$.

We were able to achieve good deposition on the aluminium substrate, but when we switched the substrate to a heated carbon felt there were problems with adhesion to the new substrate. The ongoing work is currently here, where we are searching for a way to ensure the contact between the mat and the substrate by gluing the two parts together with a seawater resistant, conductive and non-toxic glue at the interface. Once we have the adhesion problem solved, we can deposit a peanut shell derived activated carbon onto a heated carbon felt, resulting in another way to coat the electrocatalyst onto the same material. We believe that this coating technique will improve the wettability of the

electrode and the performance when applied to a seawater battery.

FIGURE 5.3: SuperP plus PAN deposition.

Bibliography

[1] S. M. Hwang, J.-S. Park, Y. Kim, W. Go, J. Han, Y. Kim, and Y. Kim, "Rechargeable seawater batteries—from concept to applications," *Advanced Materials*, vol. 31, no. 20, p. 1804936, 2019. [Cited on pages xvii, 1, 2, 12, 20, 21, 24, 28, 29, and 35.]

[2] J.-K. Kim, F. Mueller, H. Kim, S. Jeong, J.-S. Park, S. Passerini, and Y. Kim, "Eco-friendly energy storage system: Seawater and ionic liquid electrolyte," *ChemSusChem*, vol. 9, no. 1, pp. 42–49, 2016. [Cited on pages 1 and 2.]

[3] P. Sharma and V. Kumar, "Current technology of supercapacitors: A review," *Journal of Electronic Materials*, vol. 49, no. 6, pp. 3520–3532, 2020. [Cited on pages 1 and 27.]

[4] S. Senthilkumar, W. Go, J. Han, L. P. T. Thuy, K. Kishor, Y. Kim, and Y. Kim, "Emergence of rechargeable seawater batteries," *Journal of Materials Chemistry A*, vol. 7, no. 40, pp. 22 803–22 825, 2019. [Cited on pages 1, 2, 23, and 24.]

[5] Y. Kim and W.-g. Lee, *Primary Seawater Batteries*. Singapore: Springer Nature Singapore, 2022, pp. 37–90. [Online]. Available: https://doi.org/10.1007/978-981-19-0797-5_2 [Cited on pages 1, 5, 7, 8, and 9.]

[6] Y. Qiao, C. Zhang, F. Kong, Q. Zhao, A. Kong, and Y. Shan, "Activated biochar derived from peanut shells as the electrode materials with excellent performance in zinc-air battery and supercapacitance," *Waste Management*, vol. 125, pp. 257–267, 2021. [Cited on pages 2, 3, 15, 17, 18, and 79.]

[7] S. Senthilkumar, S. O. Park, J. Kim, S. M. Hwang, S. K. Kwak, and Y. Kim, "Seawater battery performance enhancement enabled by a defect/edge-rich, oxygen self-doped porous carbon electrocatalyst," *Journal of Materials Chemistry A*, vol. 5, no. 27, pp. 14 174–14 181, 2017. [Cited on pages 3, 15, 18, 46, 68, 77, 78, and 79.]

[8] L. Pandey, S. Sarkar, A. Arya, A. Sharma, A. Panwar, R. Kotnala, and A. Gaur, "Fabrication of activated carbon electrodes derived from peanut shell for high-performance supercapacitors," *Biomass Conversion and Biorefinery*, pp. 1–10, 2021. [Cited on pages 3, 17, and 81.]

[9] Y. Zhan, H. Zhou, F. Guo, B. Tian, S. Du, Y. Dong, and L. Qian, "Preparation of highly porous activated carbons from peanut shells as low-cost electrode materials for supercapacitors," *Journal of Energy Storage*, vol. 34, p. 102180, 2021. [Cited on pages 3, 17, 18, 43, 44, and 78.]

[10] B. Viswanathan, *Energy sources: fundamentals of chemical conversion processes and applications*. Newnes, 2016. [Cited on pages 6 and 10.]

[11] I. Kallquist, F. Lindgren, M.-T. Lee, A. Shavorskiy, K. Edstrom, H. Rensmo, L. Nyholm, J. Maibach, and M. Hahlin, "Probing electrochemical potential differences over the solid/liquid interface in li-ion battery model systems," *ACS applied materials & interfaces*, vol. 13, no. 28, pp. 32 989–32 996, 2021. [Cited on page 7.]

[12] V. Massaccesi, "Electrode materials for Na-ion batteries: a new route for low-cost energy storage," Thesis, Instituto Superior Técnico, Lisboa, Portugal, Jan. 2016. [Cited on pages 8, 10, 49, and 50.]

[13] X. Li, S. Guo, H. Deng, K. Jiang, Y. Qiao, M. Ishida, and H. Zhou, "An ultrafast rechargeable lithium metal battery," *Journal of Materials Chemistry A*, vol. 6, no. 32, pp. 15 517–15 522, 2018. [Online]. Available: http://xlink.rsc.org/?DOI=C8TA05354E [Cited on page 10.]

[14] K. Kubota, M. Dahbi, T. Hosaka, S. Kumakura, and S. Komaba, "Towards k-ion and na-ion batteries as "beyond li-ion"," *The chemical record*, vol. 18, no. 4, pp. 459–479, 2018. [Cited on pages xvii, 11, 13, and 14.]

[15] S. Saeidnia and M. Abdollahi, "Concerns on the growing use of lithium: The pros and cons," *Iranian Red Crescent Medical Journal*, vol. 15, no. 8, p. 629, 2013. [Cited on page 11.]

[16] M. Sawicki and L. L. Shaw, "Advances and challenges of sodium ion batteries as post lithium ion batteries," *RSC Advances*, vol. 5, no. 65, pp. 53 129–53 154, 2015. [Cited on pages 12 and 14.]

[17] Y. Kim and W.-g. Lee, "Secondary seawater batteries," in *Seawater Batteries*. Springer, 2022, pp. 91–293. [Cited on pages xvii, 12, 15, 22, 23, 24, 25, and 40.]

[18] K. Abraham, "How comparable are sodium-ion batteries to lithium-ion counterparts?" *ACS Energy Letters*, vol. 5, no. 11, pp. 3544–3547, 2020. [Cited on pages 12, 14, and 15.]

[19] P. K. Nayak, L. Yang, W. Brehm, and P. Adelhelm, "From lithium-ion to sodium-ion batteries: advantages, challenges, and surprises," *Angewandte Chemie International Edition*, vol. 57, no. 1, pp. 102–120, 2018. [Cited on pages xvii and 13.]

[20] A. Y. Tsivadze, T. Kulova, and A. Skundin, "Fundamental problems of lithium-ion rechargeable batteries," *Protection of Metals and Physical Chemistry of Surfaces*, vol. 49, no. 2, pp. 145–150, 2013. [Cited on page 13.]

[21] R. Korthauer, *Lithium-ion batteries: basics and applications*. Springer, 2018. [Cited on page 14.]

[22] B. Viswanathan, P. I. Neel, and T. Varadarajan, "Methods of activation and specific applications of carbon materials," *India, Chennai*, 2009. [Cited on page 16.]

[23] M.-A. Perea-Moreno, F. Manzano-Agugliaro, Q. Hernandez-Escobedo, and A.-J. Perea-Moreno, "Peanut shell for energy: properties and its potential to respect the environment," *Sustainability*, vol. 10, no. 9, p. 3254, 2018. [Cited on pages 16 and 17.]

[24] J. Ani, K. Akpomie, U. Okoro, L. Aneke, O. Onukwuli, and O. Ujam, "Potentials of activated carbon produced from biomass materials for sequestration of dyes, heavy metals, and crude oil components from aqueous environment," *Applied Water Science*, vol. 10, no. 2, pp. 1–11, 2020. [Cited on page 16.]

[25] M. S. Reza, C. S. Yun, S. Afroze, N. Radenahmad, M. S. A. Bakar, R. Saidur, J. Taweekun, and A. K. Azad, "Preparation of activated carbon from biomass and its' applications in water and gas purification, a review," *Arab Journal of Basic and Applied Sciences*, vol. 27, no. 1, pp. 208–238, 2020. [Cited on page 16.]

[26] N. M. Nor, L. C. Lau, K. T. Lee, and A. R. Mohamed, "Synthesis of activated carbon from lignocellulosic biomass and its applications in air pollution control—a review," *Journal of Environmental Chemical Engineering*, vol. 1, no. 4, pp. 658–666, 2013.

[27] N. Abuelnoor, A. AlHajaj, M. Khaleel, L. F. Vega, and M. R. Abu-Zahra, "Activated carbons from biomass-based sources for co2 capture applications," *Chemosphere*, vol. 282, p. 131111, 2021.

[28] J. Jjagwe, P. W. Olupot, E. Menya, and H. M. Kalibbala, "Synthesis and application of granular activated carbon from biomass waste materials for water treatment: A review," *Journal of Bioresources and Bioproducts*, vol. 6, no. 4, pp. 292–322, 2021.

[29] S. Bagheri, N. Muhd Julkapli, and S. Bee Abd Hamid, "Functionalized activated carbon derived from biomass for photocatalysis applications perspective." *International Journal of Photoenergy*, vol. 2015, 2015. [Cited on page 16.]

[30] P. Dubey, V. Shrivastav, P. H. Maheshwari, and S. Sundriyal, "Recent advances in biomass derived activated carbon electrodes for hybrid electrochemical capacitor applications: Challenges and opportunities," *Carbon*, vol. 170, pp. 1–29, 2020. [Cited on pages xvii and 16.]

[31] J. Górka, C. Vix-Guterl, and C. Matei Ghimbeu, "Recent progress in design of biomass-derived hard carbons for sodium ion batteries," *C*, vol. 2, no. 4, p. 24, 2016. [Cited on pages 17 and 18.]

[32] M. Muthu Balasubramanian, M. Subramani, D. Murugan, and S. Ponnusamy, "Groundnut shell–derived porous carbon-based supercapacitor with high areal mass loading using carbon cloth as current collector," *Ionics*, vol. 26, no. 12, pp. 6297–6308, 2020. [Cited on pages 17 and 19.]

[33] R.-w. Fu, Z.-h. Li, Y.-r. Liang, L. Feng, X. Fei, and D.-c. Wu, "Hierarchical porous carbons: design, preparation, and performance in energy storage," *New Carbon Materials*, vol. 26, no. 3, pp. 171–179, 2011. [Cited on pages 17, 18, and 65.]

[34] X. Liu, C. Ma, J. Li, B. Zielinska, R. J. Kalenczuk, X. Chen, P. K. Chu, T. Tang, and E. Mijowska, "Biomass-derived robust three-dimensional porous carbon for high volumetric performance supercapacitors," *Journal of Power Sources*, vol. 412, pp. 1–9, 2019. [Cited on pages 18, 43, 44, 61, 62, 66, 68, 78, and 89.]

[35] C.-H. Zhao, B.-J. Peng, and Z.-B. Hu, "Hierarchical porous carbon/selenium composite derived from hydrothermal treated peanut shell as high-performance lithium ion battery cathode," *Chemical Papers*, vol. 74, no. 4, pp. 1289–1299, 2020. [Cited on page 19.]

[36] S. Park, B. SenthilKumar, K. Kim, S. M. Hwang, and Y. Kim, "Saltwater as the energy source for low-cost, safe rechargeable batteries," *Journal of Materials Chemistry A*, vol. 4, no. 19, pp. 7207–7213, 2016. [Cited on page 21.]

[37] A. G. Borthwick, "Marine renewable energy seascape," *Engineering*, vol. 2, no. 1, pp. 69–78, 2016. [Cited on page 21.]

[38] "4 TO ONE." [Online]. Available: https://www.4toone.com/main/?skin=eng_index.html [Cited on pages 24, 40, and 47.]

[39] J. Park, J.-S. Park, S. Senthilkumar, and Y. Kim, "Hybridization of cathode electrochemistry in a rechargeable seawater battery: Toward performance enhancement," *Journal of Power Sources*, vol. 450, p. 227600, 2020. [Cited on pages xvii, 27, 42, 72, and 87.]

[40] J. Han, S. M. Hwang, W. Go, S. Senthilkumar, D. Jeon, and Y. Kim, "Development of coin-type cell and engineering of its compartments for rechargeable seawater batteries," *Journal of Power Sources*, vol. 374, pp. 24–30, 2018. [Cited on pages 28, 40, 41, and 47.]

[41] J.-K. Kim, E. Lee, H. Kim, C. Johnson, J. Cho, and Y. Kim, "Rechargeable seawater battery and its electrochemical mechanism," *ChemElectroChem*, vol. 2, no. 3, pp. 328–332, 2015. [Cited on page 29.]

[42] P. Brennan, "Cosmic Milestone: NASA Confirms 5,000 Exoplanets," 03 2022. [Online]. Available: https://www.jpl.nasa.gov/news/cosmic-milestone-nasa-confirms-5000-exoplanets [Cited on page 30.]

[43] "Earth's Water." [Online]. Available: https://olc.worldbank.org/sites/default/files/sco/E7B1C4DE-C187-5EDB-3EF2-897802DEA3BF/Nasa/chapter1.html [Cited on pages xvii and 30.]

[44] Y. Kim and W.-g. Lee, *Seawater and Its Resources*. Singapore: Springer Nature Singapore, 2022, pp. 1–35. [Online]. Available: https://doi.org/10.1007/978-981-19-0797-5_1 [Cited on pages xxi, 31, 32, 33, 34, 35, and 36.]

[45] P. Webb, *Introduction to Oceanography*. Rebus Community, 2019. [Cited on pages xxi, 32, 34, and 35.]

[46] R. Buck, S. Rondinini, A. Covington, F. Baucke, C. M. Brett, M. Camoes, M. Milton, T. Mussini, R. Naumann, K. Pratt *et al.*, "Measurement of ph. definition, standards, and procedures (iupac recommendations 2002)," *Pure and applied chemistry*, vol. 74, no. 11, pp. 2169–2200, 2002. [Cited on page 32.]

[47] J. Wiater, "Electric shock hazard limitation in water during lightning strike," *Sea*, vol. 200, p. 5000, 2012. [Cited on pages xxi, 32, and 33.]

[48] R. H. Tyler, T. P. Boyer, T. Minami, M. M. Zweng, and J. R. Reagan, "Electrical conductivity of the global ocean," *Earth, Planets and Space*, vol. 69, no. 1, pp. 1–10, 2017. [Cited on page 33.]

[49] Z. Zheng, Y. Fu, K. Liu, R. Xiao, X. Wang, and H. Shi, "Three-stage vertical distribution of seawater conductivity," *Scientific reports*, vol. 8, no. 1, pp. 1–10, 2018. [Cited on page 33.]

[50] Y. Zhang, S. T. Senthilkumar, J. Park, J. Park, and Y. Kim, "A new rechargeable seawater desalination battery system," *Batteries & Supercaps*, vol. 1, no. 1, pp. 6–10, 2018. [Cited on pages xvii, 36, and 37.]

[51] M. Son, S. Park, N. Kim, A. T. Angeles, Y. Kim, and K. H. Cho, "Simultaneous energy storage and seawater desalination using rechargeable seawater battery: Feasibility and future directions," *Advanced Science*, vol. 8, no. 18, p. 2101289, 2021. [Cited on page 40.]

[52] "Alfa Aesar." [Online]. Available: https://www.alfa.com/pt/ [Cited on page 41.]

[53] J. Marcuzzo, A. Cuña, N. Tancredi, H. Polidoro, S. Otani, and C. Otani, "Microporous activated carbono fiber felt produced from brasilian textile pan fiber," *X Encontro Brasileiro sobre Adsorção. Guarujá, SP, Brasil*, 2014. [Cited on pages 41 and 42.]

[54] "Electrochemical Instruments-Galvanostat/Potentiostat Manufacturer Gamry Instruments." [Online]. Available: https://www.gamry.com/ [Cited on page 47.]

[55] A. Mohammed and A. Abdullah, "Scanning electron microscopy (sem): A review," in *Proceedings of the 2018 International Conference on Hydraulics and Pneumatics—HERVEX, Băile Govora, Romania*, 2018, pp. 7–9. [Cited on pages 49 and 51.]

[56] B. Ruan, "Study of new materials for sodium-ion batteries," 2018. [Cited on pages 50, 51, and 54.]

[57] K. Praveen, C. Pious, S. Thomas, and Y. Grohens, "Relevance of plasma processing on polymeric materials and interfaces," in *Non-Thermal Plasma Technology for Polymeric Materials*. Elsevier, 2019, pp. 1–21. [Cited on page 51.]

[58] M. Sarkar, M. Hasanuzzaman, F. Gulshan, and A. Rashid, "Surface, mechanical and shape memory properties of biodegradable polymers and their applications," in *Encyclopedia of Materials: Plastics and Polymers*, M. Hashmi, Ed. Oxford: Elsevier, 2022, pp. 1092–1099. [Online]. Available: https://www.sciencedirect.com/science/article/pii/B978012820352100050X [Cited on page 51.]

[59] R. Mogensen, "Realization of sodium-ion batteries: From electrode to electrolyte materials," Ph.D. dissertation, Acta Universitatis Upsaliensis, 2020. [Cited on pages xviii, 52, 54, and 55.]

[60] X. Yao, E. Olsson, J. Zhao, W. Feng, W. Luo, S. Tan, M. Huang, Y. Zhao, J. Huang, Q. Cai, and L. Mai, "Voltage plateau variation in a bismuth-potassium battery," *J. Mater. Chem. A*, vol. 10, pp. 2917–2923, 2022. [Online]. Available: http://dx.doi.org/10.1039/D1TA09292H [Cited on page 52.]

[61] M. Winter and R. J. Brodd, "What are batteries, fuel cells, and supercapacitors?" *Chemical reviews*, vol. 104, no. 10, pp. 4245–4270, 2004. [Cited on pages xviii, 53, and 54.]

[62] W. Wang, X. Wei, D. Choi, X. Lu, G. Yang, and C. Sun, "Chapter 1 - electrochemical cells for medium- and large-scale energy storage: fundamentals," in *Advances in Batteries for Medium and Large-Scale Energy Storage*, ser. Woodhead Publishing Series in Energy, C. Menictas, M. Skyllas-Kazacos, and T. M. Lim, Eds. Woodhead Publishing, 2015, pp. 3–28. [Online]. Available: https://www.sciencedirect.com/science/article/pii/B9781782420132000017 [Cited on page 53.]

[63] N. H. N. Azman, M. S. Mamat@ Mat Nazir, L. H. Ngee, and Y. Sulaiman, "Graphene-based ternary composites for supercapacitors," *International Journal of Energy Research*, vol. 42, no. 6, pp. 2104–2116, 2018. [Cited on pages xviii, 54, and 55.]

[64] J. Ferreira, T. Salgueiro, R. Veloso, J. Ventura, and J. Espain, "High porosity bio-waste electrocatalyst for seawater batteries," in preparation. [Cited on pages 61, 77, and 97.]

[65] E. Mistar, S. Ahmad, A. Muslim, T. Alfatah, and M. Supardan, "Preparation and characterization of a high surface area of activated carbon from bambusa vulgaris—effect of naoh activation and pyrolysis temperature," in *IOP Conference Series: Materials Science and Engineering*, vol. 334, no. 1. IOP Publishing, 2018, p. 012051. [Cited on page 64.]

[66] K. J. Kim, S.-W. Lee, T. Yim, J.-G. Kim, J. W. Choi, J. H. Kim, M.-S. Park, and Y.-J. Kim, "A new strategy for integrating abundant oxygen functional groups into carbon felt electrode for vanadium redox flow batteries," *Scientific reports*, vol. 4, no. 1, pp. 1–6, 2014. [Cited on pages 67 and 68.]

[67] N. Guanhua, S. Qian, X. Meng, W. Hui, X. Yuhang, C. Weimin, and W. Gang, "Effect of nacl-sds compound solution on the wettability and functional groups of coal," *Fuel*, vol. 257, p. 116077, 2019. [Cited on page 68.]

[68] P. Biesheuvel, S. Porada, and J. Dykstra, "The difference between faradaic and non-faradaic electrode processes," *arXiv preprint arXiv:1809.02930*, 2018. [Cited on page 85.]

[69] "Determining the Onset Potential in Cyclic Voltammetry." [Online]. Available: https://resources.pcb.cadence.com/blog/2020-determining-the-onset-potential-in-cyclic-voltammetry [Cited on page 85.]

[70] A. G. El-Deen, J.-H. Choi, K. A. Khalil, A. A. Almajid, and N. A. Barakat, "A tio 2 nanofiber/activated carbon composite as a novel effective electrode material for capacitive deionization of brackish water," *RSC Advances*, vol. 4, no. 110, pp. 64 634–64 642, 2014. [Cited on page 88.]

[71] X. Mao, T. A. Hatton, and G. C. Rutledge, "A review of electrospun carbon fibers as electrode materials for energy storage," *Current Organic Chemistry*, vol. 17, no. 13, pp. 1390–1401, 2013. [Cited on pages 98, 99, and 101.]

[72] Z. Khan, F. Kafiah, H. Z. Shafi, F. Nufaiei, S. A. Furquan, and A. Matin, "Morphology, mechanical properties and surface characteristics of electrospun polyacrylonitrile (pan) nanofiber mats," *IJAENT*, vol. 2, no. 3, pp. 15–22, 2015. [Cited on page 100.]

[73] L. Sabantina, M. Á. Rodríguez-Cano, M. Klöcker, F. J. García-Mateos, J. J. Ternero-Hidalgo, A. Mamun, F. Beermann, M. Schwakenberg, A.-L. Voigt, J. Rodríguez-Mirasol *et al.*, "Fixing pan nanofiber mats during stabilization for carbonization and

creating novel metal/carbon composites," *Polymers*, vol. 10, no. 7, p. 735, 2018. [Cited on page 101.]

[74] G. K. Sharma and N. R. James, "Carbon black incorporated carbon nanofiber based polydimethylsiloxane composite for electromagnetic interference shielding," *Carbon Trends*, vol. 8, p. 100177, 2022. [Cited on page 101.]